Study on the Mode of Action of Antitumor Macrolide Aplyronine A

Yuichiro HIRAYAMA

February 2014

Study on the Mode of Action of Antitumor Macrolide Aplyronine A

Yuichiro HIRAYAMA

Doctoral Program in Chemistry

Submitted to the Graduate School of
Pure and Applied Sciences
in Partial Fulfillment of the Requirements
for the Degree of Doctor of philosophy in
Science

at the
University of Tsukuba

Acknowledgment

My current and past associates in Kigoshi group:

Dr. Mitsuru Ueda	Dr. Akiyuki Ikedo	Dr. Kenichi Kobayashi
Dr. Takashi Yoshizumi	Mr. Yuta Ogawa	Mr. Yoshihito Nagano
Mr. Hironori Nishimura	Mr. Yusuke Fujii	Mr. Hidekazu Watanabe
Mr. Takuya Yamada	Dr. Yosuke Satoh	Dr. Takuma Takemura
Mr. Dai Kawamura	Mr. Keiji Kojima	Mr. Yuta Ebihara
Ms. Yumi Ochiai	Mr. Yamato Miyazawa	Mr. Toru Watanabe
Mr. Tomoya Ishitsuka	Mr. Nozomi Ogihara	Ms. Miyuki Sugiyama
Mr. Keisuke Tomita	Mr. Shinichi Kobayashi	Mrs. Yuki Ogihara (Saito)
Ms. Eri Yaguchi	Mr. Yuzo Mogi	Mr. Akihiro Usui
Mr. Yuto Onozaki	Mr. Satoshi Tanabe	Mr. Baro Gise
Mr. Hirotaka Oka	Mr. Yusuke Sakai	Mr. Ryosuke Fujisawa
Mr. Shota Funakubo	Mr. Kozo Yoneda	Mr. Atsushi Kawamura
Mr. Koichi Takeno	Ms. Yuko Katoh	Mr. Ryo Nakajima
Ms. Mami Shimanuki	Mr. Masaki Tsunoda	Mr. Keisuke Niida
Ms. Maiko Matsuki	Ms. Sachiko Matsumoto	Mr. Kota Yamagishi
Mr. Yuhei Sone	Ms. Tomomi Nakamura	Mr. Satoru Inomata
Mr. Takahiro Kaneko	Mr. Kizuku Kimura	Mr. Shuya Shioda
Mr. Kenta Tanabe	Mr. Kota Tsuchiya	Mr. Tomotaka Ogura
Mr. Masahiro Hida	Ms. Miho Komai	Mr. Keita Saito
Mr. Kazuaki Suzuki	Mr. Taiki Sunaba	Mr. Kentaro Futaki

Graduate School of Pure and Applied Sciences

University of Tsukuba

February 2014

Yuichiro Hirayama

Table of Contents

List of abbreviation

Ac	acetyl	MALDI	matrix-assisted laser desorption/ionization
ADP	adenosine diphosphate	Me	methyl
ApA	aplyronine A	MS	mass spectrometry
aq.	aqueous	MTT	3-(4,5-dimethyl-2-thiazolyl)-2,5-diphenyl-tetrazolium bromide
ATP	adenosine triphosphate		
Boc	*tert*-butoxycarbonyl	NHS	*N*-hydroxysuccinimide
Bu	butyl	NMR	nuclear magnetic resonance
CBB	coomassie brilliant blue	ODS	octadodecylsilyl
DCC	dicyclohexylcarbodiimide	PAGE	poly-acrylamide gel electrophoresis
DIPEA	*N,N*-diisopropylethylamine	PBS	phosphate buffered saline
DMF	*N,N*-dimethylformamide	PDB	protein data bank
DMSO	dimethylsulfoxide	PEG	polyethylene glycol
DNA	deoxyribonucleic acid	Phth	phthalimide
DTT	dithiothreitol	PVDF	polyvinylidene difluoride
EC_{50}	effective concentration 50%	Py	pyridine
EDC	1-ethyl-3-(3-dimethylamiinopropyl) carbodiimide hydrochloride	PMF	peptide mass fingerprinting
		rt	room temperature
EDTA	ethylenediaminetetraacetic acid	SD	subdomain
ESI	electrospray ionization	SDS	sodium dodecyl sulfate
Et	ethyl	TFA	trifluoroacetic acid
F-actin	filamentous actin	TLC	tin layer chromatography
FBS	fetal bovine serum	Tris	tris(hydroxymethyl)aminomethane
G-actin	globular actin	Ts	*p*-toluenesulfonyl
HOAt	1-hydroxy-7-azabenzotriazole	T/C	test/control
HOBt	1-hydroxybenzotriazole	UV	ultraviolet
HPLC	high performance liquid chromatography	WB	western blotting
HRMS	high resolution mass spectrometry		
IC_{50}	inhibitory concentration 50%		
IR	infrared spectroscopy		
liq.	liquid		
Lys	lysine		

Chapter 1.
General introduction

1.1. Cancer

Cancer is a group of diseases characterized by uncontrolled growth and spread of abnormal cells. One in eight deaths worldwide is due to cancer.[1] Worldwide, cancer causes more deaths than AIDS, tuberculosis, and malaria combined. When countries are grouped according to economic development, cancer is the leading cause of death in developed countries and the second leading cause of death in developing countries (Table 1-1). The burden of cancer is increasing in step with the aging of the population. In Japan, one of the world's fastest aging societies, cancer is the top cause of mortality, accounting for 29% of deaths in 2013.[2] Population aging is quickly progress in the developing countries. Thus, cancer is a global health problem that should be put in serious effort to tackle.

1.1.1. Principal methods of curing cancer

Principal cancer therapies are surgery, radiotherapy, and chemotherapy. Surgery has been used to remove all of localized tumors or reduce the size of large tumors. Radiotherapy is the medical use of ionizing radiation to kill cancer cells in the treatment area. Chemotherapy is the use of antitumor drugs to treat cancer. These drugs not only kill cancer cells but also keep them from growing and spreading. Among of these treatments, surgery and radiotherapy achieve good therapeutic effect for localized tumors. However they are not effective against metastatic cancer and inadaptable to leukemic disease. In contrast, chemotherapy has the potential to be adaptable to metastatic cancer and leukemic disease, since anticancer drugs are carried to the whole body via the blood stream. Furthermore chemotherapy is given before or after surgery and/or radiotherapy to reduce tumor size and inhibition of metastasis, so chemotherapy has been to play the

important role in curing cancer. However chemotherapy has a low cure rate than other two methods, and

anticancer drugs sometime would also affect and kill normal cells and induce serious side effects such as hair

loss, mouth sores, nausea, and vomiting. Therefore to improve the cure rate and reduce the side effects,

developments of new anticancer drugs with novel antitumor mechanism that has high selectivity for cancer

has been strongly anticipated.

Table 1-1. Leading Causes of Death

	Worldwide		Developing		Developed	
	rank	%	rank	%	rank	%
Heart diseases	1	15.1	1	14.5	2	19.3
Malignant neoplasms	2	12.6	2	10.4	1	26.6
Cerebrovascular diseases	3	9.7	3	9.8	3	9.4
Lower respiratory infections	4	7.1	4	7.7	4	3.8
Perinatal conditions	5	5.4	5	6.2		0.4
Chronic obstructive pulmonary disease	6	5.1	6	5.4	5	3.5
Diarrhoeal diseases	7	3.7	7	4.2		0.2
HIV/AIDS	8	3.5	8	4.0		0.2
Tuberculosis	9	2.5	9	2.9		0.2
Road traffic accidents	10	2.2	10	2.3		1.4
Diabetes mellitus	11	1.9		1.8	7	2.7
Malaria	12	1.5		1.8		0.0
Suicide	13	1.4		1.4	9	1.5
Cirrohsis of the liver	14	1.3		1.3	10	1.4
Nephritis and nephrosis	15	1.3		1.2	8	1.6

Source: World Health Organization, The global burden of disease: 2004 update.

1.1.2. Anticancer drugs from natural products

More than 200 antitumor drugs have been used in clinical practice. Among these antitumor drugs, small-molecule drugs account for approximately 80%, and natural inspired drugs (i.e., natural products, derived from natural product, and totally synthetic drugs but the pharmacophore is/was from natural product) constitute over 70% of small-molecule drugs.[3] This fact suggests that natural products are important for development of antitumor drugs. Diversity of the complex structure with the chirality and activities of natural products have promise as a good source to investigate for antitumor agents which have novel mode of action. Historically, drugs were discovered from plants and fungi as natural medicines and others. Attention is currently focused on natural products which are derived from marine organism. Many marine organisms such as sponge, sea squirt, nudibranch and microorganism, keep a store of bioactive substances as chemical defenses and a lot of bioactive secondly metabolizes have been found from marine organism. Among them, many compounds exhibit antitumor activity. Examples of marine antitumor compounds classified as a typical mode of action are described below (Figure 1-1).

<u>Enzyme inhibitor</u>

Bryostatin-1[4] is a protein kinase C (PKC) inhibitor, isolated from the bryzoan *Bugula neritina*. PKC is one of the families of serine/threonine-specific protein kinase, and plays important roles in several signal transduction cascades involving cell growth, malignant alteration, and others.[5] Therefore, PKC inhibitors have a potential as antitumor agents.

Aeroplysinin[6] is a bromotyrosine derivative which is included in the sponge *Verongia aerophoba*. It prevents angiogenesis that is important for cancer growth by inhibition of protein tyrosine kinase.[7]

<u>DNA replication inhibitor</u>

Ecteinascidin 743 (ET743)[8] is a DNA-alkylating agent and isolated from the sea squirt *Ecteinascidia turbinate*. DNA-alkylating agents interfere with a DNA replication by alkylation of DNA. Since cancer cells

that undergo cell division frequently have great sensitivity for DNA lesion, the agents exhibit antitumor activity.

Spindle poison

Many marine natural products interact to tubulin as spindle poison. Historically, tubulin is one of the most important targets of antitumor agents, so the detail of tubulin and tubulin-interactive agents is described in next section.
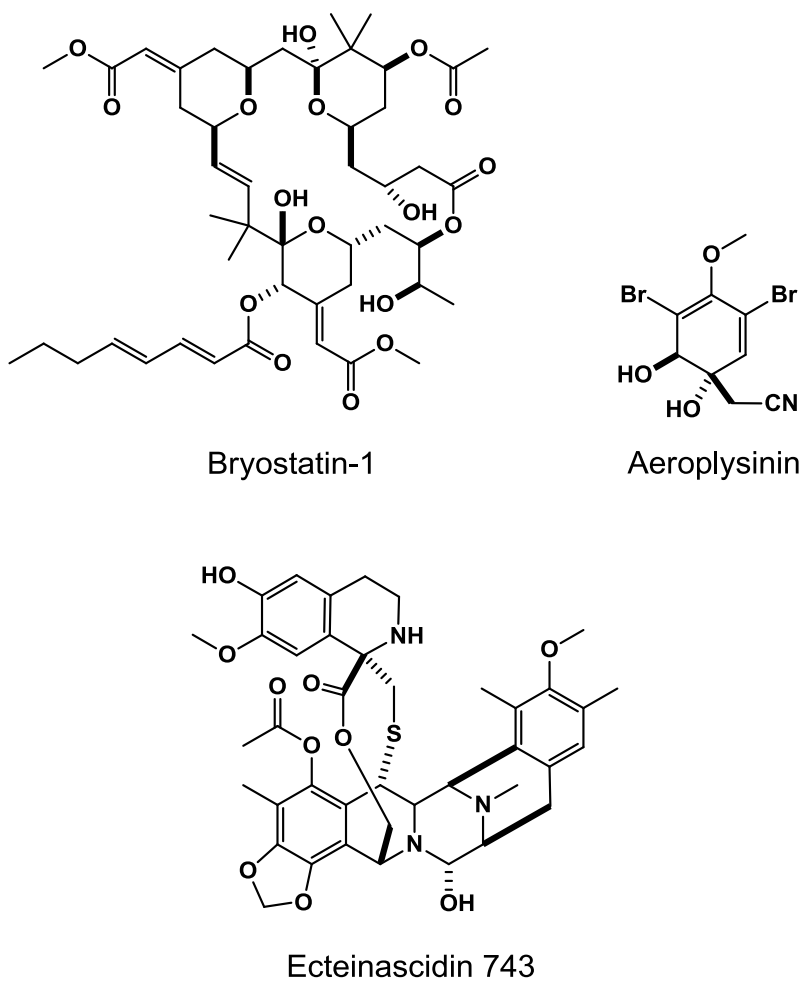
Figure 1-1. Antitumor agents from marine origin

1.2. Microtubule (Tubulin)

Microtubule is one of the cytoskeletons and formed by polymerization of α- and β-tubulin heterodimer (Figure 1-2).[9] Microtubules have several key roles that are important for cell proliferation, trafficking, signaling, and migration in eukaryotic cells. Especially, microtubules form mitotic spindle and play a primary role in the division of chromosome at metaphase. Since this process is controlled by dynamics of tubulin assembly and disassembly, inhibition of tubulin disrupts cell division and causes cell death by apoptosis. Therefore, tubulin is an important antitumor target along with DNA, and tubulin-interactive agents have been studied for a long time.
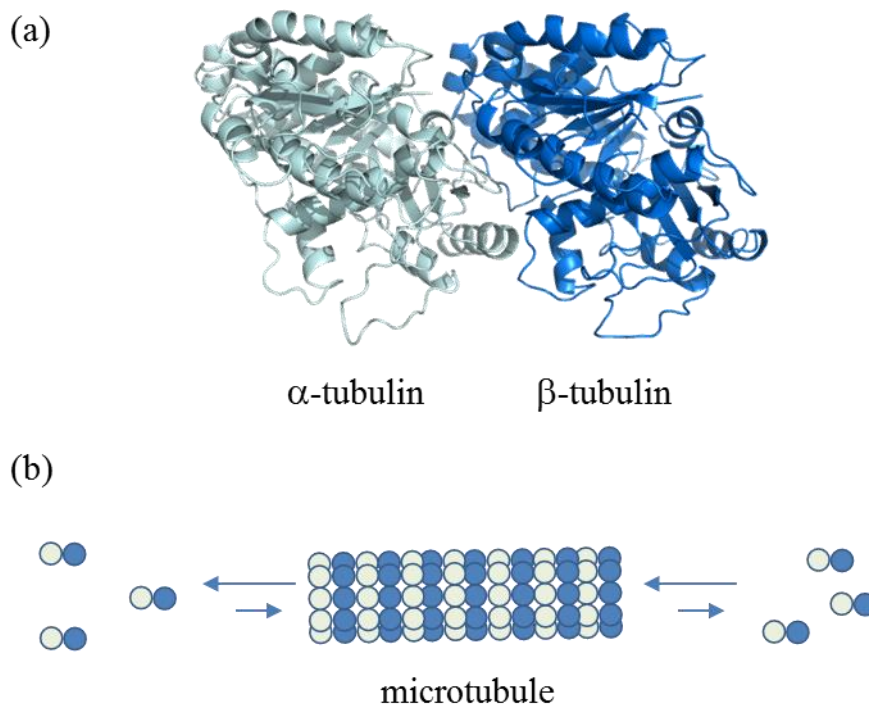
Figure 1-2. (a) Structure of α/β-tubulin heterodimer; (b) The dynamics of microtubule

1.2.1. Tubulin-interactive agents

Paclitaxel (taxol),[10] which were isolated from *Taxus brevifolia,* and vinblastine,[11] which were isolated from *Vinca rosea,* are famous tubulin-interactive agents, and they have been used as anticancer drugs in clinical practice for a long time (Figure 1-3). Colchicine is also a well-known tubulin-interactive agent while it has not been clinically used. Tubulin-interactive agents are often classified into two main groups, microtubule-stabilizing and microtubule-destabilizing agents. Microtubule-stabilizing agents enhance tubulin-polymerization and include the taxans (paclitaxel and docetaxel[12]), epothilone A,[13] discodermolide,[14] and others. Many microtubule-stabilizing agents bind to the same or to overlapping binding-site of paclitaxel. Microtubule-destabilizing agents inhibit tubulin-polymerization and include the vinca alkaloids (vinblastine and vincristine[15]), colchicine, halichondrine B,[16] dolastatine 10,[17] and others. These microtubule-destabilizing agents bind to the same or similar binding sites of vinblastine or colchicine. Meanwhile, several tubulin-interactive agents, such as laurimalide[18] and peloruside A[19] bind to novel site of tubulin.

Tubulin-interactive natural products have diversity and complex structures. In general they are present in only minute amount in natural organisms which are uncultivable. These may become the serious problem to develop in clinical. It is noteworthy that the identification and investigation of tubulin-interactive agents were nonetheless ongoing. For example, research team of Eisai Research Institute and the Kishi group developed eribulin,[20] which approved as a new antitumor drug for metastatic breast cancer, through the studies on halichondrin B (Figure 1-4).
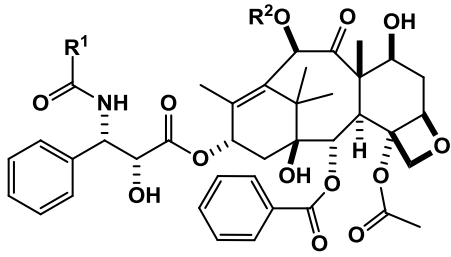
Paclitaxel   R^1 = Phe   R2 = Ac
Docetaxel   R^1 = t-BuO R^2 = H
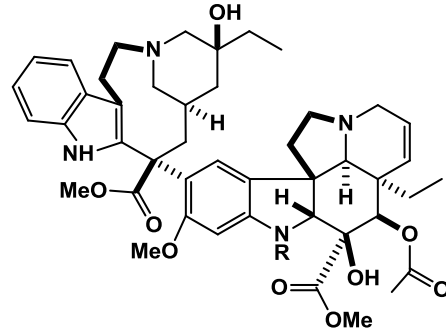
Vinblastine R = Me
Vincristine R = CHO
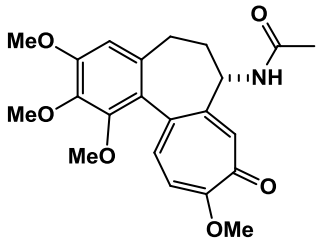
Colchicine
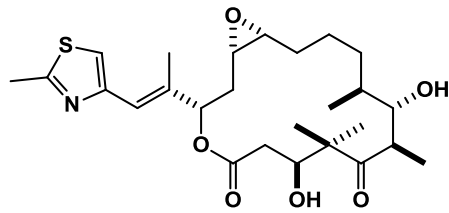
Epothilone A
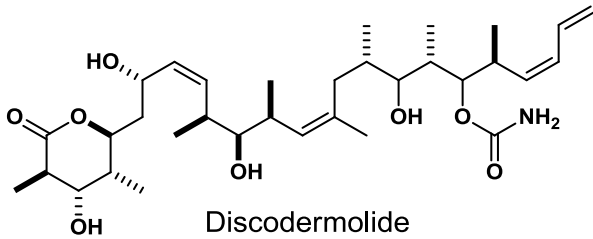
Discodermolide
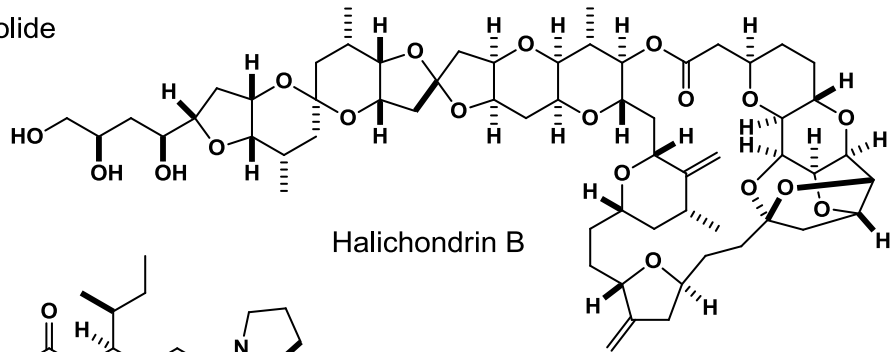
Halichondrin B
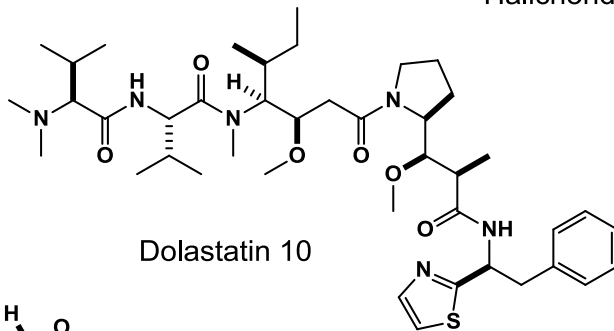
Dolastatin 10
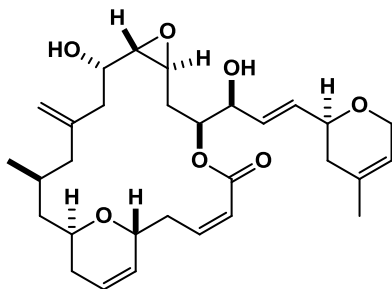
Laulimalide
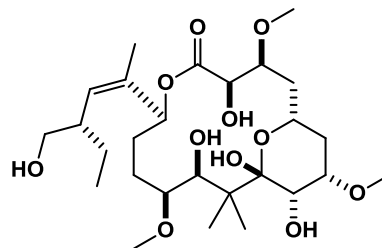
Peloruside A

Figure 1-3. Tubulin-interactive agents

7
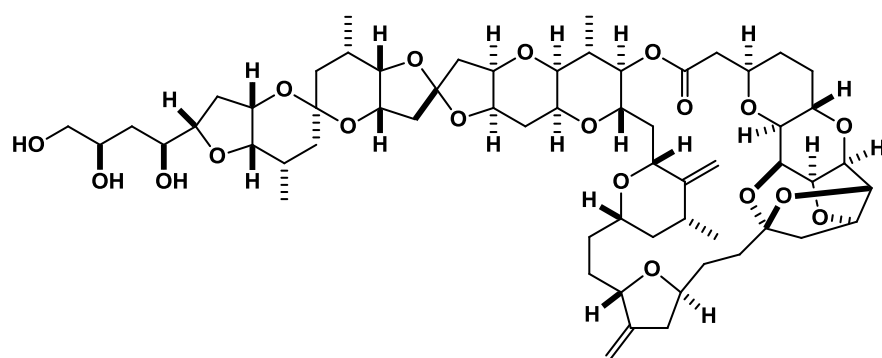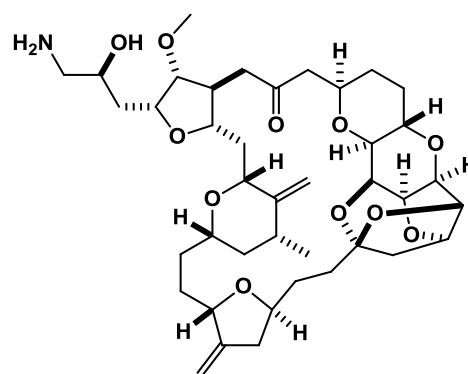
Halichondrin B

Eribulin

Figure 1-4. Anticancer drug Eribulin was an analogue of halichondrin B.

1.3. Target identification

Identification of target biomolecules and study on the mode of action of a bioactive compound are important for the development of new drugs and contribute to the elucidation of biological system such as signal pathway and protein-protein interaction. Recent technological developments in high-throughput screening and spectroscopic analysis for minute compounds have enabled to discover new bioactive small molecules. However target biomolecules and the mode of action of most of such small compounds are still unclear.

Identification of biomolecules is performed using various approaches.[21] If the target is a known biomolecule, it can be predicted by cancer cell line screening, bioassays for typical cancer targets, or computational inference. However, in the case that a compound interacts with unknown target biomolecules and/or has a novel mode of action, identification of target molecules require genetic approach or direct biochemical methods. Genetic approach identifies the target proteins by investigating the genetic modification which changes the sensitivity of a compound. Direct biochemical method is the approach to observe the interaction with target proteins by using labeling compounds called chemical probes. This approach does not require the use of genetic engineering and has been often used for the target identification of natural products. The detail of the method is described in the next section.

1.3.1. Chemical probes

A chemical probe is composed of a natural product as a ligand, tag/label groups, and a linker moiety which connects a ligand and tag/label groups. The chemical probe interacts with the target molecules of its ligand and is able to specifically label these. Target proteins that were labeled by the chemical probe can be detected and purified by using the tag/label group of the chemical probe to identify the target molecules. One of the frequently used tag/label groups is biotin. Biotin has a strong and specific interaction with avidin, and various avidin derivatives, such as avidin-resin and horse radish peroxidase (HRP) conjugate avidin for chemiluminescence detection, are commercially available (Figure 1-5). Therefore, biotin is one of the most commonly used group for target identification. The linker group separates the tag/label group from the ligand

in order for the tag/label group not to affect the interactions between the ligand and its target proteins. The

linker group also prevents the ligand from affecting the interaction between the tag and its target. PEG linker,

peptide linker and alkyl chain linker are commonly used as the linker group.
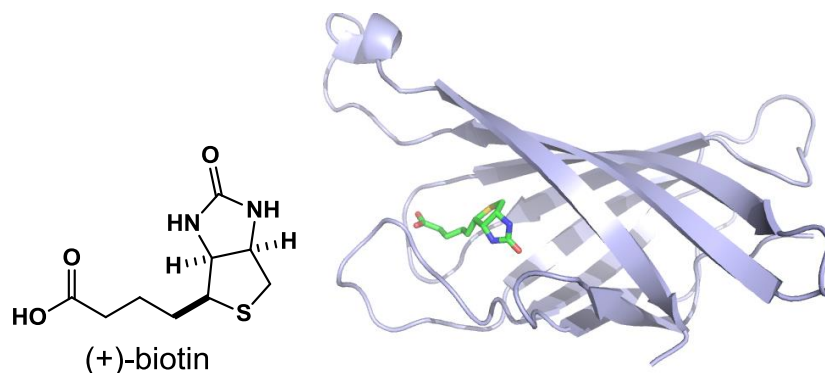
Figure 1-5. Structures of biotin and biotin-avidin complex (PDB code:2AVI)

In the case that the interaction with target proteins is weak or the amount of target proteins is minute,

photolabeling experiments are useful. Chemical probes that have a photoreacting group, such as

benzophenone, diazirine and azide, are called photoaffinity probes (Figure 1-6). Since photoaffinity probes

covalently bind to adjacent proteins, the connections between the ligand and its target proteins are not

cleaved even if the target proteins are denatured and digested. Therefore, by using photoaffinity probes,

target protein is detectable by Western blotting analysis, and the binding site of ligands can be determined.

benzophenone   diazirine   azide
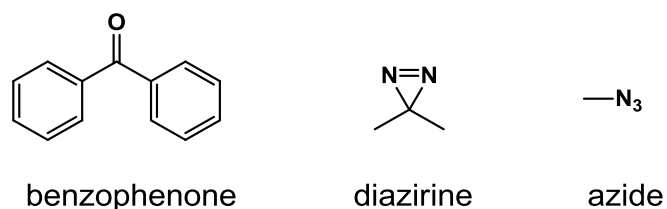
Figure 1-6. Typical photoreacting groups.

1-4. Aplyronine A

1.4.1. Isolation and biological activities of aplyronine A

As described in section 1.3, a lot of natural products that exhibit interest activities were discovered, however many of their modes of action are still unclear. Aplyronine A (ApA, **1**) is one of the such natural products. ApA is a 24-membered macrolide, which was isolated in 1993 from the Japanese sea hare *Aplysia kurodai* by Yamada and co-workers (Figure 1-7).[22] ApA has C24-34 side-chain moiety which bears a terminal *N*-methyl enamide group and two unique amino acid portions (*N,N,O*-trimethylserin and *N,N*-dimethylalanine) as structural features. ApA displays strong cytotoxicity against HeLa S3 cells. Furthermore, ApA exhibit potent antitumor activities against various mouse xenograft models (Table 1-2). Interestingly, ApA is shown to not affect the target molecules of known antitumor agents, such as DNA, microtubule, and cycle regulating enzymes.[23] In 1996, Karaki and co-workers ascertained that ApA inhibits the polymerization of actin by forming a 1:1 complex with actin.[24] Thus ApA is expected to be a new type of anticancer agent which interacts with actin.
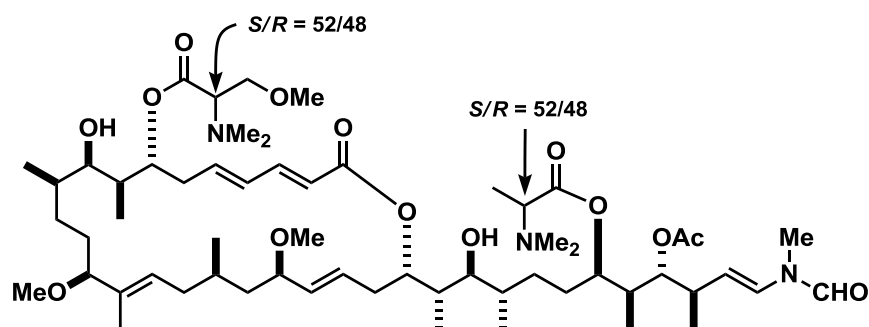
Figure 1-7. Structure of aplyronine A (**1**)

Table 1-2. Antitumor activities of aplyronine A

Tumor	Life prolong effect (T/C)	Dose (mg/kg/day)
P388 murine leukemia	545%	0.08
Lewis lung carcinoma	556%	0.04
Ehrlich carcinoma	398%	0.04
Colon 26 carcinoma	255%	0.08
B16 melanoma	201%	0.04

1.4.2. Actin

Actin is a cytoskeletal protein as with tubulin. Actin is one of the most abundant proteins in eukaryotic cells, and exists as a dynamic equilibrium mixture between globular actin (G-actin, monomer) and fibrous actin (F-actin, polymer) in cells (Figure 1-8). Microfilaments composed of F-actin, controlls several cell functions, such as cell muscle contraction, cell motility, division of cytoplasm, and adhesion. Almost actin-interactive agents inhibit the division of cytoplasm to lead multinucleated and finally induce apoptosis. Thus, actin is expected to be a new target of antitumor drug. However the study on the actin-interactive agents is less-advanced to develop actin-targeting antitumor drugs.

Many actin-targeting agents have been reported (Figure 1-9). Phalloidin[25] and jasplakinolide[26] enhance to polymerize actin, while latrunculin A (LatA)[27], bistramide A[28], and pectenotoxin A[29] inhibit the polymerization of actin. Many macrolides also depolymerize F-actin, which involve kabiramides,[30] micarolide B (MyB),[31] reigispongeolide A,[32] and iejimalide A.[33] All of these macrolides have similar side chain structure to ApA in contrast with diversity of macrolactone moiety. Thus it is inferred that the side chain structure is important for actin-binding ability. Actually X-ray crystal structures of kabiramide C-actin complex and reigiapongeolide A-actin complex were reported,[34] which showed that their side-chain moieties insert into the cleft between subdomains (SD) 1 and 3 of actin. It is suggested that ApA also interacts with actin by using its side chain moiety.

13
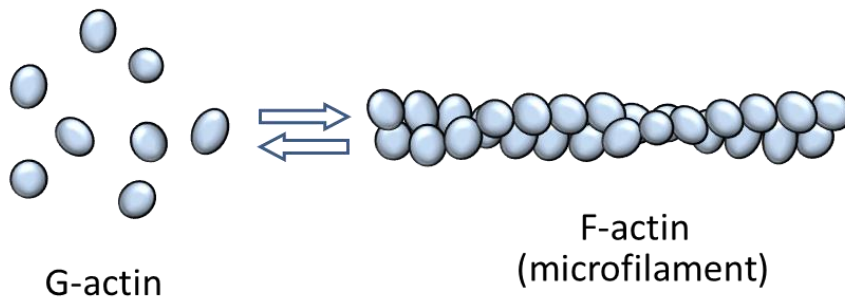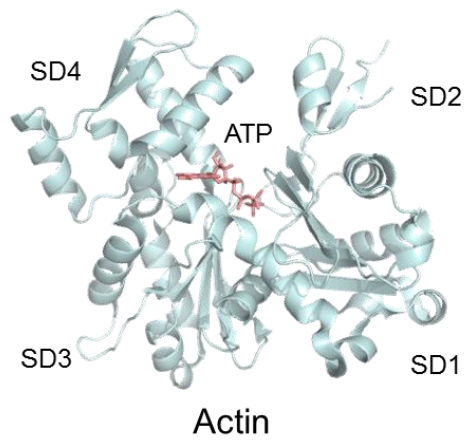
Figure 1-8. Actin exists in equilibrium between G-actin and F-actin in cells.
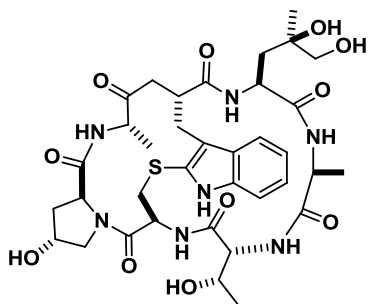
Phalloidin
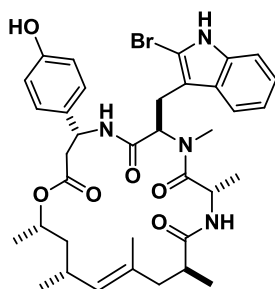
Jasplakinolide
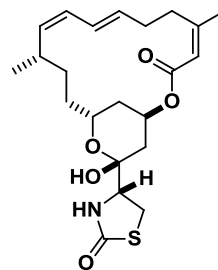
Latrunculin A
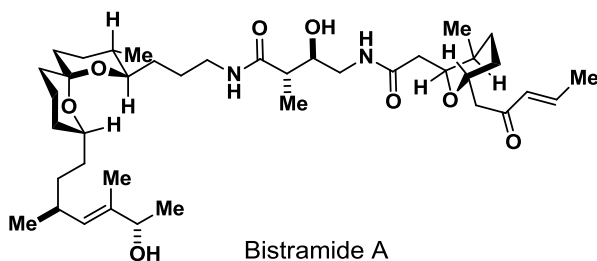
Bistramide A
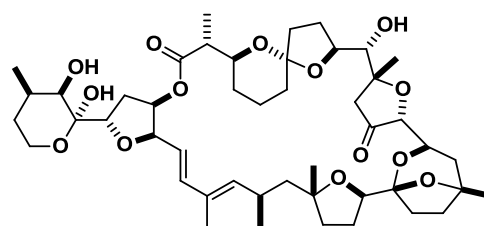
Pectenotoxin-2
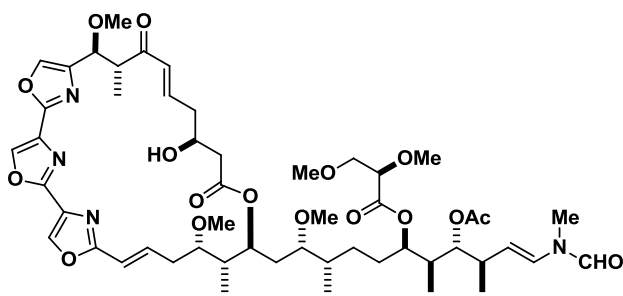
Mycarolide B
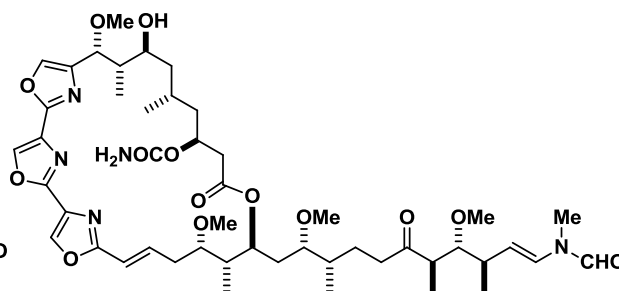
Kabiramide A
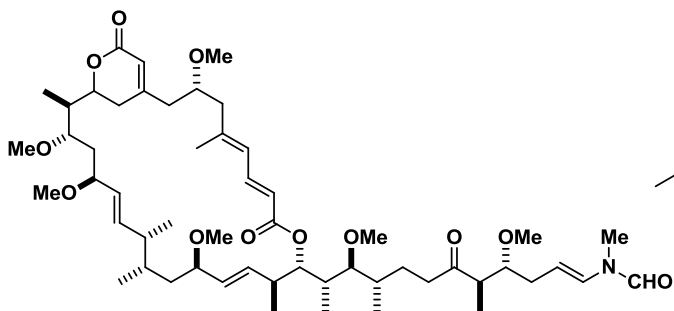
Reidispongiolide A
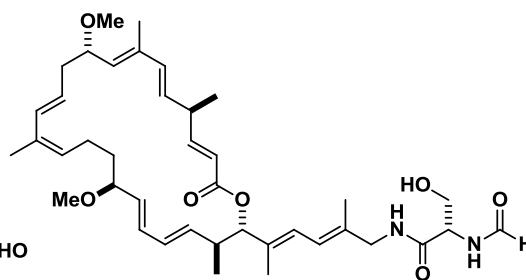
Iejimalide A

Figure 1-9. Actin-targeting agents.

1.4.3. Structure-activity relationships of ApA

Total synthesis of ApA has been accomplished in 1996, and structure-activity relationships (SAR) study of ApA have been performed. For example, ApA side chain analogue **3** exhibited one-tenth of actin-depolymerization activity of ApA, while the macrolactone analogue **4** showed no activity (Table 1-3). It was suggested that side chain moiety of ApA has a key role of actin-depolymerizing activity. In addition, fluorescent photoaffinity probe **5** possessing the side chain moiety of ApA as ligand was synthesized (Figure 1-10), and found to photolabeled actin.[35] Photolabeling of actin with probe **5** was inhibited by competition of ApA or MyB. On the other hand, LatA, that bind to actin at the ATP binding site between SD 2 and 4, was not able to inhibit the labeling of actin. These results indicated that ApA directly bind to actin not at LatA binding site but at MyB binding site.

The side chain analogue **3** did not exhibit cytotoxicity, which suggested that there was poor correlation between potent cytotoxicity and actin-depolymerizing activity of ApA. Structures and bioactivities of ApA and seven minor congeners of ApA were shown in Table 1-3. Cytotoxicity of the congeners which have serine ester moiety at C7 (aplyronines D, E, F and G) are comparable to or better than ApA. In contrast, congeners which have serine ester moiety at C9 (aplyronine B and H) exhibit one-tenth cytotoxicity of ApA. Furthermore, cytotoxicity of aplyronine C (**2**), which has no serine ester moiety, decline to one-thousandth. These results suggested that serine ester moiety of ApA play a key role for its potent cytotoxicity. On the other hand, aplyronines A-C exhibit comparable actin-depolymerizing activity. Therefore serine ester moiety does not affect the actin-depolymerizing activity. Further SAR study revealed that not only trimethylserine ester moiety but also conjugated double bond and two hydroxyl group are also important for cytotoxicity and have little effect for actin-depolymerizing activity. However, macrolactone analogue **4**, which has these moieties that are important for cytotoxicity, exhibits neither cytotoxicity nor actin-depolymerizing activity. Thus the actin-binding activity is also a necessarily condition for the potent cytotoxicity of ApA but is not a sufficient condition.

In 2006, Hirata and co-workers reported the X-ray crystal structure of actin-ApA complex (Figure 1-11).[36] The X-ray analysis revealed that ApA interacts with the hydrophobic cleft between SD 1 and 3 of actin by using its side chain. On the other hand, trimethylserine ester of ApA protrudes from actin surface and does not affect interaction with actin. From these findings, it is probable that ApA binds to other biomolecules and the trimethylserine ester moiety play an important role in binding to these biomolecules. Therefore, the author aimed to clarify the mode of action of ApA through the identification of the other biomolecules that bind to ApA.

Table 1-3. Structures and biological activities of aplyronines and its derivatives
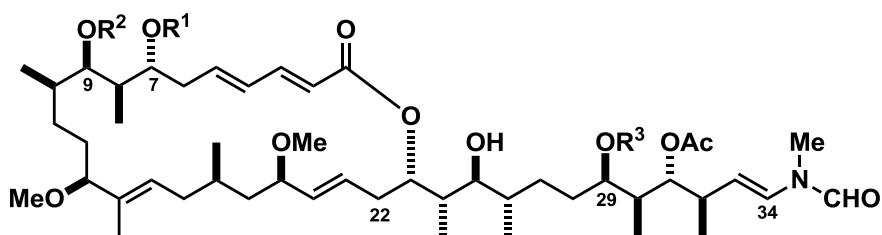
Compounds	R^1	R^2	R^3	Cytotoxicity[a] IC_{50} (ng/mL)	Actin-depolymerizing activity[b] EC_{50} (µM)
aplyronine A (**1**)	TMSer	H	DMAla	0.48	31
aplyronine B	H	TMSer	DMAla	3.11	33
aplyronine C (**2**)	H	H	DMAla	21.2	32
aplyronine D	TMSer	H	DMGly	0.075	— [c]
aplyronine E	= 22-methylaplyronine A			0.201	— [c]
aplyronine F	TMSer	H	MMAla	0.201	— [c]
aplyronine G	DMSer	H	DMAla	0.127	— [c]
aplyronine H	H	DMSer	DMAla	10.4	— [c]
analogue **3**				inactive	330
analogue **4**				> 1000	inactive

[a] against HeLa S3 cells. [b] EC_{50} is the concentrations required to depolymerize F-actin (40 µM) to 50% of its control amplitude. [c] not determined. TMSer = *N,N,O*-trymethylserine, DMSer = *N,O*-dimethylserine, DMAla = *N,N*-dimethylalanine, DMGly = *N,N*-dimethylglycine, MMAla = *N*-monomethylalanine.
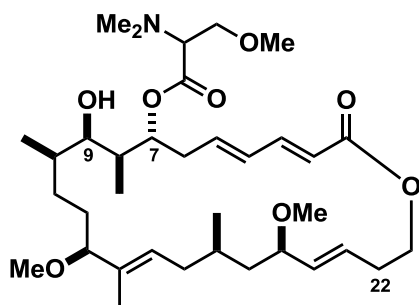
ApA macrolactone analogue **4**

ApA side chain analogue **3**

18
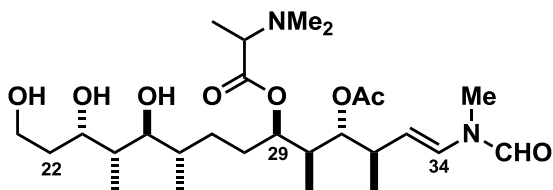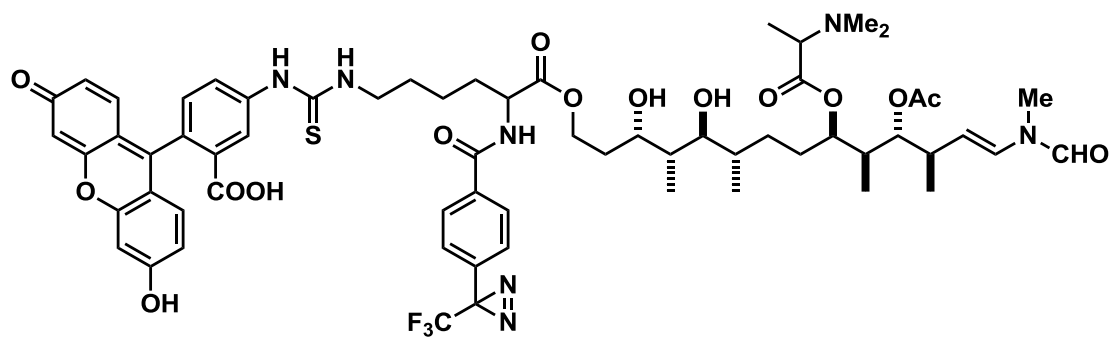
Figure 1-10. Fluorescent photoaffinity probe **5** with ApA side chain.
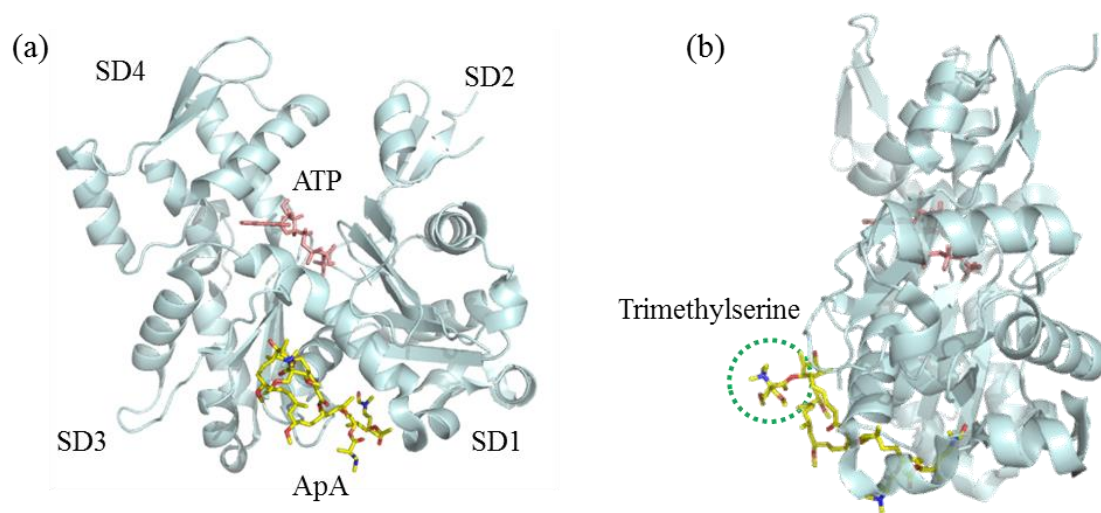
Figure 1-11. (a) Structure of the actin-ApA complex; (b) the same complex rotated by 90°.

References

1. American Cancer Society. *Global Cancer Facts & Figures 2nd Edition.* Atlanta: American Cancer Society; 2011.

2. Ministry of health, Labour and welfare, Labour and welfare statistical database (in Japanese).

3. Newman, D. J.; Cragg, G. M. *J. Nat. Prod.* **2012**, *75*, 311–335.

4. Pettit, G. R.; Herald, C. L.; Doubek, D. L.; Herald, D. L.; Arnold, E.; Clardy, J. *J. Am. Chem. Soc.* **1982**, *104,* 6846−6848.

5. Roffey, J.; Rosse, C.; Linch, M.Hibbert, A.; McDonald, N. Q.; Parker, P. *J. Curr. Opin. Cell Biol.* **2009**, *21*, 268–279.

6. Fattorusso, E.; Minale, L.; Sodano, G. *J. Chem. Soc., Perkin Trans. 1* **1972**, 16–18.

7. Rodríguez-Nieto, S.; Gonzalez-Iriarte, M.; Carmona, R.; Muñoz-Chápuli, R.; Medina, M. A.; Quesada, A. R. *FASEB J.* **2002**, *16*, 261–263.

8. (a) Rinehart, K. L.; Holt, T. G.; Fregeau, N. L.; Keifer, P. A.; Wilson, G. R.; Perun, T. J.; Sakai, R.; Thompson, A. G.; Stroh, J. G.; Shield, L. S.; Seigler, D. S. *J. Nat. Prod.* **1990**, *53*, 771-792. (b) Rinehart, K. L.; Holt, T. G.; Fregeau, N. L.; Stroh, J. G.; Keifer, P. A.; Sun, F; Li, L. H.; Martin, D. G. *J. Org. Chem.* **1990**, *55*, 4512–4515.

9. (a) Kingston, D. G. I. *J. Nat. Prod.* **2009**, *72*, 507–515. (b) Dumontet, C.; Jordan, M. A. *Nat. Rev. Drug Discov.* **2010**, *9*, 790–803.

10. Wani, M. C.; Taylor, H. L.; Wall, M. E.; Coggon, P.; McPhail, A. T. *J. Am. Chem. Soc.* **1971**, *93*, 2325–2327.

11. Noble, R. L.; Beer, C. T.; Cutts, J. H. *Ann. N.Y. Acad. Sci.* **1958**, *76*, 882–894.

12. Guenard, D.; Gueritte-Voegelein, F.; Potier, P. *Acc. Chem. Res.* **1993**, *26*, 160–167.

13. Hofle, G.; Reichenbach, H. In *Anticancer Agents from Natural Products*; Cragg, G. M., Kingston, D. G. I., Newman, D. J., Eds.; CRC Press: Boca Raton, FL, 2005; pp. 413 - 450.

14. Gunasekera, S. P.; Gunasekera, M.; Longley, R. E. *J. Org. Chem.* **1990**, *55*, 4912–4915.

15. Svoboda, G. H.; Johnson, I. S.; Gorman, M.; Neuss, N. *J. Pharm. Sci.* **1962**, *51*, 707–720.

16. Hirata, Y.; Uemura, D. *Pure Appl. Chem.* **1986**, *58*, 701–710.

17. Bai, R.; Pettit, G. R.; Hamel, E. *Biochem. Pharmacol.* **1990**, *39*, 1941–1949.

18. Mooberry, S. L.; Tien, G.; Hernandez, A. H.; Plubrukarn, A.; Davidson, B. S. *Cancer Res.* **1999**, *59*, 653–660.

19. West, L. M.; Northcote, P. T.; Battershill, C. N. *J. Org. Chem.* **2000**, *65*, 445–449.

20. Towle, M. J., Salvato, K. A., Budrow, J., Wels, B. F., Kuznetsov, G., Aalfs, K. K., Welsh, S., Zheng, W., Seletsky, B. M., Palme, M. H., Habgood, G. J., Singer, L. A., Dipietro, L. V., Wang, Y., Chen, J. J., Quincy, D. A., Davis, A., Yoshimatsu, K., Kishi, Y., Yu, M. J., Littlefield, B. A. *Cancer Res.* **2001**, *61*, 1013−1021.

21. Schenone, M.; Dancik, V.; Wagner, B. K.; Clemons, P. A. *Nat. Chem. Biol.* **2013**, *9*, 232–240.

22. (a) Yamada, K.; Ojika, M.; Ishigaki, T.; Yoshida, Y.; Ekimoto, H.; Arakawa, M. *J. Am. Chem. Soc.* **1993**,

115, 11020–11021. (b) Ojika, M.; Kigoshi, H.; Ishigaki, T.; Yamada, K. *Tetrahedron Lett.* **1993**, *34,* 8501–8504. (c) Ojika, M.; Kigoshi, H.; Ishigaki, T.; Nishiwaki, M.; Tsukada, I.; Mizuta, K.; Yamada, K. *ibid.* **1993**, *34,* 8505–8508. (d) Ojika, M.; Kigoshi, H.; Ishigaki, T.; Nishiwaki, M.; Tsukada, I.; Tsuboshi, T.; Ogawa, T.; Yamada, K. *J. Am. Chem. Soc.* **1994**, *116,* 7441–7442. (e) Ojika, M.; Kigoshi, H.; Yoshida, Y.: Ishigaki, T.; Nishiwaki, M.; Tsukada, I.; Arakawa, M.; Ekimoto, H.; Yamada, K.. *Tetrahedron* **2007**, *63,* 3138–3167. (f) Yamada, K.; Ojika, M.; Kigoshi, H.; Suenaga, K. *Nat. Prod. Rep.* **2009**, *26,* 27–43.

23. Suenaga, K.; Kigoshi, H. *J. Synth. Org. Chem. Jpn.* **2006**, *64,* 1273−1281.

24. Saito, S.; Watabe, S.; Ozaki, H.; Kigoshi, H.; Yamada, K.; Fusetani, N.; Karaki, H. *J. Biochem.* (Tokyo) **1996**, *120,* 552−555.

25. Wieland, T.; Faulstich, H. *CRC Crit. Rev. Biochem.* **1978**, *5,* 185−260.

26. Bubb, M. R.; Senderowicz, A. M. J.; Sausville, E. A.; Duncan, K. L. K.; Korn, E. D. *J. Biol. Chem.* **1994**, *269,* 14869−14871.

27. Kashman, Y.; Groweiss, A.; Shmueli, U. *Tetrahedron Lett.* **1980**, *21,* 3629–3632.

28. Gouiffe`s, D.; Moreau, S.; Helbecque, N.; Bernier, J. L.; Henichart, J. P.; Barbin, Y.; Laurent, D.; Verbist, J. F. *Tetrahedron* **1988**, *44,* 451–459.

29. Yasumoto, T.; Murate, M.; Oshima, Y.; Sano, M.; Matsumoto, G. K.; Clardy, J. *Tetrahedron* **1985**, *41,* 1019–1025

30. Matsunaga, S.; Fusetani, N.; Hashimoto, K. *J. Am. Chem. Soc.* **1986**, *108,* 847-849.

31. Fusetani, N.; Yasumuro, K.; Matsunaga, S.; Hashimoto, K. *Tetrahedron Lett.* **1989**, *30,* 2809-2812.

32. Carbonelli, S.; Zampella, A.; Randazzo, A.; Debitus, C.; Gomez-Paloma, L. *Tetrahedron* **1999**, *55,* 14665–14674.

33. Kobayashi, J.; Cheng, J.; Ohta, T.; Nakamura, H.; Nozoe, S.; Hirata, Y.; Ohizumi, Y.; Sasaki, T. *J. Org. Chem.* **1988**, *53,* 6147–6150.

34. (a) Klenchin, V. A., Allingham, J. S., King, R., Tanaka, J., Marriott, G. and Rayment, I. *Nat. Struct. Biol.* **2003**, *10,* 1058–1063. (b) Allingham, J. S., Zampella, A., D'Auria, M. V. and Rayment, I. *Proc. Natl. Acad. Sci. USA* **2005**, *102,* 14527–14532.

35. Kuroda, T.; Suenaga, K.; Sakakura, A.; Handa, T.; Okamoto, K.; Kigoshi, H. *Bioconjugate Chem.* **2006**, *17,* 524−529.

36. Hirata, K.; Muraoka, S.; Suenaga, K.; Kuroda, K.; Kato, K.; Tanaka, H.; Yamamoto, M.; Takata, M.; Yamada, K.; Kigoshi, H. *J. Mol. Biol.* **2006**, *356,* 945−954.

Chapter 2.

Identification of the New Target Proteins of Aplyronine A

Abstract

To identify the target proteins of an antitumor macrolide aplyronine A, biotin probes of aplyronines were synthesized. By using biotin probes of aplyronines A and C, Arp2 and 3 (actin-related proteins) were purified from cell lysate along with actin. However aplyronine photoaffinity probes were found not to covalently bind to Arp2 or Arp3. Thus, actin-related proteins might indirectly bind to ApA as the ternary adducts of the actin/ApA complex or through the oligomeric actin. Through in situ photolabeling experiments with photoaffinity probes of ApA, tubulin as well as actin were specifically labeled. Since ApA competitively inhibited the labeling of tubulin by photoaffinity probes, tubulin might be the new target protein of ApA.

2.1. Introduction

Aplyronine A (ApA) is a marine natural product that shows potent antitumor activity.[1] However the molecular targets and mechanisms of action of ApA have remained unclear. The author has attempted the identification of new target proteins of ApA by chemical probe approach. Identification of target biomolecules by using chemical probes requires three steps: synthesis of chemical probes, purification of binding proteins, and identification of purified proteins.

Syntheses of chemical probes which maintain the activities of original natural products are important. However, there is no general answer to design chemical probes due to the diversity of structure and property of natural products. Thus we have to consider the best way for each original compound. In general, to develop active chemical probes, structure-activity relationships (SAR) studies are important. Also we need to verify the bioactivities of synthetic derivatives.

With the desired chemical probes in hand, we can attempt the purification of binding biomolecules with chemical probes. Purification of target proteins also involved several optimizations, such as preparation and labeling conditions of proteins. After target biomolecules are purified, we should confirm the specificity of interaction of biomolecules with the ligands. Generally, competitive experiments using excess ligands and the control experiments with negative probe are useful to confirm the specificity of binding property of the probes.

If we successfully purify target proteins, next we attempt the identification of these proteins. Protein identification can be performed by using mass spectrometry analysis, such as peptide mass fingerprinting (PMF) analysis[1] and de novo sequence analysis. For identification of proteins by PMF analysis, observed mass values of digested peptide are compared with the theoretical mass data from worldwide database.

In this chapter, the various biotin-conjugated aplyronine derivatives are synthesized and used for the purification and identification of new target proteins of aplyronine A.

2.2. Synthesis of the biotin derivatives of ApA

2.2.1. Design of ApA-biocytin and ApA-bio

The design of a chemical probe is important to identify the target proteins of ApA. Previous SAR studies of ApA revealed that both side-chain moiety and macrolactone moiety of ApA are important, and it is proposed that ApA interacts with two or more target proteins. Therefore it is difficult to expect which substituent group can be modified without significant loss of activity. Although the total synthesis of ApA was already accomplished, it is still difficult to synthesize various ApA derivatives by the synthesis. Therefore the author considered that chemical probes would be derivatized from natural ApA.

It has been suggested that the *N*-methyl enamide moiety, which is common to various actin-depolymerizing macrolides, is important for their cytotoxicities.[2] On the other hand, in 1998, Watabe and co-workers reported the derivative of kabiramide D (KaD), an actin-depolymerizing macrolide that possesses a similar side-chain structure to ApA (Figure 2-1).[3] The derivative of KaD was synthesized by acidic hydrolysis of the *N*-methyl enamide moiety, which is a common structure to ApA, followed by reductive amination with biocytin. Although the cytotoxicity and actin-depolymerizing activity of the biocytinylated KaD were not reported, they reported that it maintained the actin-binding activity.

Because there is a space inside the 1,3-cleft of the actin molecule (Figure 2-2), the author anticipated that ApA could be modified at C34 without a significant loss of activity by elongating a tethered biotin moiety with hydrophilic groups. Therefore ApA-biocytin probe (ApA-biocytin, **6**) and ApA-PEG linked biotin probe (ApA-bio, **7**) were designed (Figure 2-3).
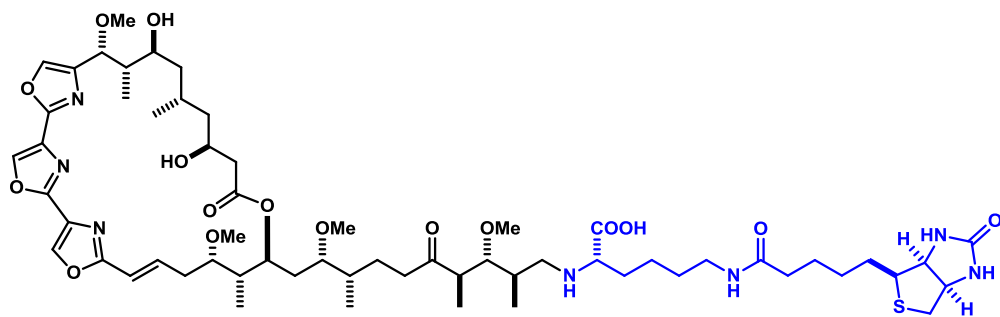
Figure 2-1. Biocytinylated kabiramide D.
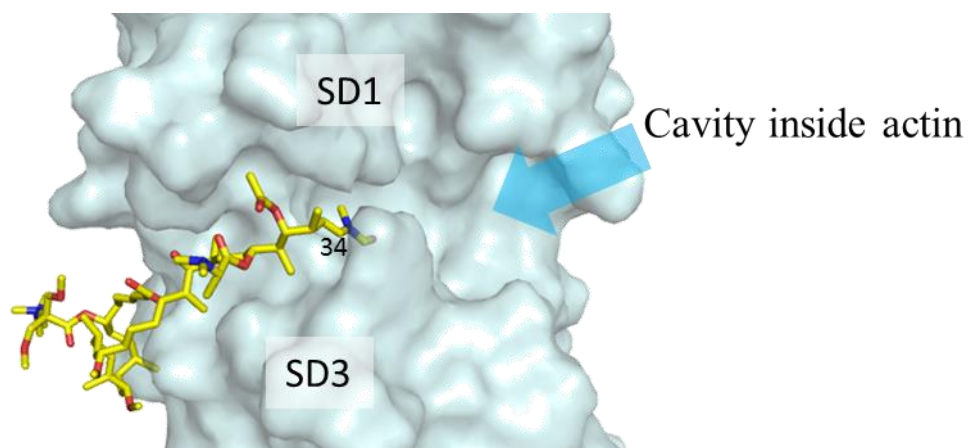
Figure 2-2. Binding mode of ApA to actin (PDB code:1WUA).
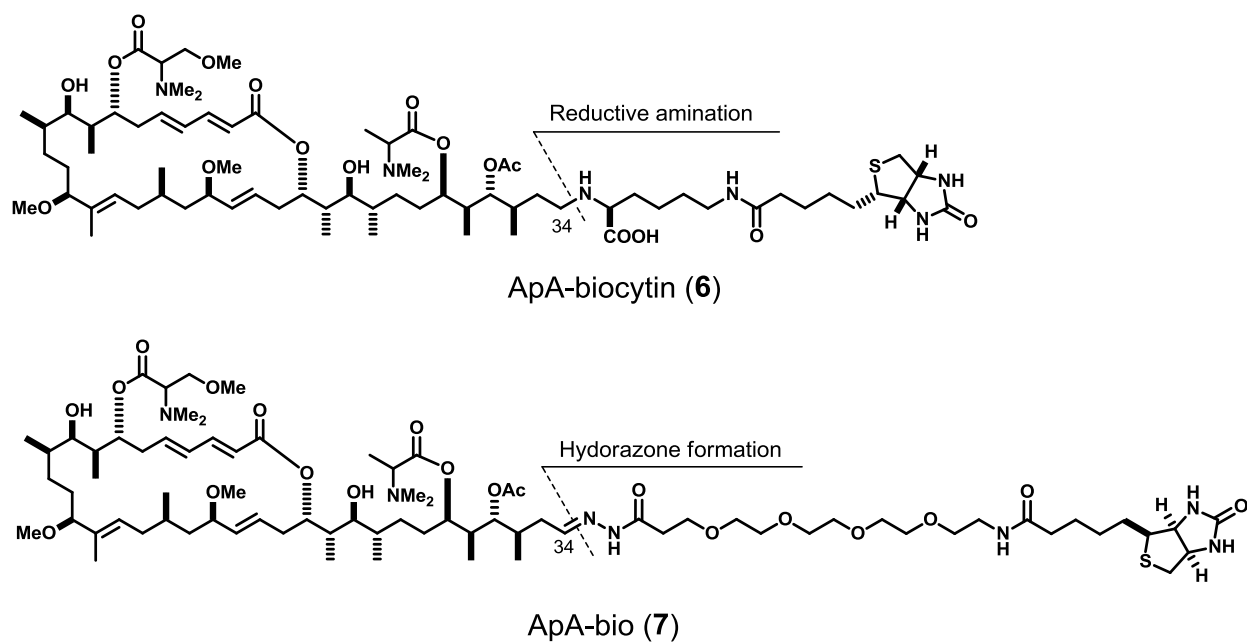
Figure 2-3. Structures of ApA biotin probes.

2.2.2. Synthesis of ApA-biocytin and ApA-bio*   *These experiments were performed by co-workers.

ApA-biocytin and ApA-bio were synthesized from ApA (Scheme 2-1). Acidic hydrolysis of **1** afforded the C34 aldehyde **8**.[5] Reductive amination of **8** with biocytin (**9**) gave ApA-biocytin (**6**) (24%). The coupling reaction of **8** with EZ-Link biotin-PEG$_4$-hydrazide gave ApA-bio (**7**) (38%). For comparison, model biotin probe (model-bio, **10**) was also prepared from the 3-phenylpropionaldehyde.
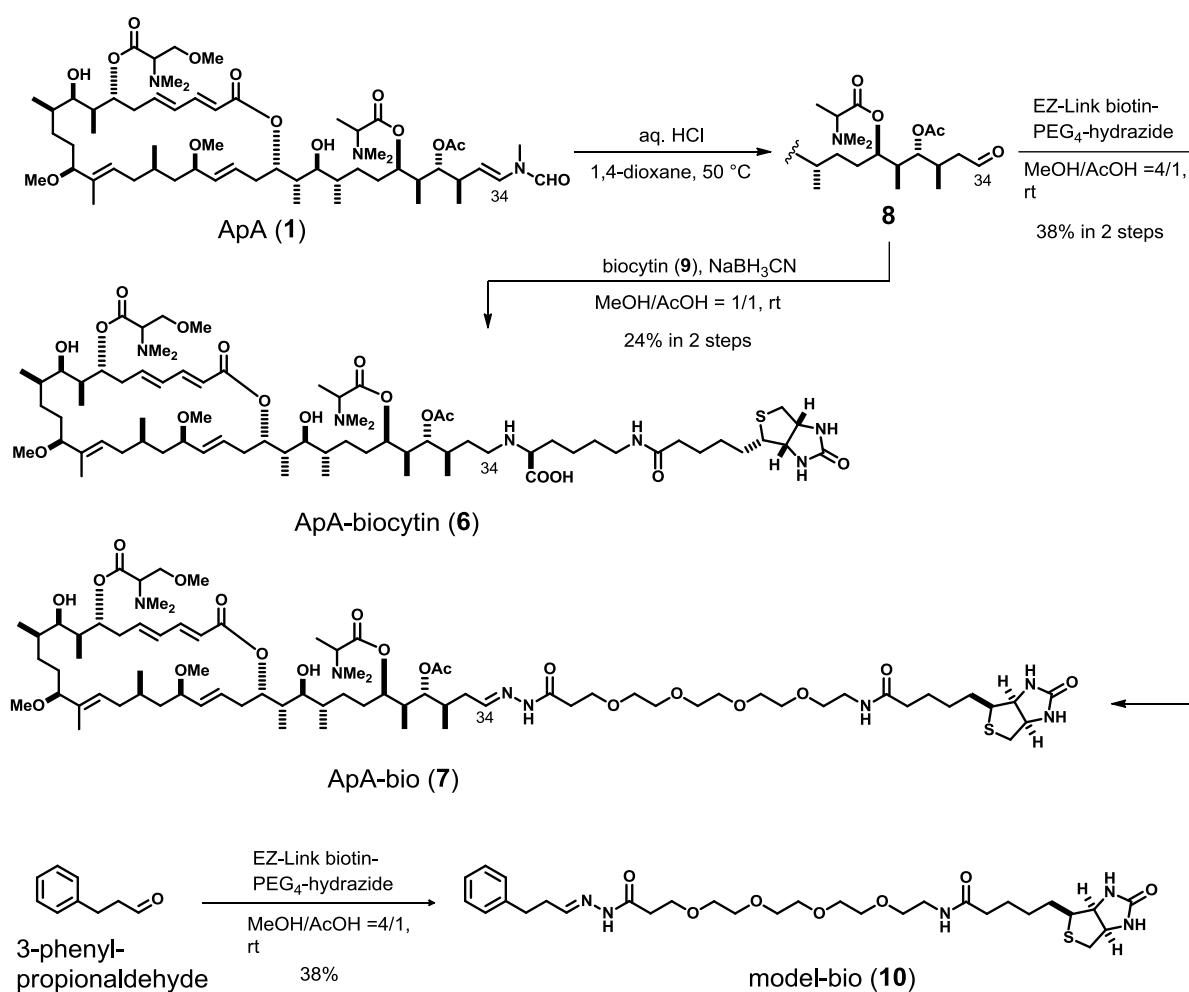
Scheme 2-1. Synthesis of ApA biotin probes.

2.2.3. Biological activity of ApA-biotin derivatives

The cytotoxicities and in vitro actin-depolymerizing activities of ApA analogues and model compounds were compared to those of ApA (Table 2-1). ApA-biocytin (**6**) was found to be 1500 times less cytotoxic than ApA (IC_{50} 15000 pM), whereas ApA-bio (**7**) was only approximately 10 times less active than ApA (IC_{50} 96 pM). ApA-biocytin (**6**) bears a carboxyl group, which may influence its ability to permeate into living cells or give it lower affinity for target molecules, thus causing a decrease in cytotoxicity. Meanwhile, ApA-biocytin (**6**) and ApA-bio (**7**) showed potent actin-depolymerizing properties, which were comparable to those of natural ApA. In contrast, both biocytin (**9**) and model-bio (**10**) which lack the whole parts of ApA, did not exhibit both cytotoxicity and actin-depolymerizing activity.

Table 2-1. Biological activities of biotinylated ApA derivatives.

Compound	Cytotoxicity against HeLa S3 cells IC_{50} (nM)	Actin-depolymerizing activity[a] EC_{50} (μM)
ApA (**1**)	0.010	1.6
ApA-biocytin (**6**)	15	2.1
ApA-bio (**7**)	0.096	1.8
biocytin (**9**)	>10,000	>100
model-bio (**10**)	>10,000	>100

[a] Activity was monitored by measuring the fluorescence intencity of pyrenyl actin. Values indicate the concentrations required to depolymerize F-actin (3 μM) to 50% of its control amplitude.

2.2.4. Labeling experiments with Actin

The biotinylated ApA derivatives were then examined to determine their specificities for binding to actin. When the binding proteins were competitively eluted by an excess ApA, only the actin that were attached to ApA-biocytin (**6**) or ApA-bio (**7**) were eluted (Figure 2-4a). In contrast, actin was eluted in all lanes by boiling the resins in SDS buffer (Figure 2-4b). Thus, considerable amounts of actin were nonspecifically absorbed to the hydrophobic agarose resin because of the presence of the lipophilic parts of the actin molecule (i.e., the SD 1,3-cleft). Despite this behaviour, resin-bound ApA-biocytin (**6**) and ApA-bio (**7**) were found to exhibit high affinity for actin and to have the same binding properties as ApA.
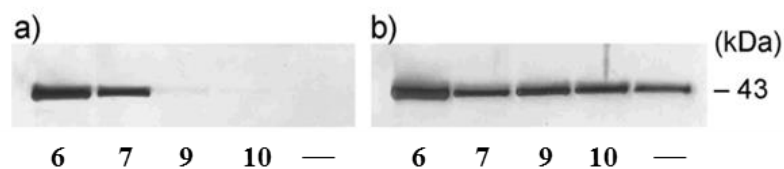
Figure 2-4. Interaction of biotinylated ApA derivatives with actin. Actin in G-buffer was treated with **6**, **7**, **9**, **10** or DMSO that were preloaded on NeutrAvidin agarose. Binding actin was eluted a) by treatment with 5 μM ApA or b) by boiling in SDS buffer, and detected with silver stain.

2.2.5. Design of Aplyronine photoaffinity biotin probes

Since ApA-bio (**7**) maintained the activities of ApA, it was revealed that the *N*-methyl enamide moiety is a good substituent for elongating the linker to synthesize their chemical probes. Thus ApA photoaffinity biotin probe (ApA-PB, **11**) that possesses a diazirine group as a photoaffinity group, was designed based on the design of ApA-bio (**7**). Since ApA-PB (**11**) can bind covalently, a weak interaction between ApA and intracellular proteins can be detected and the binding mode of target proteins with ApA-PB (**11**) can be analyzed. Furthermore, ApC photoaffinity biotin probe (ApC-PB, **12**) that has ApC instead of ApA, was also designed as a negative control.
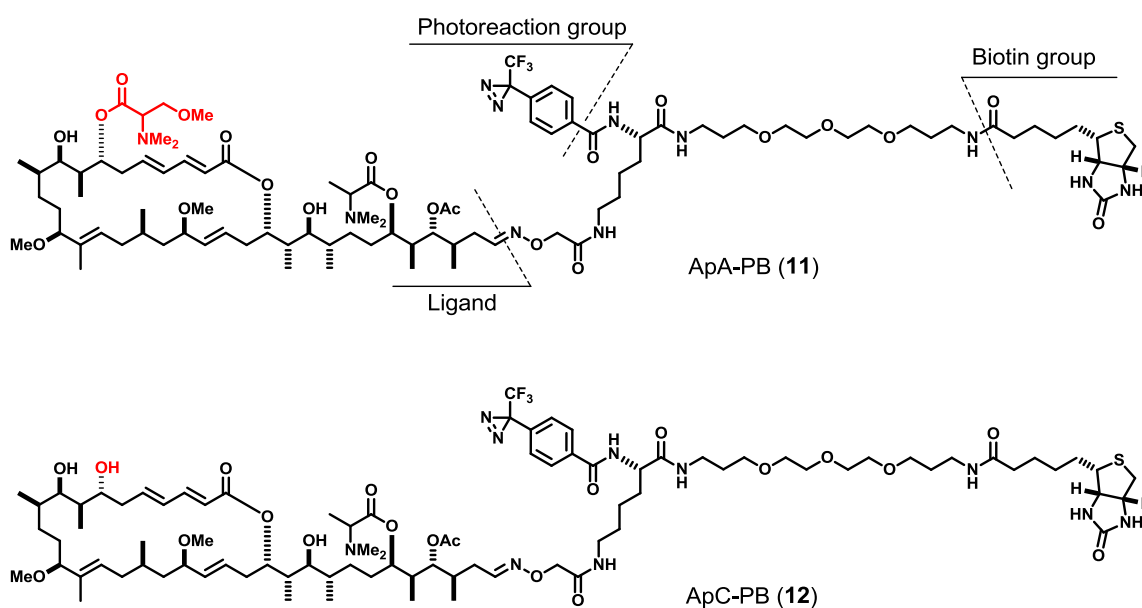
Figure 2-5. Structures of aplyronine photoaffinity biotin probes

30

2.2.6. Synthesis of alkoxyamine 19

Alkoxyamine **19** that has aryl diazirine moiety and biotin group was synthesized (Scheme 2-2). Condensation of bis[2-(3-aminopropoxy)ethyl]ether with (+)-biotin *N*-hydroxysuccinimidyl ester gave amine **13**[6] (67%). Condensation of carboxylic acid **14**[7] with amine **13** yielded amide **15** (74%). Deprotection of the Boc group of amide **15** followed by the coupling with succinyl ester **17**[8] in the presence of DIPEA gave the amide **18** (82%). Deprotection of the Phth group in **18** yielded alkoxyamine **19** (quant.).
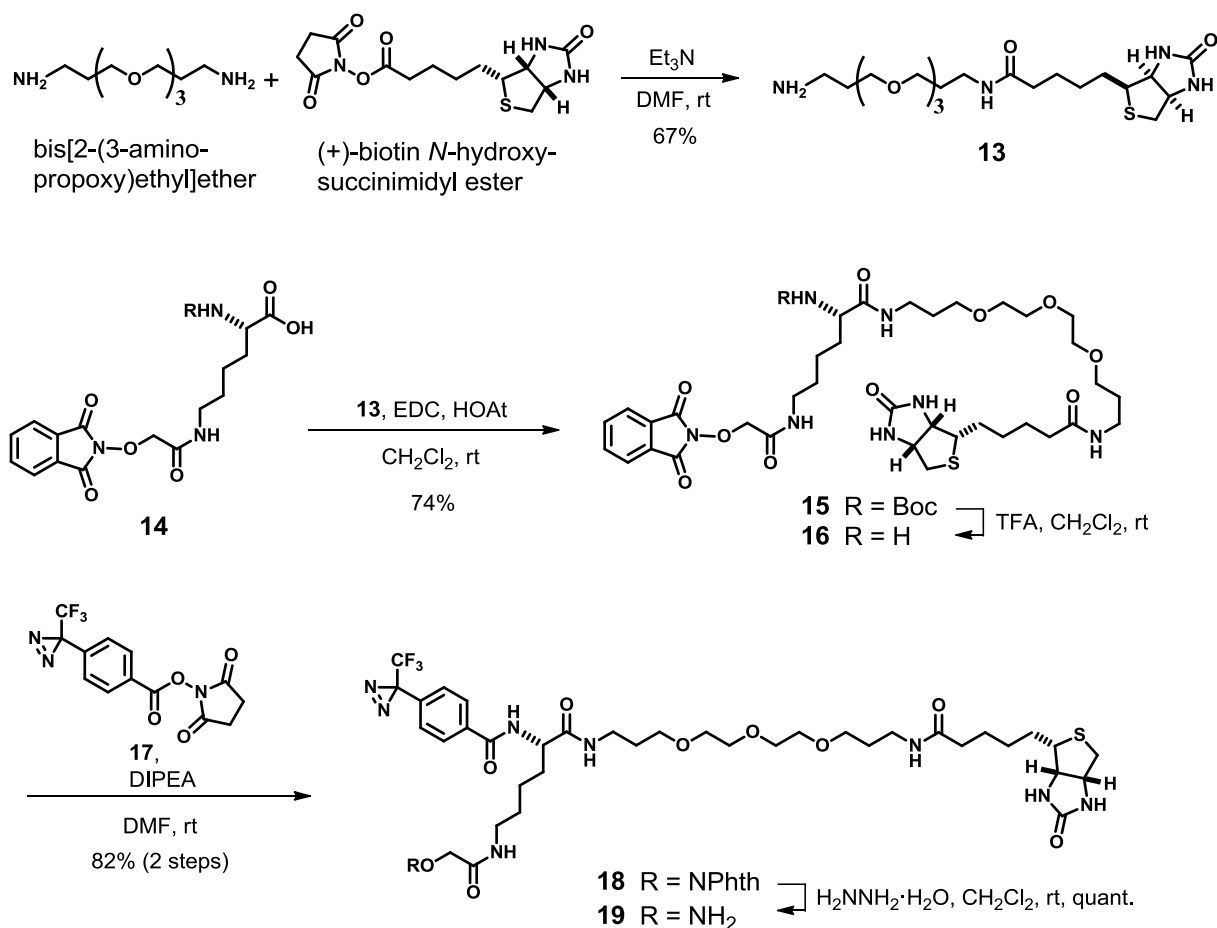
Scheme 2-2. Synthesis of alkoxyamine **19**

2.2.7. Synthesis of ApA-PB and ApC-PB*   * Synthesis of ApC-PB was performed by co-workers.

ApA-PB (**11**) and ApC-PB (**12**) were synthesized from ApA (Scheme 2-3). Acidic hydrolysis of ApA afforded the aldehyde **8**. The oximation reaction of **8** with alkoxyamine **19** gave ApA-PB (**11**) (71%). Due to the scarcity of ApC from natural sources (e.g., 3×10^{-7}% yield based on wet wt), ApC was prepared from the conversion of ApA. Methanolysis of ApA with 0.1% triethylamine preferentially cleaved the trimethylserine ester to give ApC in 41% yield (with 38% of recovered ApA). Subsequent acidic hydrolysis of ApC followed by condensation with alkoxyamine **19** gave ApC-PB (**12**) (41%).
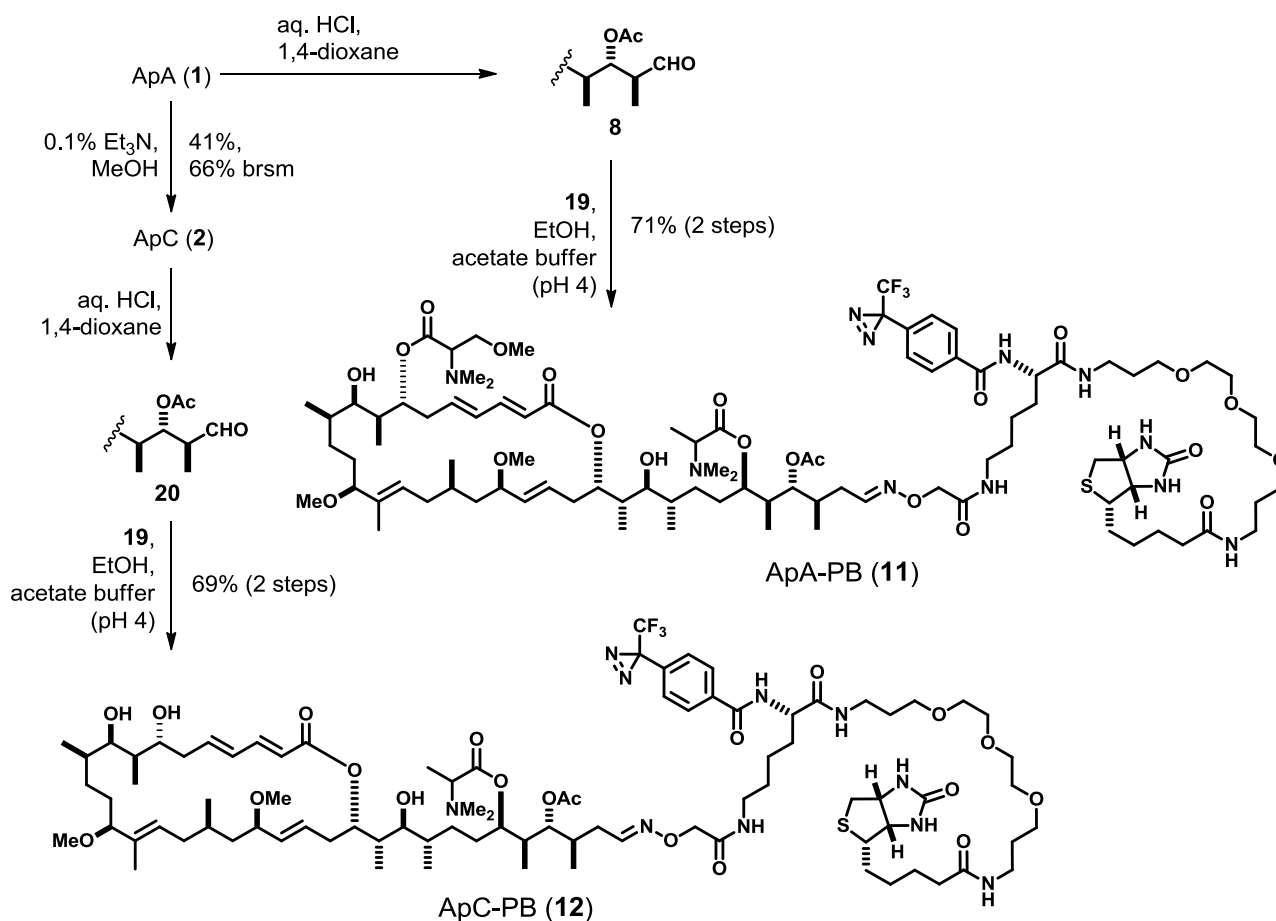
Scheme 2-3. Synthesis of ApA-PB (**11**) and ApC-PB (**12**)

2.2.8. Biological activity of Aplyronines photoaffinity biotin probes

Biological activities of aplyronine photoaffinity biotin probes were compared with those of natural compounds (Table 2-2). ApA-PB (**11**) showed potent cytotoxicity against HeLa S3 cells (IC$_{50}$ 1.2 nM), whereas the ApC-PB (**12**) was 260 times less cytotoxic than ApA-PB (IC$_{50}$ 310 nM).

Since the diazirine group is degraded by UV irradiation, we did not perform actin-depolymerizing assay, which needs UV irradiation. Instead, ApA-PB (**11**) was shown to potently inhibit F-actin sedimentation, which was confirmed by ultracentrifugation (Figure 2-6). F-actin was prepared by polymerization of G-actin (3 μM) in the presence of MgCl$_2$, followed by treatment with ApA or ApA-PB (**11**) (3 μM) to depolymerize the F-actin. After ultracentrifugation (150,000×g), the proteins contained in the supernatant (S) and the precipitate (P) were analyzed by SDS-PAGE analysis. Actin did not polymerize without the MgCl$_2$ and not precipitate by ultracentrifugation, thus protein bands were mostly detected in the S fraction (lane 1). When the MgCl$_2$ was added, actin was polymerized and precipitated by ultracentrifugation, thus protein bands were detected in the P fraction (lane 2). Treatment with ApA caused complete depolymerization of F-actin and the protein bands were detected in the S fraction (lane 3). Similarly, upon treatment with ApA-PB (**11**), the protein bands were also mostly observed in the S fraction (lane 4), which established that ApA-PB (**11**) had an actin-depolymerizing property while the activity was slightly weaker than ApA.

Table 2-2. Biological activities of aplyronine photoaffinty biotin derivatives.

Compounds	Cytotoxicity against HeLa S3 cells IC$_{50}$ (nM)	Actin-depolymerizing activity[a] EC$_{50}$ (μM)
ApA (**1**)	0.010	1.3
ApC (**2**)	17	1.4
ApA-PB (**11**)	1.2	— [b,c]
ApC-PB (**12**)	310	— [b]

[a] Values indicate the concentrations required to depolymerize F-actin (3 μM) to 50% of its control amplitude. [b] Not examined. [c] Confirmed by ultracentrifugation.
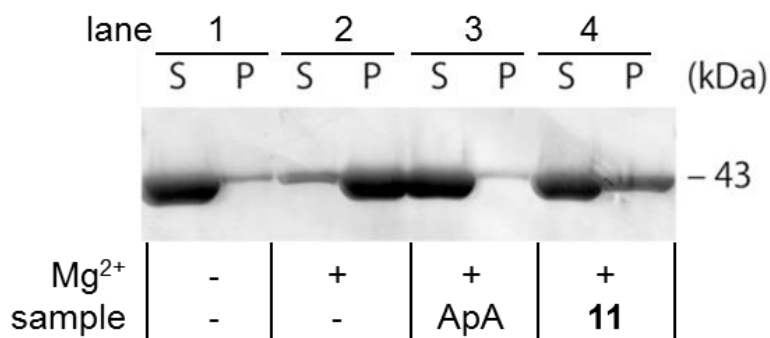
Figure 2-6. F-actin sedimentation assay. After F-actin was incubated with ApA or ApA-PB (**11**), the remaining F-actin was precipitated by ultracentrifugation. The proteins in the supernatant (S) and the precipitate (P) were detected by CBB stain.

2.3. Purification and identification of target proteins from cell lysate

2.3.1. Purification and identification of target proteins by ApA-bio

The pull-down assay with ApA-bio (**7**) in the whole cell lysate of HeLa S3 was conducted (Figure 2-7). To minimize interference with intrinsic biotin-binding molecules, NeutrAvidin agarose was pretreated with an excess amount of ApA-bio (**7**), on which the lysate of HeLa S3 cells was loaded. After incubation, the resin was washed with 0.1% Triton PBS. The binding proteins were eluted by boiling in SDS buffer or competition of ApA, and detected with silver stain (Figure 2-8).
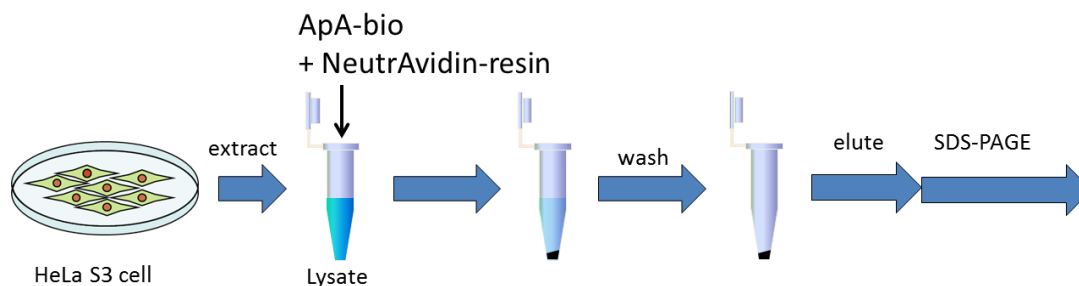
Figure 2-7. Outline of the pull-down assay.

When the binding proteins were eluted by boiling, four bands with molecular masses of 40, 43, 47 and 200 kDa were clearly detected along with several nonspecific bands (Figure 2-8, a). These four bands were identified as miyosin II heavy chain (200 kDa), actin related proteins 2 and 3 (Arp2 and 3, 40 and 47 kDa), and actin (43 kDa), respectively, through the PMF. To confirm the identification of PMF, immunoblotting analysis were carried out. Only in the presence of ApA-bio (**7**), myosin II, actin, Arp2 and Arp3 were detected with each moleculer masses of 200 kDa, 43 kDa, 40 kDa and 47 kDa (Figure 2-8, b–e), therefore the PMF analysis result was correct.

To confirm the specificity of interaction of these proteins with ApA-bio (**7**), same competitive experiments were carried out except the elution condition from the resin. When binding proteins were

competitively eluted by treatment of excess ApA (Figure 2-9), actin (43 kDa) were clearly detected. Arp2 (40 kDa) and Arp3 (47 kDa) were also slightly detected, but myosin II (200 kDa) was not detected. Thus, ApA-bio (**7**) may specifically interact with Arp2 and Arp3 as well as actin, but not with myosin II. Since myosin II is known to bind to F-actin, this protein may interact with the abundant actin that nonspecifically bound to the resin.

To further analyze the interaction between ApA-bio (**7**) and actin, biotinylated proteins were detected with a HRP conjugated streptavidin (Figure 2-10). Upon treatment with ApA-bio (**7**), a weak band corresponding to actin (43 kDa) was observed, along with nonspecific bands (120 and 74–72 kDa, biotin carboxylase). In the same experiments, compounds derived from ApA-bio (**7**), which did not bind to proteins, were detected in the region of the lowest molecular weight (< 10 kDa). Meanwhile, the amounts of bound actin that were eluted by boiling of resins were mostly the same as those by the ApA elution (Figures 2-8 and 2-9, lane 1). These results suggested that most actins bound to ApA-bio (**7**) were competitively eluted by ApA, and that binding property between ApA-bio (**7**) and actin was non covalent, such as hydrogen bond and van der Waals interaction.
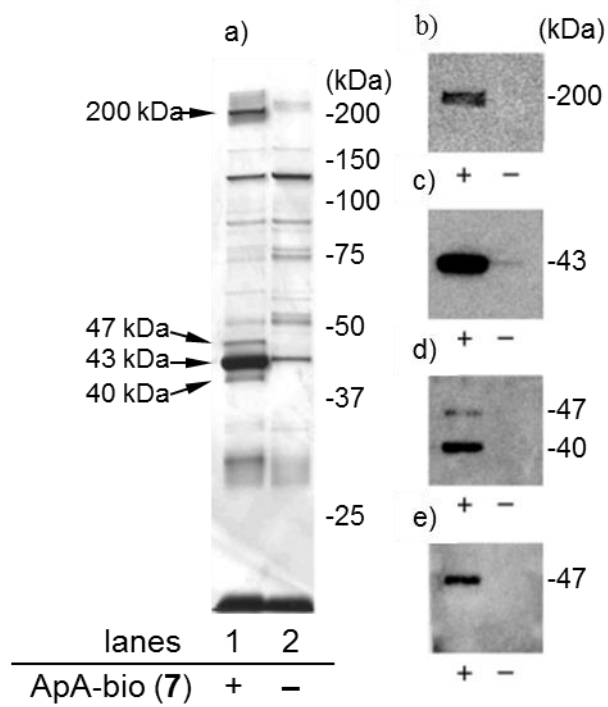
Figure 2-8. SDS-PAGE analysis of the proteins purified from HeLa S3 cell lysate by pull-down assay. Affinity-purified proteins were eluted from NeutrAvidine-resin by boiling and were detected a) with silver stain or by immunoblotting analysis using b) anti-myosin II, c) anti-actin, d) mixtures of anti-Arp2 and Arp3 or e) anti-Arp3, respectively.
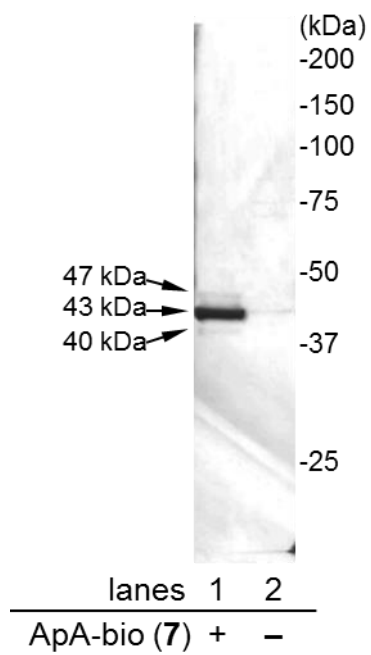
Figure 2-9. SDS-PAGE analysis of the proteins eluted by the competitive elution with ApA. Proteins were detected with silver stain.
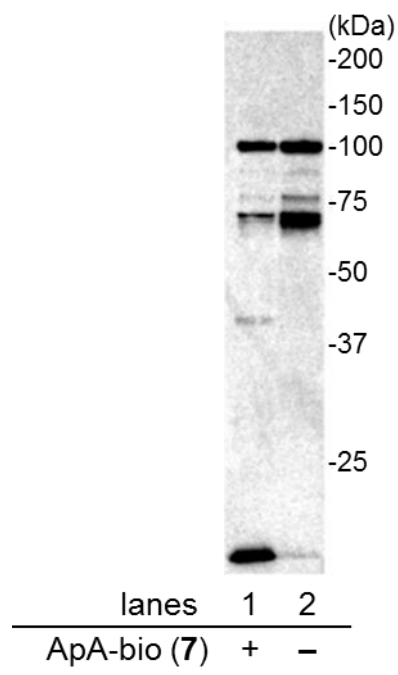
Figure 2-10. Detection of biotinylated proteins from HeLa S3 cell lysate. Proteins were purified by pull-down assay using ApA-bio (**7**), eluted by the boiling from NeutrAvidin-resin, and detected with HRP conjugate streptavidin.

2.3.2. Arp2/3

Arp2 and Arp3 are the key proteins of the Arp2/3 complex (Figure 2-11), which binds to the sides of an existing actin filament and initiates growth of a new actin filament to form branched-actin-filament networks.[9] The amino acid sequences and three-dimensional structures of Arp2 and Arp3 are highly similar (46% and 36% identity) to those of monomeric actin (Figure 2-12). The secondary structure around the ApA-binding sites of actin is closely similar to those of Arp2 and Arp3. Moreover, the remaining components of the Arp2/3 complex, Arp2/3 complex subunit 1-5 (ARPC1–5, 16–40 kDa), were not purified by the pull-down assay with ApA-bio (**7**) (see Figure 2-9). Thus, it was suggested that ApA may bind to Arp2 or Arp3 to give 1:1 complexes, as with the actin-ApA complex. Since it was difficult to further analyze the interaction of ApA with Arp2 and Arp3 by ApA-bio (**7**), their detail interactions were analyzed by using the photoaffinity probe of aplyronines as described in the next section.
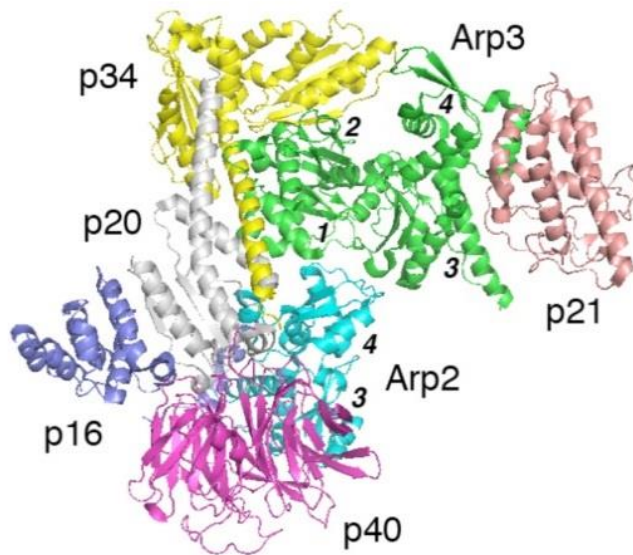
Figure 2-11. Structure of Arp2/3 complex (PDB code: 3DXM).

Actin-ApA complex (1WUA)   Arp3 (3DXM)
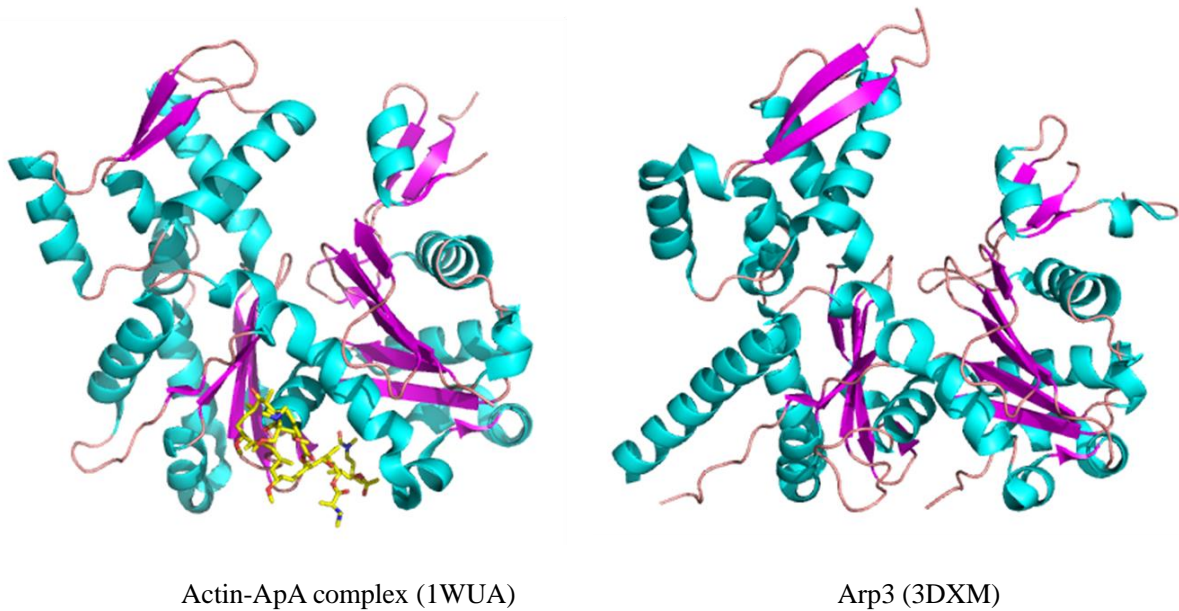
Figure 2-12. Comparison of the structures of actin and Arp3.

2.3.3. Photoaffinity labeling experiments in cell lysate with ApA-PB and ApC-PB.

The author investigated the target proteins of ApA in whole cell lysate through the reaction with photoaffinity probes followed by affinity purification (Figure 2-13). NeutrAvidin agarose was pretreated with an excess amount of ApA-PB (**11**) or ApC-PB (**12**), on which the lysate of HeLa S3 cells was loaded. After incubation for 2 h, photoreaction was carried out. The proteins were eluted by boiling in SDS buffer and detected with silver stain (Figure 2-14).
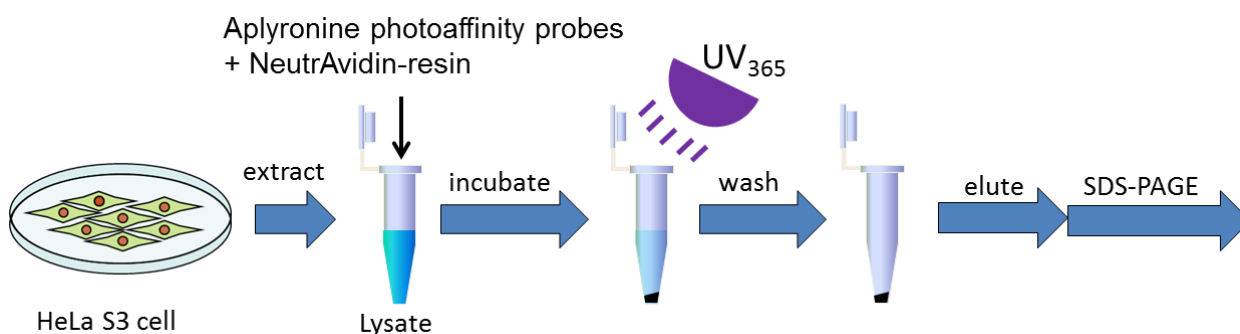
Figure 2-13. Outline of photoaffinity labeling experiments in this section.

Three strong bands corresponding to actin, Arp2, and Arp3 (43, 40, and 47 kDa, respectively) were detected with silver stain and were identified by immunoblotting analysis with anti-Arp2 and Arp3 (Figure 2-14, a and b, lane 1). Binding of these three proteins with ApA-PB (**11**) were competitively inhibited by excess ApA (lane 2). These results suggested that there are specific interactions between the ApA analogs and actin or actin-related proteins, rather than their simple absorptions on the agarose resin.

To confirm the properties of binding between ApA and its target proteins, photoreacted products were detected by HRP conjugate streptavidin. As expected, a strong band corresponding to actin was observed upon treatment with ApA-PB (**11**) (Figure 2-15, lane 1), and the band disappeared with the addition of excess ApA (lane 2). In contrast, neither Arp2 nor Arp3 was detected as a biotinylated protein. Thus, actin surely formed a covalent bond with ApA-PB, while actin-related proteins did not.

When the photolabeled products were competitively eluted with ApA, both Arp2 and Arp3 were liberated from the resin with a quantity of actin (Figure 2-16. lane 1), while the actin covalently bound to ApA

derivatives was eluted only after the boiling process (lane 1'). These results indicated that Arp2 and Arp3 might indirectly bind to ApA as the ternary adducts of the actin-ApA complex or through the oligomeric actin that interacts with ApA derivatives.

Furthermore, through affinity purification with ApC-PB (**12**), both Arp2 and Arp3 were obtained with actin from cell lysate, as with ApA-PB (**11**), in which only the actin was photolabeled (Figure 2-14–2-16, lane 3). ApC (**2**), which lacks the C7 trimethylserine ester moiety, exhibits 1000-fold less cytotoxicity, but as much actin-depolymerizing activity as ApA (**1**) as described chapter 1. Because the much less cytotoxic ApC-PB (**12**) bound to Arp2 and Arp3 in same extent as more highly cytotoxic ApA-PB (**11**), actin-related proteins were found not to be critical target proteins of ApA (**1**) for its potent antitumor activity.
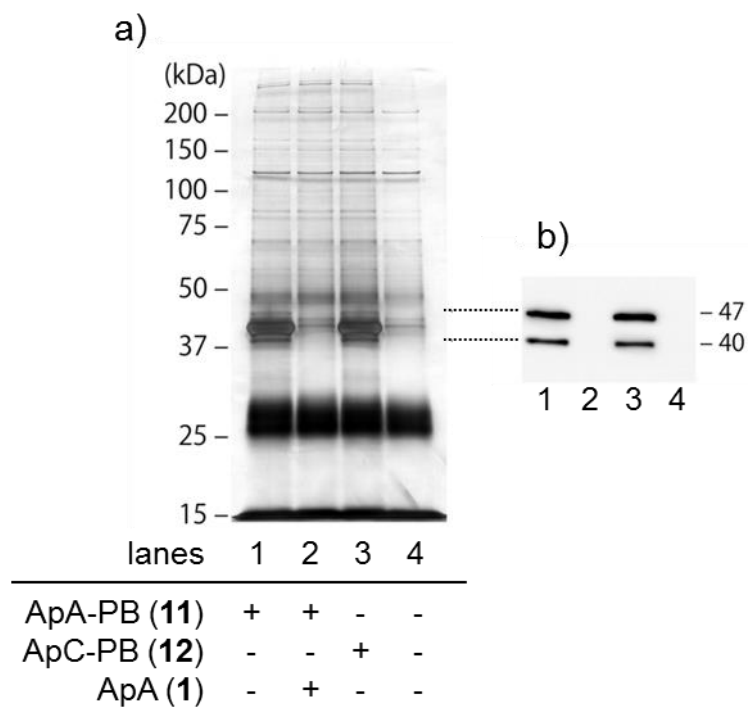
Figure 2-14. Pull-down assay using aplyronine photoaffinity probes. After photoreaction in cell lysate, labeled proteins were eluted from resin by boiling. The proteins were detected a) with silver stain, b) by immunoblotting analysis with anti-Arp2 and anti-Arp3.

lanes	1	2	3	4
ApA-PB (**11**)	+	+	-	-
ApC-PB (**12**)	-	-	+	-
ApA (**1**)	-	+	-	-

.
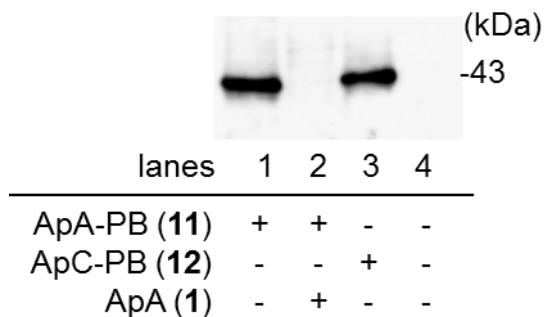
Figure 2-15. Detection of labeled proteins with aplyronine photoaffinity probes. Labeled proteins with ApA-PB (**11**) or ApC-PB (**12**) were detected by immunoblotting analysis with HRP conjugate streptavidin.

lanes	1	2	3	4	1'	2'	3'	4'
ApA-PB (**11**)	+	+	-	-	+	+	-	-
ApC-PB (**12**)	-	-	+	-	-	-	+	-
ApA (**1**)	-	+	-	-	-	+	-	-
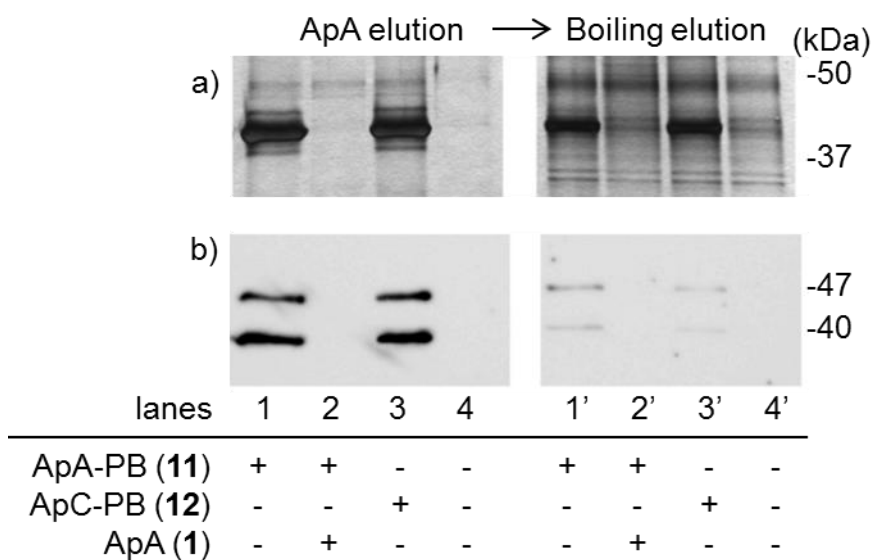
Figure 2-16. Stepwise elution. Binding proteins on the resin were eluted by treatment with ApA (10 μM, lanes 1–4) followed by boiling in SDS buffer (lanes 1'–4') and detected with a) silver stain or b) anti-Arp2 and anti-Arp3.

2.4. Purification and identification of the target proteins photolabeled in living cells

The target proteins which are important for the potent antitumor activity of ApA (**1**), were not detected by the pull-down assay in cell lysate. One of the possible reasons was the lack of interaction of target proteins with ApA-PB (**11**) due to the denaturation of target proteins upon the lysis and extraction steps. Therefore, photolabeling experiments of target proteins with ApA-PB (**11**) were conducted in living cells.

2.4.1. Photolabeling experiments of target proteins in living cells by ApA-PB

0.6 μM of ApA-PB (**11**) was incubated with living HeLa S3 cells. After the incubation for 1–48 h, photoreaction was carried out. The whole cellular proteins were extracted and the labeled proteins were detected by Western blotting (WB) analysis with HRP conjugate streptavidin (Figure 2-17). When incubation time was 48 h, no specific biotinylated proteins were detected (Figure 2-18. lane 1), suggesting that ApA-PB (**11**) caused significant damage in HeLa S3 cells. In contrast, when incubation time was reduced to 1–24 h, two bands with molecular masses of 55 and 58 kDa were slightly detected along with actin (43 kDa) (lanes 2–4). Since these three proteins were not detected without ApA-PB (**11**) (lane 5), these proteins were labeled by ApA-PB (**11**). Amount of the labeled actin were slightly increased as incubation time increased from 1 to 24 h. However the labeling efficiency of 55 and 58 kDa proteins was not changed by the incubation time.
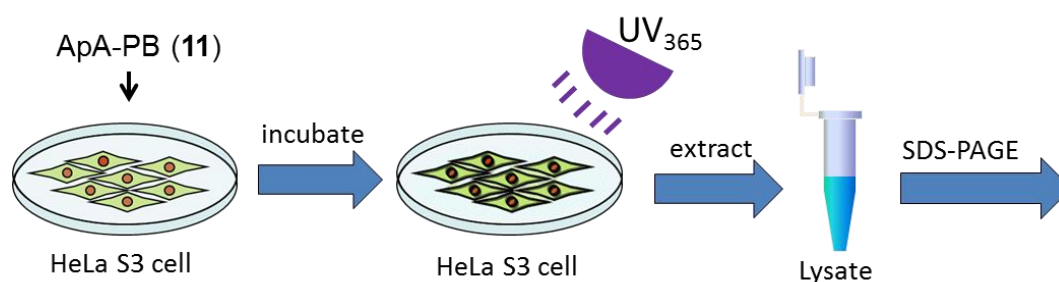
Figure 2-17. Outline of in situ photolabeling experiments.
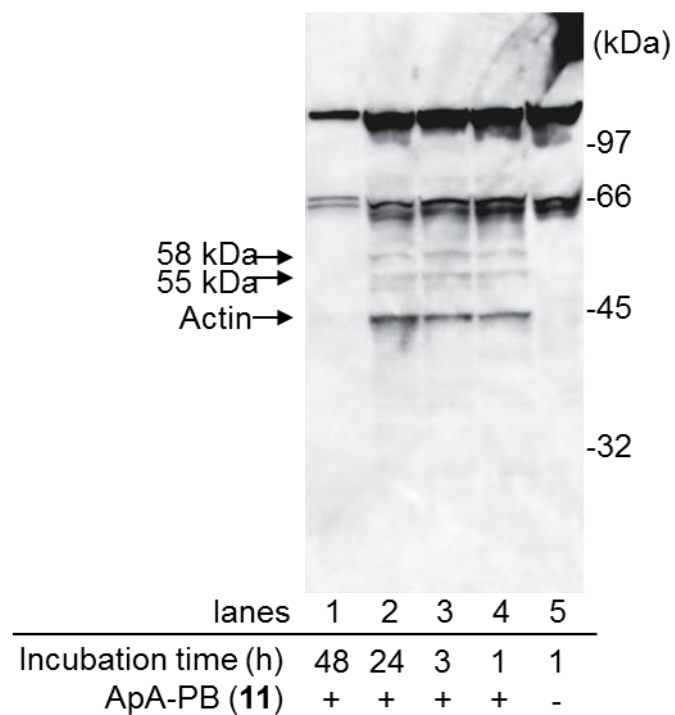
Figure 2-18. In situ photolabeling experiments with various incubation times. 0.6 µM of ApA-PB (**11**) was added to HeLa S3 cells. After incubation for 1, 3, 24 or 48 h, photoreaction was carried out. Labeled proteins were detected by Western blotting analysis with HRP conjugate streptavidin.

To improve the labeling efficiency of additional target proteins, WB condition was optimized. First the blocking condition was changed from 5% to 0.5% skim-milk in PBS-T to prevent over-blocking. Then dosed amount of ApA-PB (**11**) were examined (Figure 2-19). The labeled amount of the actin (43 kDa) and additional target proteins (55 and 58 kDa) were increased as in a dose-dependent manner. When cells were treated with 5 μM ApA-PB (**11**), two additional bands were also detected in 50 and 60 kDa (lane 4).
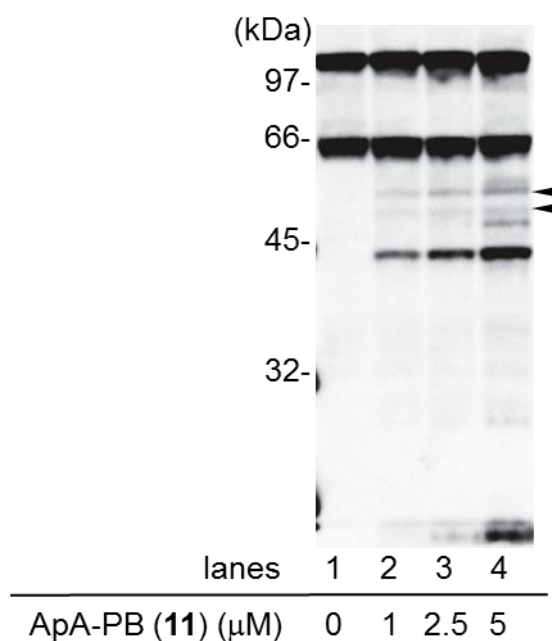
Figure 2-19. Dose-dependence on in situ photolabeling experiments. 0, 1, 2.5 or 5 μM of ApA-PB (**11**) were added to HeLa S3 cells. After photoreaction, labeled proteins were detected by WB analysis with HRP conjugate streptavidin. Arrowheads indicate 55 kDa and 58 kDa proteins.

To confirm whether detected proteins were specifically labeled with ApA-PB (**11**), competitive experiments with excess ApA (**1**) were conducted (Figure 2-20). ApA (**1**) inhibited the labeling of not only actin but also the 55 and 58 kDa proteins (lane 1), suggesting their specific interaction with ApA (**1**). On the other hand, other biotinylated proteins with the molecular weight of 50 and 60 kDa were still detected in the presence of excess actin (lane 2). Therefore these two proteins were found to be non-specific binding proteins, which did not specifically interact with natural ApA (**1**).
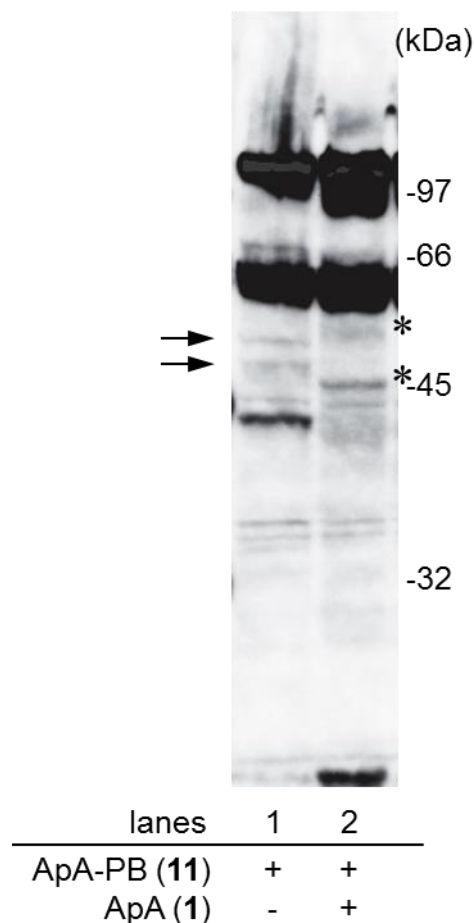
Figure 2-20. In situ photolabeling experiments in the absence/presence of excess ApA (**1**). The arrows show the 55 kDa and 58 kDa proteins which bound specifically to ApA-PB (**11**). Asterisks indicate the 50 kDa and 60 kDa proteins that non-specifically bound to ApA-PB (**11**).

2.4.2. Purification and identification of proteins photlabeled with ApA-PB.

In the section 2.4.1. the photolabeled proteins in the whole cell lysate were detected without affinity purification. To identify the two 55 and 58 kDa proteins, affinity purification of the photolabeled proteins was conducted (Figure 2-21). After photoreaction with ApA-PB (**11**) in living cells, the whole cellular proteins were extracted. The labeled proteins were purified with the use of NeutrAvidin agarose, and detected with silver stain and HRP conjugate streptavidin (Figure 2-22). A lot of proteins were nonspecifically absorbed to the resin, and affinity purified proteins that specifically purified by ApA-PB (**11**) except actin were hard to be detected by silver staining (lane 1). Meanwhile 55 and 58 kDa proteins were clearly detected with HRP conjugate streptavidin, and labeling of these proteins were inhibited in the presence of excess ApA (**1**) (lane 3). When ApC-PB (**12**) was used in the same experiments, 55 and 58 kDa were not labeled, and yet actin was labeled as with ApA-PB (**11**) (lane 2). These results indicate that 55 and 58 kDa proteins specifically bound to ApA (**1**), and were critical target proteins of ApA (**1**) for its potent antitumor activity.
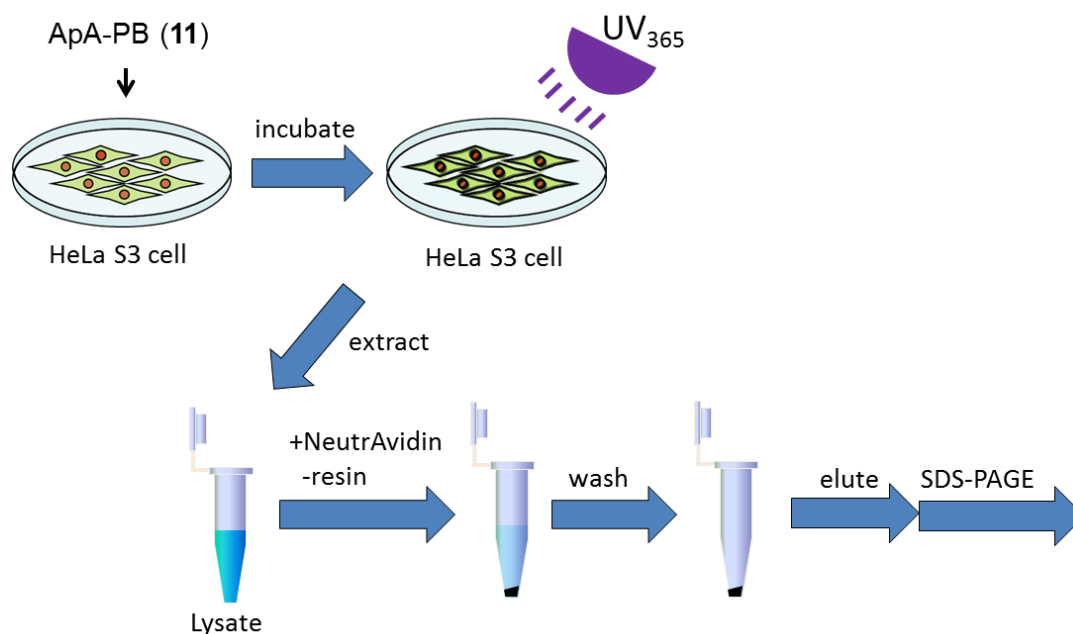
Figure 2-21. Outline of in situ photolabeling experiment and purification of labeled proteins.
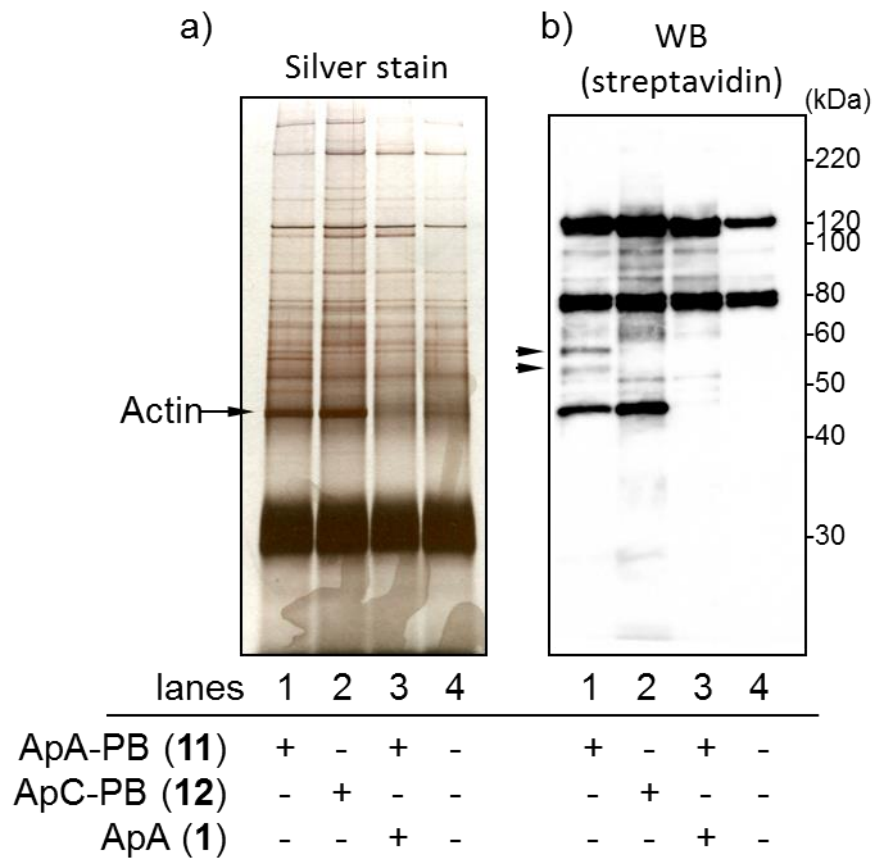
Figure 2-22. Affinity purification of the photoreacted proteins. After photoreaction with ApA-PB (**11**) or ApC-PB (**12**) in situ, labeled proteins were purified with NeutrAvidin resin. Purified proteins were detected with a) silver stain or b) HRP conjugate streptavidin. Arrowhead indicate the 55 and 58 kDa bands.

2.4.3. PMF analysis

It was confirmed that the photolabeled proteins were contained in the 55 kDa and 58 kDa bands after affinity purification. The author used PMF analysis for identification of major components in these two bands. Two bands of 55 kDa and 58 kDa were excised from the gel. After trypsin digestion, mass spectra of generated peptides were analyzed (Figures 2-23 and 2-24). The list of peptide masses were transferred into the peptide mass fingerprint search program MS-Fit. The observed masses of five peptides (K1-K5) and twelve peptides (K1-K12) were matched to the theoretical values based on the amino acid sequence of α-tubulin and β-tubulin (Tables 2-3 and 2-4, figures 2-25 and 2-26) Thus, it was determined that β-tubulin and α-tubulin were major components in the 55 kDa protein and β-tubulin was major component in the 58 kDa protein, respectively.
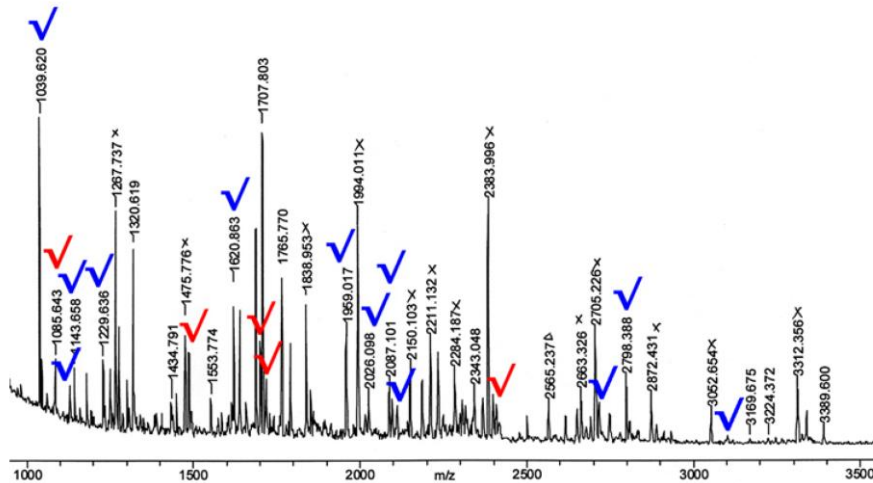
Figure 2-23. MALDI-TOF MS analysis of the tryptic peptides derived from the 55 kDa protein. Red check marks represent peptide ions that correspond to human α-tubulin; Blue check marks represent peptide ions that correspond to human β-tubulin. "x" represent the peptides derived from actin and non-specific contaminants (trypsin, keratin, etc)

Table 2-3. Tryptic peptides of the 55 kDa protein observed by the MALDI-TOF MS analysis.

• human α-tubulin (accession No. Q9BQE3)

	Observed (m/z) [a]	Calcd (m/z)	Start/end	Sequence
K1	1085.64	1085.62	113 / 121	EIIDLVLDR
K2	1487.90	1487.88	230 / 243	AVFVDLEPTVIDEVR
K3	1701.93	1701.91	65 / 79	LISQIVSSITASLR
K4	1718.90	1718.88	216 / 229	NLDIERPTYTNLNR
K5	2409.23	2409.21	244 / 264	FDGALNVDLTEFQTNLVPYPR

[a] The data represent the monoisotopic ion peaks (M+H)[+] value.

• human β-tubulin (accession No. P07437)

	Observed (m/z) [a]	Calcd (m/z)	Start/end	Sequence
K1	1039.62	1039.59	310 / 318	YLTVAAVFR
K2	1130.61	1130.60	242 / 251	FPGQLNADLR
K3	1143.66	1143.63	253 / 262	LAVNMVPFPR
K4	1229.64	1229.60	381 / 390	ISEQFTAMFR
K6	1620.86	1620.84	263 / 276	LHFFMPGFAPLTSR
K7	1959.02	1958.98	104 / 121	GHYTEGAELVDSVLDVVR
K8	2026.10	2026.08	363 / 380	MAVTFIGNSTAIQELFKR
K9	2087.10	2087.08	104 / 122	GHYTEGAELVDSVLDVVRK
K10	2110.09	2110.06 [b]	1 / 19	MREIVHIQAGQCGNQIGAK
K11	2708.44	2708.34 [b]	217 / 241	LTTPTYGDLNHLVSATMSGVTTCLR
K12	2798.39	2798.34	78 / 103	SGPFGQIFRPDNFVFGQSGAGNNWAK
K13	3102.47	3102.41	20 / 46	FWEVISDEHGIDPTGTYHGDSDLQLDR

[a] The data represent the monoisotopic ion peaks (M+H)[+] value.
[b] Putative values indicating that the Cys residue(s) in the sequences are carbamidomethylated.

53
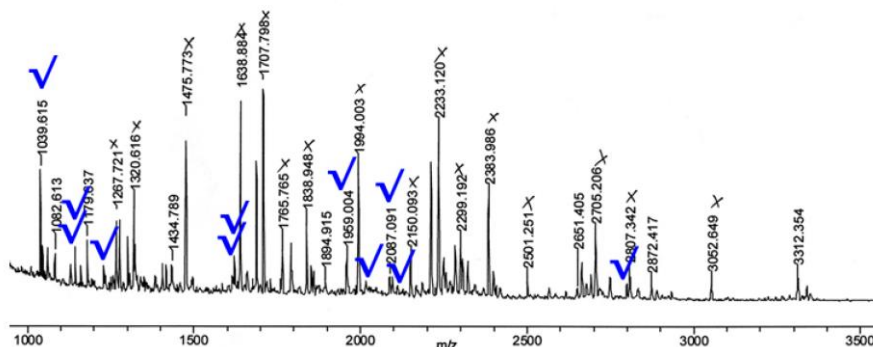
Figure 2-24. MALDI-TOF MS analysis of the tryptic peptides derived from the 58 kDa protein. Blue check marks represent peptide ions that correspond to human β-tubulin. "x" represent the peptides derived from actin and non-specific contaminants (trypsin, keratin, etc)

Table 2-4. Tryptic peptides of the 58 kDa protein observed by the MALDI-TOF MS analysis.

• human β-tubulin (accession No. P07437)

	Observed (m/z)[a]	Calcd (m/z)	Start/end	Sequence
K1	1039.62	1039.59	310 / 318	YLTVAAVFR
K2	1130.61	1130.60	242 / 251	FPGQLNADLR
K3	1143.66	1143.63	253 / 262	LAVNMVPFPR
K4	1229.64	1229.60	381 / 390	ISEQFTAMFR
K5	1615.86	1615.84	63 / 77	AILVDLEPGTMDSVR
K6	1620.86	1620.84	263 / 276	LHFFMPGFAPLTSR
K7	1959.02	1958.98	104 / 121	GHYTEGAELVDSVLDVVR
K8	2026.10	2026.08	363 / 380	MAVTFIGNSTAIQELFKR
K9	2087.10	2087.08	104 / 122	GHYTEGAELVDSVLDVVRK
K10	2110.09	2110.06[b]	1 / 19	MREIVHIQAGQCGNQIGAK
K12	2798.39	2798.34	78 / 103	SGPFGQIFRPDNFVFGQSGAGNNWAK

[a] The data represent the monoisotopic ion peaks (M+H)$^+$ value.
[b] Putative values indicating that the Cys residue(s) in the sequences are carbamidomethylated.

54

```
  1  MRECISIHVG QAGVQIGNAC WELYCLEHGI QPDGQMPSDK TIGGGDDSFN TFFSETGAGK HVPRAVFVDL EPTVIDEVRT
                                                                           K3
 81  GTYRQLFHPE QLITGKEDAA NNYARGHYTI GKEIIDLVLD RIRKLADQCT GLQGFLVFHS FGGGTGSGFT SLLMERLSVD
                                            K1
161  YGKKSKLEFS IYPAPQVSTA VVEPYNSILT THTTLEHSDC AFMVDNEAIY DICRRNLDIE RPTYTNLNR L ISQIVSSITA
                                                                    K4                K2
241  SLR FDGALNV DLTEFQTNLV PYPRIHFPLA TYAPVISAEK AYHEQLTVAE ITNACFEPAN QMVKCDPRHG KYMACCLLYR
         K5
321  GDVVPKDVNA AIATIKTKRT IQFVDWCPTG FKVGINYQPP TVVPGGDLAK VQRAVCMLSN TTAVAEAWAR LDHKFDLMYA

401  KRAFVHWYVG EGMEEGEFSE AREDMAALEK DYEEVGADSA DGEDEGEEY
```

Figure 2-25. Amino acid sequence of human α-tubulin. The sequences of the tryptic fragments (K1-K5) identical to the MS data are shown as solid underlines.

```
  1  MREIVHIQAG QCGNQIGAK F WEVISDEHGI DPTGTYHGDS DLQLDRISVY YNEATGGKYV PRAILVDLEP GTMDSVR SGP
         K10                   K13                                           K5
 81  FGQIFRPDNF VFGQSGAGNN WAK GHYTEGA ELVDSVLDVV RKEAESCDCL QGFQLTHSLG GGTGSGMGTL LISKIREEYP
         K12                   K7, K9
161  DRIMNTFSVV PSPKVSDTVV EPYNATLSVH QLVENTDETY CIDNEALYDI CFRTLKLTTP TYGDLNHLVS ATMSGVTTCL
                                                                       K11
241  R FPGQLNADL R KLAVNMVPF PR LHFFMPGF APLTSRGSQQ YRALTVPELT QQVFDAKNMM AACDPRHGRY LTVAAVFRGR
       K2          K3         K6                                                        K1
321  MSMKEVDEQM LNVQNKNSSY FVEWIPNNVK TAVCDIPPRG LKMAVTFIGN STAIQELFKR ISEQFTAMFR RKAFLHWYTG
                                                      K8                  K4
401  EGMDEMEFTE AESNMNDLVS EYQQYQDATA EEEEDFGEEA EEEA
```

Figure 2-26. Amino acid sequence of human β-tubulin. The sequences of the tryptic fragments (K1-K12) identical to the MS data are shown as solid underlines.

2.4.4. Immunoblotting analysis

To confirm that the photolabeled proteins (55 kDa and 58 kDa) were tubulin, immunoblotting analysis with anti-tubulin antibody were carried out. After in situ photoreaction and affinity purification, β-tubulins were detected by immunoblotting analysis (Figure 2-27). Native β-tubulins in HeLa S3 cells were detected in 55 kDa. As shown in lane 4, a certain amount of β-tubulin was non-specifically absorbed to the resin. However by using ApA-PB (**11**), amount of purified β-tubulin was markedly increased and the 58 kDa band was detected (lane 1). By competition of excess ApA (**1**), the amount of 55 kDa β-tubulin reduced to almost the same level as control, and the 58 kDa band was disappeared (lane 3). Therefore it was suggested that the 58 kDa was the β-tubulin which was covalently bound to ApA-PB (**11**). These results indicated that β-tubulin specifically interact with ApA (**1**). Furthermore by using ApC-PB (**12**), the amount of β-tubulin was not as much as with ApA-PB (**11**) (lane 2), as with the detection with HRP conjugate streptavidin (Figure 2-22, lane 2).

In the same immunoblotting analysis were performed with anti-α-tubulin (Figure 2-28). Native α-tubulins in HeLa S3 cells were detected in 53 kDa. Contrary to expectations, the amount of α-tubulin was the same level as control in the both case of ApA-PB (**11**) or ApC-PB (**12**) (lanes 1 and 2). No additional bands with the higher molecular weight were observed. Therefore direct interaction between α-tubulin and ApA has not been established based on these studies.

lanes	1	2	3	4
ApA-PB (**11**)	+	-	+	-
ApC-PB (**12**)	-	+	-	-
ApA (**1**)	-	-	+	-
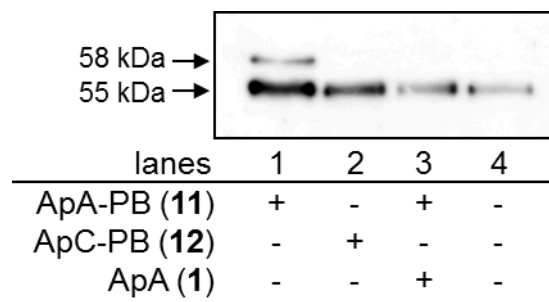
Figure 2-27. Immunoblotting analysis with anti-β-tubulin of purified proteins labeled in situ.

lanes	1	2	3	4
ApA-PB (**11**)	+	-	+	-
ApC-PB (**12**)	-	+	-	-
ApA (**1**)	-	-	+	-

Figure 2-28. Immunoblotting analysis with anti-α-tubulin of purified proteins labeled in situ.

2.5. Conclusion

ApA-bio (**7**) that has biotin group and ApA-PB (**11**) that has biotin and photoaffinity groups were synthesized. They maintained the potent cytotoxicity and actin-depolymerizing activity of ApA (**1**).

By using the ApA-bio (**7**), Arp2 and Arp3 were specifically purified as binding proteins along with actin from tumor cell lysate. Additionally with the use of ApA-PB (**11**), Arp2 and Arp3 were also specifically purified from tumor cell lysate. However, ApA-PB (**11**) did not covalently bind to Arp2 and Arp3. Thus, actin-related proteins might indirectly bind to ApA (**1**) as the ternary adducts of the actin-ApA complex or through the oligomeric actin. With the use of ApC-PB (**12**), Arp2 and Arp3 were also purified as with ApA-PB (**11**), therefore Arp2 and Arp3 were not important proteins for potent cytotoxicity of ApA (**1**).

After photoreaction with ApA-PB (**11**) in living cells, two labeled proteins were detected along with actin and identified as α- and β-tubulin. Since the labeling of tubulin was inhibited by competition of excess ApA (**1**) along with actin, tubulin might specifically interact with ApA (**1**). Furthermore ApC-PB (**12**) did not interact with tubulin. It is suggested that tubulin is a critical target protein of ApA (**1**) for its potent antitumor activity.

2.6. Experimental

The synthesis of ApA-biocytin (**6**) and ApA-bio (**7**), and PMF analysis of Arp2 and Arp3 were performed by co-workers.

2.6.1. General

Chemicals and solvents were the best grade available and were used as received from commercial sources. To protect aryl diazirine derivatives from the light, all synthetic and biological experiments with aryl diazirine derivatives were conducted with light-shaded glass or plastic equipment, or under a yellow-filtered light hood. For bioassays, the experiments that used cell lysate and proteins were performed on ice unless otherwise noted. The protein concentration was measured with a Bio-Rad Protein Assay Kit (Bradford's method) with BSA as a standard.

TLC analysis was conducted on E. Merck precoated silica gel 60 F_{254} (0.25 mm layer thickness), HPTLC Silica gel 60 RP-18 WF_{254}S, or HPTLC Silica gel $60F_{254}$. Fuji Silysia silica gels BW-820 MH and FL-60D, Merck Aluminum oxide 90 standardized, and Nacalai tesque COSMOSIL $75C_{18}$-OPN were used for open column chromatography. NMR spectra were recorded on a Bruker Biospin AVANCE 600 spectrometer (600 MHz for ^{1}H and 150 MHz for ^{13}C), a Bruker Biospin AVANCE 400 spectrometer (400 MHz for ^{1}H and 100 MHz for ^{13}C) or a JEOL JNM-EX270 spectrometer (270 MHz for ^{1}H). Chemical shifts are reported in parts per million (ppm) with coupling constants (J) in hertz relative to the solvent peaks, δ_H 3.30 (residual CHD_2OD) and δ_C 49.0 for CD_3OD, δ_H 7.26 (residual chloroform) and δ_C 77.0 for ($CDCl_3$), or δ_H 2.50 (residual $CHD_2S(O)CD_3$) and δ_C 39.5 for $[(CD_3)_2S= O]$, respectively. For the quantification of minute amounts of samples by ^{1}H NMR analyses, 1,4-dioxane, dichloromethane or benzene (10 mM in CD_3OD) was added to the sample solutions as a standard (1:60 v/v). Optical rotations were measured with a JASCO DIP-1000 polarimeter. IR spectra were recorded on a JASCO FT/IR-230 spectrometer. High-resolution electrospray ionization mass spectra (HR-ESIMS) were measured on a QSTAR Pulsar *i* spectrometer (Applied Biosystems) or an AccuTOF CS spectrometer (JEOL). Matrix-assisted laser desorption/ionization

59

with time-of-flight mass spectrometry (MALDI-TOF MS) was performed using a Bruker ultrafleXtreme spectrometer with α-cyano-4-hydroxycinnamic acid (CHCA) as a matrix.

2.6.2. Cell culture and cytotoxicity assay.

HeLa S3 cells (suspension culture-adapted human cervical carcinoma cell line, ATCC CCL-2.2) were cultured in Eagle's minimal essential medium (E-MEM) supplemented with fetal bovine serum (FBS, 10%) in a humidified atmosphere containing CO_2 (5%) at 37 °C. The cytotoxicities of ApA and its derivatives were measured by the 3-(4,5-dimethylthiazol-2-yl)-2,5-diphenyl tetrazolium bromide (MTT) method. HeLa S3 cells were seeded at 2×10^3 cells per well in 96-well plates. After incubation overnight at 37 °C, aplyronines and these derivatives (1 pM – 1 µM) were added, and the cells were incubated for 96 h at 37 °C. After MTT was added, the mixtures were incubated for 4 to give insoluble formazan derivative from MTT. After removal of the medium, the formazan derivative was dissolved with N,N-dimethylformamide and absorbance at 540 nm was measured on Infinite F200 PRO (TECAN). The IC_{50} value (concentration required for 50% inhibition of cell growth) was determined using a growth curve by comparison of negative control wells.

2.6.3. In vitro actin-depolymerizing assay.

The actin-depolymerizing activities of ApA (**1**) and model compounds were measured based on their ability to attenuate the fluorescence of pyrene-conjugated (pyrenyl) actin. Actin polymerization was started by the addition of a 0.15 M solution of $MgCl_2$ (3.3 µL) to a solution of actin (3 µM, from rabbit skeletal muscle, Cytoskeleton Inc., 10% of total actin is pyrenyl-actin) in 500 µL of G-buffer [2 mM Tris·HCl (pH8.0), 0.2 mM $CaCl_2$, 0.2 mM ATP, 0.5 mM 2-mercaptoethanol]. After incubation for 1 h at 25 °C, ApA (**1**) and its derivatives were added, and the time course of polymerization (or depolymerization) was continuously monitored by measuring fluorescence of pyrenyl-actin with spectrofluorometer (Hitachi, F-4500, equipped with a magnetic stirrer) at 25 °C at 365nm excitation and 407nm emission wavelengths.

   In another assay of F-actin sedimentation (centrifugation method), to a solution of actin (3 µM, from

rabbit skeletal muscle, Cytoskeleton) in G-buffer (500 μL) was added a 0.15 M solution of MgCl$_2$ (3.3 μL), and the mixture was stirred at 25 °C for 1 h. To the solutions of F-actin were added samples (3 μM), and the resulting mixtures were stirred at 25 °C for 1 h and then ultracentrifuged (150,000 × g, 22 °C, 1 h). The supernatants (lyophilized) and the precipitates were dissolved in 1 × SDS buffer (100 μL, Sigma) and boiled at 95 °C for 5 min. SDS-PAGE was performed by using a precast 10% polyacrylamide gel (ATTO), and the gels were stained with a Quick-CBB kit (Wako).

2.6.4. Interaction of biotinylated ApA derivatives with actin.

1 mM solutions of samples (5 μL) were pre-incubated with the NeutrAvidin agarose resin (10 μL, Pierce) equilibrated with G-buffer (250 μL) with a rotator at 4 °C for 2 h. After the unbound samples were removed by decantation, actin (50 μg/mL, from rabbit muscle, Sigma Co.) in G-buffer (240 μL) was added to the resin, and the mixtures were incubated with a rotator at 4 °C for 23 h. The resins were thoroughly washed with 0.1% Triton PBS (4 × 400 μL) followed by PBS (400 μL). In the case of elution by ApA (**1**), the resins were incubated with ApA (**1**) (5 μM) in G-buffer (40 μL) with a rotator at room temperature for 2 h, and the supernatants were collected by filtration. The elutes were diluted with an equal volume of 2 × SDS buffer (Sigma Co.) and boiled at 95 °C for 5 min. In the case of elution by boiling, the resins were resuspended in 2 × SDS buffer (30 μL) and boiled at 95 °C for 5 min. SDS-PAGE was performed by using a precast 10% polyacrylamide gel (ATTO Co.), and the gels were stained with a Silver Stain Kit, Protein (GE Healthcare).

2.6.5. Pull-down assay of the ApA-binding proteins in cell lysate.

1 mM solutions of samples (5 μL) were pre-incubated with NeutrAvidin agarose resin (10 μL) equilibrated with 0.1% Triton PBS (250 μL) with a rotator at 4 °C for 2 h. After unbound samples were removed by decantation, the cell lysate (277 μL, 3 mg protein, from 2×10^7 cells) was added to the resin and incubated with a rotator at 4 °C for 15 h. The resins were thoroughly washed with 0.1% Triton PBS (4 × 400 μL) followed by PBS (400 μL). Binding proteins were eluted by the ApA (**1**) or boiling as described in 2.6.4.

except for the use of 0.1% Triton-PBS instead of G-buffer. SDS-PAGE was performed by using a precast 10% polyacrylamide gel (ATTO Co.), and the gels were stained with a Silver Stain Kit, Protein (GE Healthcare). For the immunoblot analyses, proteins in the gels after electrophoresis were transferred to PVDF membranes using the Trans-Blot® SD semi-dry blotting system (Bio-Rad) according to the manufacturer's instructions. After transfection, PVDF membranes were blocked with 5% skim-milk in PBS. Proteins were detected with HRP conjugated streptavidin (1:2000, GE Healthcare), rabbit polyclonal anti-nonmuscle myosin IIB antibody (1:200, GeneTex Inc., cat. No. GTX11090), rabbit polyclonal anti-β-actin antibody (1:200, Sigma Co., cat. No. A2066), rabbit polyclonal anti-Arp2 antibody (1:200, CST Japan, cat. No. #3128S), rabbit polyclonal anti-Arp3 antibody (1:200, CST Japan, cat. No. #4738S), or mouse monoclonal anti-ACTR3 (actin-related protein 3 homolog) antibody (1:200, 2B6, Abnova Co., cat. No. H00010096-M02). For the all primary antibodies, proteins were further treated with HRP-conjugated anti-rabbit or anti-mouse IgG (1:2000, GE Healthcare). HRP-conjugated bands were visualized with an ECL or ECL-prime systems (GE Healthcare), and detected by a Fujifilm LAS-4000 MINI imaging scanner.

2.6.6. Photolabeling and affinity purification of aplyronine binding proteins in HeLa S3 cell lysate.

HeLa S3 cells (4.0×10^7 cells) in culture were washed twice with PBS and treated with 0.05% trypsin–EDTA. Suspended cells were collected by centrifugation and washed twice with PBS. The cells were lysed in 1 mL of lysis buffer [10 mM Tris·HCl (pH 7.4), 0.15 M NaCl, 1% Triton X-100, 10 mg/mL leupeptin] with a pestle at 4 °C. To remove most of the intrinsic biotin-binding proteins, the suspensions were centrifuged (15,000 rpm, 30 min) and treated with NeutrAvidin agarose resin (200 μL, Pierce) equilibrated with 0.1% Tween 20 in PBS (PBS-T) with a rotator for 30 min. The supernatants were collected by filtration to give the cell lysate (~1.3 mL) with a concentration of 10 mg protein/mL. Solution of ApA-PB or ApC-PB in dimethyl sulfoxide (1 mM, 5 μL) and lysis buffer (50 μL) was added to the NeutrAvidin agarose resin (40 μL) in 1.5 mL Eppendorf tubes. After the incubation with a rotator shielded from light for 30 min, the cell lysate (300

μL) was added, and the mixtures were further incubated for 2 h. For competitive inhibition assays, a 10 mM solution of ApA in dimethyl sulfoxide (5 μL) was pretreated with the cell lysate for 30 min. Then the resulting mixture was irradiated with UV lamp 0.8 mW/cm^2 on ice for 15 min. For the direct elution by boiling, the resins divided in half were thoroughly washed with PBS-T (5 × 400 μL) followed by PBS (400 μL) and resuspended in 2 × SDS buffer (30 μL). The binding proteins were eluted by boiling at 95 °C for 5 min. For the stepwise elution, the remaining half of the resins washed with PBS-T (5 × 400 μL) were incubated with ApA (**1**) (10 μM) in PBS-T (100 μL) with a rotator at room temperature for 2 h, and the supernatants were collected by filtration. The eluates were lyophilized, dissolved in 2 × SDS buffer (30 μL, Sigma Co.), and boiled at 95 °C for 5 min. The residual resins were resuspended in 2 × SDS buffer (30 μL), and binding proteins were eluted by boiling at 95 °C for 5 min. SDS-PAGE was performed by using a precast 10% polyacrylamide gel, and the gels were stained with a Silver Stain Kit, Protein. Immunoblotting analyses were performed as described in 2.6.5. Proteins were detected with HRP-conjugated streptavidin (1:3000, GE Healthcare), rabbit polyclonal anti-Arp2 antibody (1:200, CST Japan, cat. No. #3128S), or rabbit polyclonal anti-Arp3 antibody (1:200, CST Japan, cat. No. #4738S). For the both primary antibodies, proteins were further treated with HRP-conjugated anti-rabbit IgG (1:2000, GE Healthcare). The HRP-conjugated bands were visualized with an ECL-prime system (GE Healthcare), and detected by a Fujifilm LAS-4000 MINI imaging scanner.

2.6.7. In-gel digestion and PMF analysis.

After SDS-PAGE, gels were silver-stained in a mass-compatible manner[10] (Silver staining was performed except that treatment with glutaraldehyde, a cross-linking and sensitizing agent). The gel was fixed in 50% methanol, 5% acetic acid in water for 30 min. After washing with H$_2$O, the gel was sensitized for 2 min in 0.02% sodium thiosulfate and then rinsed with H$_2$O (2 × 1 min). The gel was treated with 0.25% silver nitrate solution for 30 min. After the silver nitrate solution was discarded, the gel was rinsed twice with water for 1 min and then developed in 0.004% formalin in 2% sodium carbonate for 1 min. The development was

terminated by discarding the reagent, followed by washing of the gel with 1% acetic acid. Stained spots were excised from the PAGE gel, and the gel pieces were desilverized by vortexing in 30 mM potassium ferricyanide / 100 mM sodium thiosulfate (1:1) for 10 min, followed by washing with H_2O twice. H_2O was replaced with acetonitrile to dehydrate the gel pieces. After removal of liquid phase, they were completely dried in a centrifugal evaporator. A volume of 10 mM dithiotreitol (DTT) in 25 mM ammonium bicarbonate sufficient to cover the gel pieces was added, and the DTT solution was incubated for 45 min at 56 °C. The DTT solution was replaced with roughly the same volume of 55 mM iodoacetamide in 100 mM ammonium bicarbonate. After vortexing in the dark for 30 min, the gel pieces were washed with 25 mM ammonium bicarbonate for 5 min. Washed gel pieces were incubated in acetonitrile−25 mM ammonium bicarbonate (1:1), and dehydrated by replace washed solvent with acetonitrile. The liquid phase was removed, and the gel pieces were completely dried in a centrifugal evaporator. The gel pieces were incubated with the modified trypsin (1:100 w/w, sequence-grade, #V5111, Promega) in 25 mM ammonium bicarbonate for 19 h at 37 °C. The tryptic peptide mixtures were extracted from the gel pieces with 5% formic acid−50% acetonitrile (three times). All extracts were combined and concentrated to the 10 μL in a centrifugal evaporator. The solution was desalted by using a prespotted Anchorchip™ (PAC 384/96 α-CHCA, Bruker Daltonics), according to the manufacturer's instruction for MS and MS/MS analyses. PMF searches to identify proteins were performed using MS-fit in ProteinProspector (http://prospector.ucsf.edu/prospector/mshome.htm). Database was SwissProt. Partial methionine oxidation, N-terminal acetylation and pyro-glutamate, complete cysteine carbamidomethylation, and one or no missed trypsin cleavages were factors considered in the searches.

2.6.8. Isolation of aplyronine A (1)

Aplyronine A (**1**) was isolated from the sea hare *Aplysia kurodai*. The specimens of sea hare were collected off the Pacific coast of the Shima Peninsula, Mie Prefecture, Japan. Approximately 16 kg (wet weight) of sea hare was crashed and extracted with ethanol (30 L) for 2 days. The extracted was filtered, and the filtrate was concentrated. The residue was partitioned between ethyl acetate (3 × 1 L) and water (1 L). The ethyl acetate layer was concentrated, and the residue was partitioned between 90% methanol (1 L) and hexane (4 × 0.5 L). The 90% methanol layer was concentrated, and the residue was partitioned between 60% methanol (1 L) and dichloromethane (6 × 0.5 L). The dichloromethane layer was concentrated. The residue (17.8 g) was loaded on a silica gel column (300 g) and eluted with benzene–ethyl acetate–methanol (1:1:0 → 0:1:0 → 0:4:1 → 0:1:1 → 0:0:1). The concentrated fraction (1.25 g) eluted with benzene–ethyl acetate–methanol 0:1:1 was loaded on aluminum oxide column (35 g) and eluted with ethyl acetate–methanol (1:0→19:1→1:1). The concentrated fraction (34.4 mg) eluted with ethyl acetate–methanol (19:1) was chromatographed by reversed-phase HPLC [Develosil ODS-HG-5 (ϕ 20 mm I.D. × 250 mm), methanol–0.01 M ammonium acetate (70:30), 5 mL/min] and column chromatography on aluminum oxide [0.5 g, ethyl acetate–methanol (1:1)] to give aplyronine A (**1**) (5.1 mg, 3.2×10^{-5}% based on wet wt).

## 2.6.9. Synthesis and spectroscopic data of aplyronine derivatives and model compounds.

ApA-biocytin (**6**). *   *The experiments performed by co-workers.


ApA-biocytin (**6**)
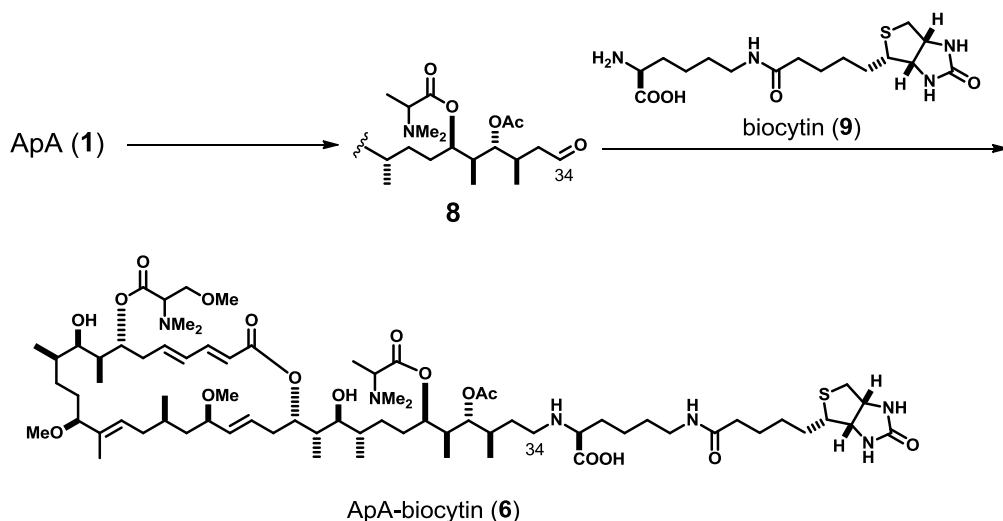
To a stirred solution of ApA (**1**) (0.50 mg, 460 nmol) in acetonitrile (0.1 mL) was added 1 M aq. HCl (0.1 mL) under a nitrogen atmosphere. After being stirred for 26 h at room temperature, the reaction mixture was diluted with ethyl acetate (5 mL), washed with water and brine, dried, and concentrated to give aldehyde **8**, which was used for the next step without further purification. The crude material was dissolved in 50% aq. methanol (0.5 mL), and biocytin (2.0 mg, 5.3 µmol, Nakalai Tesque) was added under a nitrogen atmosphere. After the mixture was stirred for 30 min, sodium cyanoborohydride (1.2 mg, 18 µmol) was added. The mixture was stirred for an additional 36 h and concentrated. The residue was applied (twice) to a Develosil 300C4-HG-5 reversed-phase HPLC column (ϕ 4.6 mm I.D. × 250 mm). Samples were eluted by acetonitrile–20 mM ammonium acetate (4:6) at a flow rate of 0.5 mL/min, with monitoring at 220 nm, to give a ApA-biocytin (**6**) (157 µg, 24%, based on NMR quantification, t_R = 15.1 min). Compound **6**: ^{1}H NMR (600 MHz, CD$_3$OD) δ 7.21 (dd, J = 15.4, 10.5 Hz, 1H), 6.39 (br dd, J = 15.2, 10.5 Hz, 1H), 6.23 (m, 1H), 5.98 (d, J = 15.4 Hz, 1H), 5.64 (ddd, J = 15.4, 10.9, 3.6 Hz, 1H), 5.56 (br d, J = 10.8 Hz, 1H), 5.10 (m, 1H), 4.94–4.58 (m, 5H), 4.48 (m, 1H), 4.30 (m, 1H), 3.67 (m, 2H), 3.59–3.50 (m, 2H), 3.45–3.07 (m, 6H), 3.36 [3.41]

(s, 3H), 3.18 (s, 3H), 3.16 (s, 3H), 2.92 (br dd, J = 13.0, 4.9 Hz, 1H), 2.88 (m, 1H), 2.70 (br d, J = 13.0 Hz, 1H), 2.52–2.38 (m, 2H), 2.39 (s, 3H), 2.38 (s, 3H), 2.35 (s, 3H), 2.33 (s, 3H), 2.28 (br d, J = 14.0 Hz, 1H), 2.19 (br t, J = 7.1 Hz, 2H), 2.10–1.95 (m, 6H), 2.04 [2.03] (s, 3H), 1.94–1.77 (m, 6H), 1.76–1.50 (m, 12H), 1.52 [1.51] (br s, 3H), 1.47–1.38 (m, 4H), 1.36–1.22 (m, 4H), 1.30 [1.29] (d, J = 7.2 Hz, 3H), 1.18–1.08 (m, 4H), 1.03 (d, J = 7.2 Hz, 3H), 1.01 (d, J = 7.3 Hz, 3H), 1.00 (d, J = 6.9 Hz, 3H), 0.98 (d, J = 7.3 Hz, 3H), 0.97 (d, J = 6.9 Hz, 3H), 0.92 (br d, J = 7.0 Hz, 3H), 0.77 [0.78] (d, J = 6.1 Hz, 3H). Chemical shifts of the minor diastereomer are within brackets. HRMS (ESI) m/z 696.4544 (calcd for $C_{73}H_{128}N_6O_{17}S)/2$ [M+2H]$^{2+}$, Δ +1.4 mmu).

ApA-bio (**7**) *   *The experiments performed by co-workers.


ApA-bio (**7**)
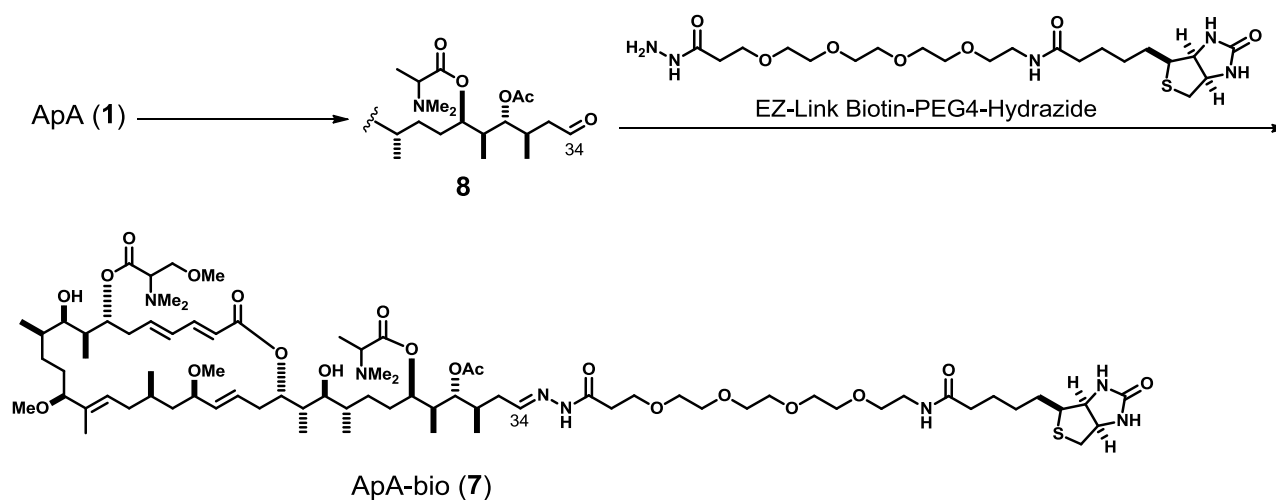
To a stirred solution of ApA (1.0 mg, 930 nmol) in 1,4-dioxane (0.3 mL) was added 2 M aq. HCl (0.1 mL) under a nitrogen atmosphere. After being stirred for 80 min at 50 °C, the reaction mixture was neutralized with sodium bicarbonate (3 mL) and extracted with chloroform (2 mL × 4). The combined extracts were washed with brine and concentrated to give aldehyde **8**, which was used for the next step without further purification. To the stirred solution of aldehyde **8** in methanol–acetic acid (4:1, 0.4 mL) was added EZ-Link Biotin-PEG$_4$-Hydrazide (2.5 mg, 5 µmol, Thermo Scientific) in dimethyl sulfoxide (20 µL) under a nitrogen atmosphere. After the mixture was stirred for 48 h at room temperature, acetone (50 µL) was added. After additional stirring for 30 min, the reaction mixture was azeotropically concentrated with toluene and applied (five times) to a Develosil ODS-HG-5 reversed-phase HPLC column (ϕ 4.6 mm I.D. × 250 mm). Samples were eluted by methanol–40 mM ammonium acetate (73:27) at a flow rate of 1 mL/min, with monitoring at 254 nm, and then lyophilized from water twice to give ApA-bio (**7**) (540 µg, 38%, based on NMR quantification, t_R = 25.3 min, E/Z = 2/1 for the C34 isomers). Compound **7**: ^{1}H NMR (600 MHz, CD$_3$OD) δ 7.48 [7.30] (t, *J* = 5.7 Hz, 1H), 7.20 (dd, *J* = 15.1, 10.7 Hz, 1H), 6.38 (br dd, *J* = 15.3, 10.7 Hz, 1H), 6.22 (m, 1H), 5.97 (d, *J* = 15.1 Hz, 1H), 5.64 (ddd, *J* = 15.4, 10.9, 3.6 Hz, 1H), 5.55 (br d, *J* = 10.7 Hz, 1H), 5.10 (m, 1H), 4.97 (m, 1H), 4.95–4.78 (m, 2H), 4.68 (m, 1H), 4.48 (dd, *J* = 7.8, 5.0 Hz, 1H), 4.30 (dd, *J* = 7.8, 4.6 Hz,

1H), 3.77 [3.79] (t, J = 6.0 Hz, 2H), 3.68 (t, J = 5.9 Hz, 2H), 3.67 (t, J = 5.8 Hz, 2H), 3.66–3.58 (m, 12 H),

3.55 (m, 1 H), 3.53 (t, J = 6.0 Hz, 2H), 3.52 (m, 1 H), 3.37–3.14 (m, 5H), 3.34 [3.41] (s, 3H), 3.18 (s, 3H),

3.16 (s, 3H), 3.08 (m, 1H), 2.92 (br dd, J = 12.8, 5.0 Hz, 1H), 2.88 (m, 1H), 2.70 (br d, J = 12.8 Hz, 1H),

2.52–2.35 (m, 3H), 2.47 (t, J = 6.0 Hz, 1H), 2.39 (s, 3H), 2.38 (s, 3H), 2.35 (s, 3H), 2.33 (s, 3H), 2.28 (br d,

J = 14.0 Hz, 1H), 2.22 (br t, J = 7.3 Hz, 2H), 2.11–1.90 (m, 4H), 2.04 [2.03] (s, 3H), 1.76–1.49 (m, 13H),

1.51 [1.52] (br s, 3H), 1,43 (m, 2H), 1.39–1.23 (m, 4H), 1.31 [1.29] (d, J = 7.1 Hz, 3H), 1.18–1.07 (m, 2H),

1.03 (d, J = 7.0 Hz, 3H), 1.01 (d, J = 7.0 Hz, 3H), 0.99 (d, J = 6.8 Hz, 3H), 0.98 (d, J = 7.3 Hz, 3H), 0.92

[0.91] (d, J = 6.8 Hz, 3H), 0.90 [0.89] (d, J = 7.1 Hz, 3H), 0.77 [0.76] (d, J = 6.0 Hz, 3H). Chemical shifts

of the minor hydrazone stereoisomer are within brackets. HRMS (ESI) m/z 761.9811 (calcd for

$C_{78}H_{137}N_7O_{20}S$)/2 $[M+2H]^{2+}$, Δ –0.9 mmu).

3-phenylpropionaldehyde   model-bio (**10**)


To a stirred solution of 3-phenylpropionaldehyde (3.4 mg, 25 µmol) in methanol–acetic acid (4:1, 2 mL) was added EZ-Link Biotin-PEG$_4$-Hydrazide (12.6 mg, 25 µmol) in dimethyl sulfoxide (100 µL) under a nitrogen atmosphere. After being stirred for 24 h at 50 °C, the reaction mixture was concentrated and applied (twice) to a Develosil ODS-HG-5 HPLC column (ϕ 20 mm I.D. × 250 mm). Samples were eluted by 80% aqueous methanol at a flow rate of 5 mL/min, with monitoring at 215 nm (t_R = 12.5 min) to give Model-bio **10** (5.9 mg, 38%, E/Z = 2/1 for the imine carbonyl carbon). Compound **10**: ^{1}H NMR (600 MHz, CD$_3$OD) δ 7.47 [7.31] (t, J = 5.5 Hz, 1H), 7.26 (br t, J = 7.6 Hz, 2H), 7.22 (br d, J = 7.6 Hz, 2H), 7.16 (br t, J = 7.6 Hz, 1H), 4.47 (ddd, J = 7.8, 5.0, 0.7 Hz, 1H), 4.09 (dd, J = 7.8, 4.6 Hz, 1H), 3.75 (t, J = 6.1 Hz, 2H), 3.63–3.57 (m, 12H), 3.52 (t, J = 5.5 Hz, 2H), 3.34 (t, J = 5.5 Hz, 2H), 3.19 (m, 1H) 2.91 (dd, J = 12.7, 5.0 Hz, 1H), 2.85 (t, J = 7.4 Hz, 2H), 2.69 (br d, J = 12.7 Hz, 1H), 2.60 [2.57] (dt, J = 5.5, 7.8 Hz, m, 2H), 2.45 (t, J = 6.1 Hz, 2H), 2.20 (t, J = 7.3 Hz, 2H), 1.72 (m, 1H), 1.69–1.60 (m, 2H), 1.59 (m, 1H), 1.43 (tt, J = 7.3, 7.3 Hz, 2H). Chemical shifts of the minor hydrazone stereoisomer are within brackets. ^{13}C NMR (150 MHz, CD$_3$OD) δ 176.1 (s), 170.1 (s), 166.1 (s), 153.1 [149.1] (d), 142.1 [142.5] (s), 129.5 (d, 2C), 129.1 (d, 2C), 127.2 [127.1] (d), 71.6 (t, 2C), 71.5 (t, 2C), 71.4 (t), 71.3 (t), 70.6 (t), 68.0 (t), 63.4 (d), 61.6 (d), 57.0 (d), 41.0 (t), 40.4 (t), 36.7 (t), 36.3 (t), 35.0 [34.1] (t), 33.7 [33.4] (t), 29.8 (t), 29.5 (t), 26.8 (t); IR (chloroform) 3466, 3265 (br.), 3006, 2926, 1698, 1523, 1455, 1350, 1249, 1111 cm^{-1}; [α]$_D^{19}$ +28 (*c* 0.37, methanol); HRMS (ESI) *m/z* 644.3108 (calcd for C$_{30}$H$_{47}$N$_5$NaO$_7$S [M+Na]$^+$, Δ +1.7 mmu).

Biotin-PEO$_4$-amine **13**.[6]

bis[2-(3-aminopropoxy)ethyl]ether   (+)-biotin *N*-hydroxysuccinimidyl ester

NH$_2$ +   NH$_2$ **13**

To a stirred solution of bis[2-(3-aminopropoxy)ethyl]ether (650 μL, 2.95 mmol) and triethylamine (70 μL, 0.50 mmol) in *N,N*-dimethylformamide (1 mL) was added (+)-biotin *N*-hydroxysuccinimidyl ester (100.8 mg, 0.295 mmol) in 5 mL of *N,N*-dimethylformamide dropwise for 45 min. After being stirred at room temperature for 2 h, the mixture was concentrated under vacuum and azeotropically dried with toluene twice. The residual oil was triturated with diethyl ether (15 mL) and stirred for 1 h. The solid was collected by filtration, dissolved in methanol–ethyl acetate (4:1), and loaded on aluminum oxide column (5 g). Samples were eluted with methanol–ethyl acetate (4:1) to give the biotin-PEO$_4$-amine **13** (88.4 mg, 67%). Compound **13**: ^{1}H NMR (270 MHz, CD$_3$OD) δ 4.48 (dd, *J* = 4.1, 7.7 Hz, 1H), 4.29 (dd, *J* = 4.6, 7.7 Hz, 1H), 3.66–3.48 (m, 12H), 3.25 (t, *J* = 7.0 Hz, 2H), 3.23–3.16 (m, 1H), 2.92 (dd, *J* = 4.6. 12.7 Hz, 1H), 2.75 (t, *J* = 6.8 Hz, 2H), 2.69 (d, *J* = 12.7 Hz, 1H), 2.19 (t, *J* = 7.3 Hz, 2H), 1.80–1.38 (m, 10H).

PEG-linked biotin amide **15**.
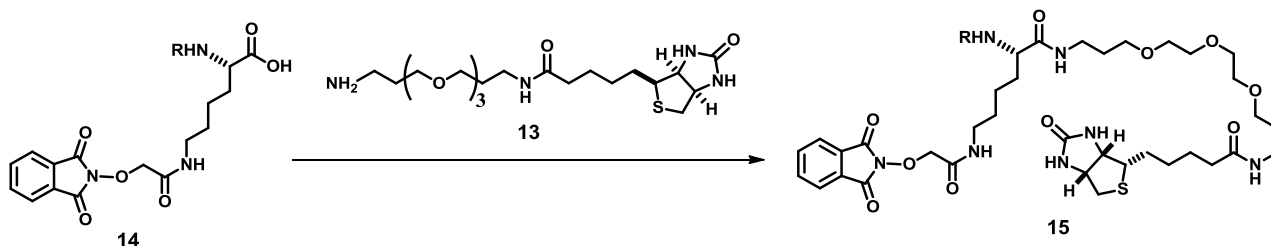
To a stirred solution of carboxylic acid **14**[7] (58.3 mg, 0.130 mmol) and biotin-PEO4-amine **13** (45.4 mg, 0.102 mmol) in dry dichloromethane (8 mL) were added 1-hydroxy-7-aza-benzotriazole (HOAt) (21 mg, 0.16 mmol) and 1-ethyl-3-(3-dimethylaminopropyl) carbodiimide hydrochloride (EDC·HCl) (40 mg, 0.21 mmol). After being stirred at room temperature for 2 h, the reaction mixture was washed with sat. sodium hydrogen carbonate aq. (10 mL × 2), and the washings were extracted with chloroform (2 mL × 2). The combined organic layer and the extracts were dried with Na_2SO_4 and concentrated. The crude material was purified with an ODS column (2 g, acetonitrile) and a recycling HPLC [JAIGEL-1H, JAIGEL-2H (φ 20 mm I.D. × 300 mm), chloroform, 3.8 mL/min, UV254 nm] to give amide **15** (65 mg, 74%) as a colorless oil.

Compound **15**: $[\alpha]_D^{22}$ +11.5 (c 0.87, chloroform); ^{1}H NMR (600 MHz, $CDCl_3$) δ 7.90–7.78 (m, 5H), 7.31–7.26 (m, 1H), 6.78 (br s, 1H), 6.10 (br s, 1H), 5.64 (br d, J = 8.4 Hz, 1H), 5.19 (br s, 1H), 4.70 (s, 2H), 4.50 (dd, J = 5.0, 7.7 Hz, 1H), 4.35–4.29 (m, 1H), 4.08 (dt, J = 7.4, 7.6 Hz, 1H), 3.68–3.48 (m, 12H), 3.40–3.29 (m, 6H), 3.14 (dt, J = 4.3, 7.6 Hz, 1H), 2.91 (dd, J = 5.0, 12.9 Hz, 1H), 2.73 (d, J = 12.9 Hz, 1H), 2.17 (t, J = 7.3 Hz, 2H), 2.10–1.30 (m, 12H), 1.78 (tt, J = 5.9 Hz, 4H), 1.42 (s, 9H); ^{13}C NMR (150 MHz, $CDCl_3$) δ 172.9, 172.5, 166.9, 163.7 (2C), 163.4, 155.9, 135.1 (2C), 128.5 (2C), 124.1 (2C), 79.6, 77.2, 70.5, 70.4, 70.1, 70.0, 69.8, 69.5, 62.0, 60.0, 55.7, 54.5, 40.6, 38.9, 37.9, 37.3, 35.8, 32.3, 29.0, 28.8 (2C), 28.4 (3C), 28.2 (2C), 25.5, 22.9; IR (chloroform) 3362, 3005, 2933, 2870, 1792, 1735, 1704, 1539, 1469, 1456, 1369 cm^{-1}; HRMS (ESI) m/z 900.4174 (calcd for $C_{41}H_{63}N_7NaO_{12}S$ [M+Na]$^+$, Δ −2.1 mmu).

Diazirine amide **18**.
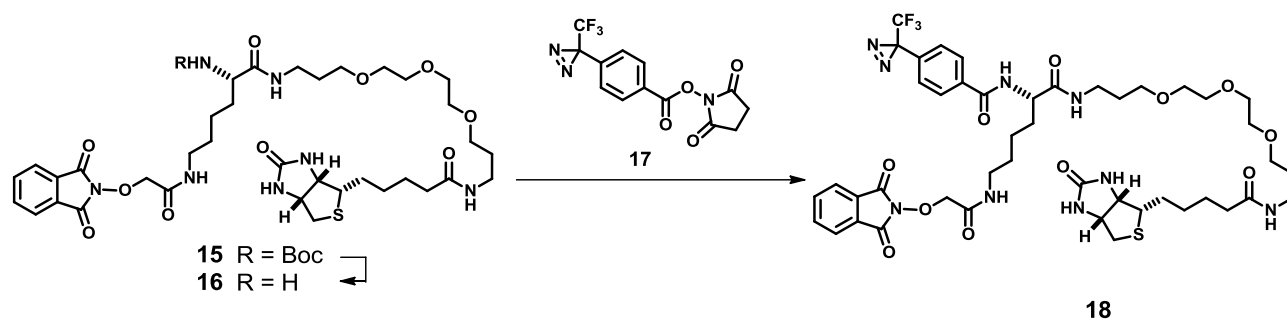
A solution of amide **15** (14.7 mg, 16.7 μmol) in a 1:1 mixture of dry dichloromethane and trifluoroacetic acid (1 mL) was stirred for 30 min at 0 °C, and azeotropically concentrated with toluene in vacuo to give crude amine trifluoroacetic acid salt. To a stirred solution of the crude amine trifluoroacetic acid salt in dry *N,N*-dimethylformamide (0.5 mL) were added diazirine succinyl ester **17**[8] (11.9 mg, 36.4 μmol) and diisopropylethylamine (10 μL, 57 μmol) under a nitrogen atmosphere. After being stirred for 3 h at room temperature, the resulting mixture was concentrated. The crude material as purified with a recycling HPLC [JAIGEL-1H, JAIGEL-2H (φ 20 mm I.D. × 300 mm), chloroform, 3.8 mL/min, UV254 nm] to give diazirine amide **18** (13.5 mg, 82%) as a colorless oil. Compound **18**: $[\alpha]_D^{25}$ +6.3 (*c* 0.49, chloroform); ^{1}H NMR (400 MHz, CDCl$_3$) δ 8.67 (br d, *J* = 7.8 Hz, 1H), 7.94 (br t, *J* = 5.5 Hz, 1H), 7.92 (d, *J* = 8.5 Hz, 2H), 7.85–7.77 (m, 4H), 7.38 (br t, *J* = 5.5 Hz, 1H), 7.17 (d, *J* = 8.5 Hz, 2H), 6.98 (br s, 1H), 6.96 (br t, *J* = 5.5 Hz, 1H), 4.90 (br s, 1H), 4.71 (d, *J* = 15.6 Hz, 1H), 4.68 (d, *J* = 15.6 Hz, 1H) 4.49–4.44 (m, 2H), 4.30 (dd, *J* = 4.6, 7.8 Hz, 1H), 3.75–3.26 (m, 18H), 3.04 (dt, *J* = 4.6, 6.9 Hz, 1H), 2.84 (dd, *J* = 5.0, 12.8 Hz, 1H), 2.60 (d, *J* = 12.8 Hz, 1H), 2.02 (t, *J* = 7.8 Hz, 2H), 1.80–1.25 (m, 16H); ^{13}C NMR (100 MHz, CDCl$_3$) δ 173.3, 173.0, 166.95, 166.93, 163.9, 163.8 (2C), 135.3 (2C), 134.8, 132.4, 128.6 (2C), 128.2 (2C), 126.6 (2C), 124.2 (2C), 77.4, 70.8, 70.4, 70.10, 70.07, 69.9, 69.5, 62.1, 60.1, 55.7, 54.8, 40.7, 38.6, 38.0, 37.0, 35.5, 31.3, 29.3, 28.9, 28.8, 28.1, 28.0, 25.4, 23.1. Two carbon signals [Ar–C(=N$_2$)CF$_3$] were not detected; IR (chloroform) 3360, 3004, 2928, 2864, 1792, 1734, 1693, 1656, 1544, 1456, 1345 cm^{-1}; HRMS (ESI) *m/z* 1012.3847 (calcd for C$_{45}$H$_{58}$F$_3$N$_9$NaO$_{11}$S [M+Na]$^+$, Δ +2.1 mmu).

Alkoxyamine **19**

---

18 → 19
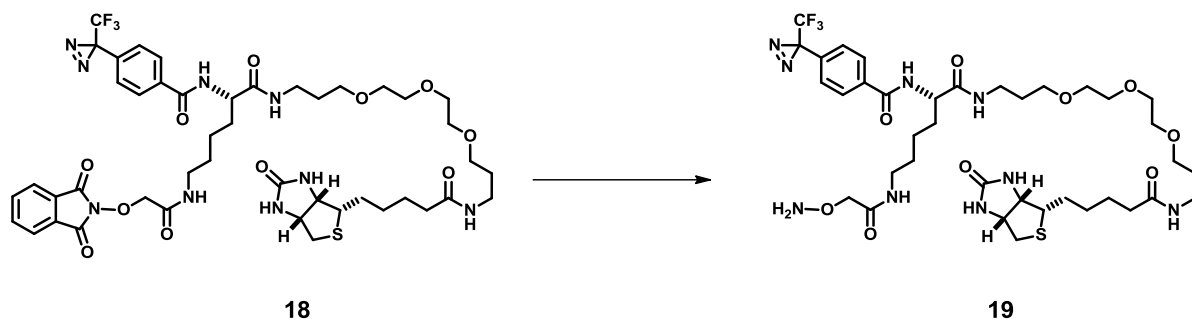
Diazirine amide **18** (1.4 mg, 1.4 µmol) was dissolved in dry dichloromethane (0.3 mL), and hydrazine monohydrate 1.0 µL (21 µmol) was added. After being stirred at room temperature for 10 min, the resulting mixture was filtered, and the filtrate was azeotropically concentrated with toluene to give alkoxyamine **19** (quant. monitored by TLC analysis: R_f 0.23, chloroform–methanol = 4/1), which was immediately used for the next step without further purification.

ApA-PB (**11**).

ApA-PB (**11**)
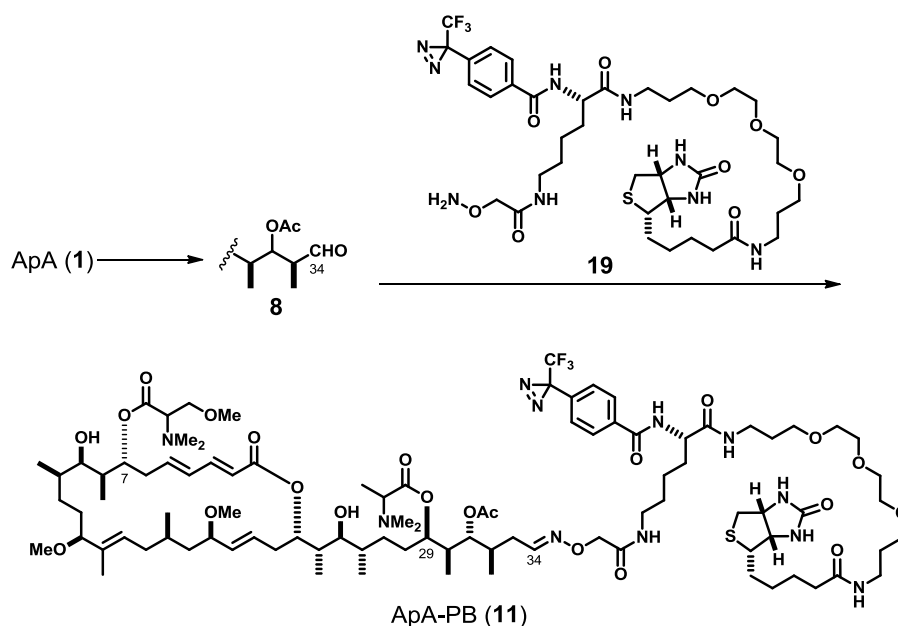
A solution of ApA (**1**) (0.32 mg, 300 nmol) in a 3:1 mixture of 1,4-dioxane (150 μL) and 2 M aq. HCl (50 μL) was stirred for 1 h at 50 °C. The resulting mixture was diluted with sat. sodium hydrogen carbonate aq. (250 μL) and water (2 mL) and extracted with chloroform (1 mL × 5). The combined extracts were washed with brine and concentrated to give aldehyde **8** (quant. monitored by HPTLC analysis: R_f 0.49, chloroform–methanol = 9/1), which was used for the next step without further purification.

A solution of the aldehyde **8** prepared from ApA (0.16 mg, 150 nmol) as described above and the alkoxyamine **19** in a 10:1 mixture of ethanol and 50 mM acetate buffer (pH 4.0) (0.22 mL) was stirred at room temperature for 22 h under a nitrogen atmosphere. The reaction mixture was directly applied to a Develosil ODS-HG-5 HPLC column (ϕ 20 mm I.D. × 250 mm). Samples were eluted with methanol–20 mM ammonium acetate (80:20) at a flow rate of 5 mL/min, with monitoring at 254 nm (t_R = 49–55 min) to give ApA-PB (**11**) (103 nmol, 69%, based on NMR quantification, E/Z = 7/3 for the C34 isomers). Compound **11**: ^{1}H NMR (600 MHz, CD$_3$OD) δ 7.97 (d, *J* = 8.7 Hz, 2H), 7.54 [6.80][1] (t, *J* = 6.0 Hz, 1H), 7.35 (d, *J* = 8.7 Hz, 2H), 7.20 (dd, *J* = 10.8, 15.1 Hz, 1H), 6.38 [6.39][2] (dd, *J* = 10.8, 15.3 Hz, 1H), 6.25–6.20 (m, 1H), 5.97 (br d, *J* = 14.8 Hz, 1H), 5.63 (ddd, *J* = 4.0, 10.6, 14.8 Hz, 1H), 5.55 (br d, *J* = 11.2 Hz, 1H), 5.12–5.07 (m, 1H),

4.95 (s, 2H), 5.00–4.80 (m, 3 H), 4.79 [4.78]^2 (d, J = 10.0 Hz, 1H), 4.48 (dd, J = 4.9, 7.9 Hz, 1H), 4.45 (dd, J = 5.3 Hz, 9.0 Hz, 1H), 4.36 [4.44]^1 (s, 2H), 4.29 (dd, J = 4.4, 7.9 Hz, 1H), 3.70–3.52 (m, 16H), 3.51 (t, J = 6.0 Hz, 2H), 3.50 (t, J = 6.1 Hz, 2H), 3.38 [3.34]^2 (s, 3H), 3.38–3.32 (m, 3H), 3.24 (t, J = 6.7 Hz, 2H), 3.21–3.16 (m, 1H), 3.18 (s, 3H), 3.15 (s, 3H), 3.07 (br d, J = 9.9 Hz, 1H), 2.91 (dd, J = 4,9, 12.7 Hz, 1H), 2.69 (d, J = 12.7 Hz, 1H), 2.54–2.25 (m, 5H), 2.38 [2.39]^2 (s, 6H), 2.34 [2.34]^1 [2.32]^3 [2.33]^{1,3} (s, 6H), 2.17 (t, J = 7.2 Hz, 2H), 2.20–2.10 (m, 1H), 2.04 [2.04]^1 [2.02]^3 [2.03]^{1,3} (s, 3H), 2.10–1.90 (m, 3H), 1.84–1.56 (m, 29H), 1.50 [1.51]^2 (s, 3H), 1.30 [1.29]^3 (d, J = 6.9 Hz, 3H), 1.18–1.06 (m, 3H), 1.04–0.95 (m, 12H), 0.91 (d, J = 6.9 Hz, 3H), 0.89 (d, J = 6.8 Hz, 3H), 0.76 [0.75]^2 (d, J = 5.8 Hz, 3H). Chemical shifts of the minor diastereomers are within brackets: [ ]^1 7:3 at C34 stereoisomers. [ ]^2 1:1 at C7 trimethylserine moiety. [ ]^3 3:1 at C29 dimethylalanine moiety. HRMS (ESI) m/z 648.3506 (calcd for [C$_{94}$H$_{152}$F$_3$N$_{11}$Na$_3$O$_{22}$S]/3 [M+3Na]$^{3+}$, Δ +1.3 mmu).

ApC (**2**).

ApA   ApC
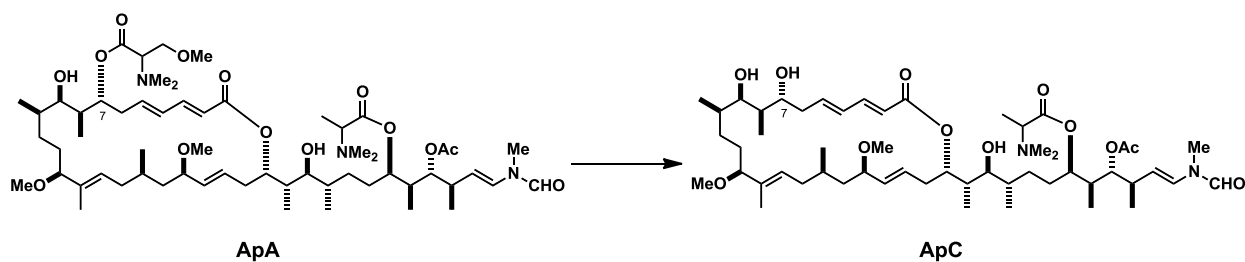
A solution of ApA (**1**) (0.65 mg, 600 nmol) in 0.1% triethylamine–methanol (14 mL) was stirred at 50 °C for 9 days. The reaction mixture was concentrated and applied to a Develosil ODS-HG-5 HPLC column (ϕ 20 mm I.D. × 250 mm). The fractions eluted with methanol–20 mM ammonium acetate (75:25) at a flow rate of 5 mL/min, with monitoring at 254 nm gave ApC (**2**) (245 nmol, 41%, based on NMR quantification, t_R = 43–47 min) and recovered ApA (226 nmol, 38%, t_R = 58–63 min) as colorless oils. All of the spectroscopic data of **2** prepared from ApA (**1**) were identical to those of the natural ApC.

ApC-PB (**12**).*   *The experiments performed by co-workers.
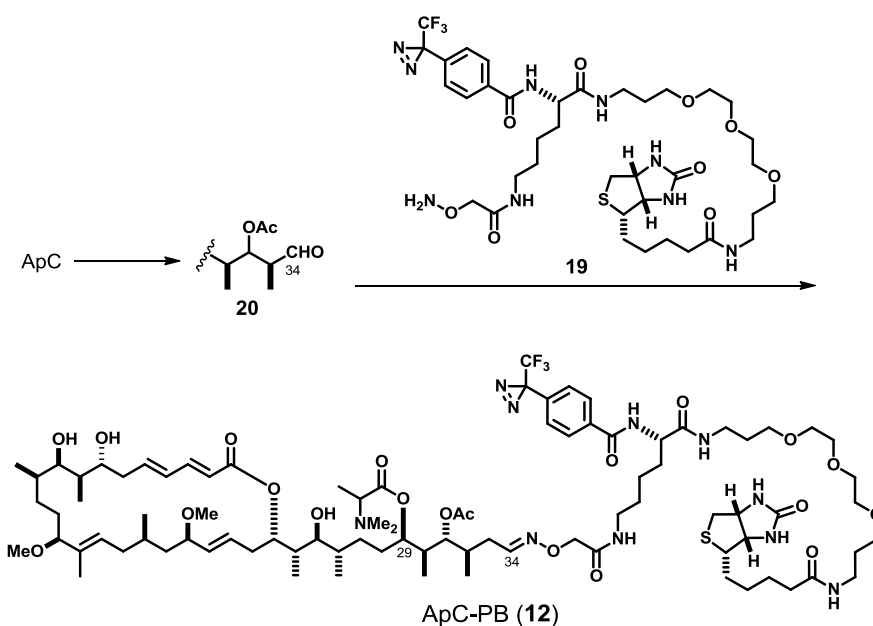
ApC-PB (**12**)

ApC-PB (**12**) was prepared from ApC (**2**) (170 μg, 179 nmol) and alkoxyamine **19** in 47% yield using the same procedure as that for ApA-PB (**11**). Compound **12**: t_R = 41–46 min [Develosil ODS-HG-5 (φ 20 mm I.D. × 250 mm), methanol–20 mM ammonium acetate (80:20), 5 mL/min, UV 254 nm]; ^{1}H NMR 600 MHz, CD$_3$OD) δ 7.96 (d, *J* = 8.5 Hz, 2H), 7.54 [6.80][1] (t, *J* = 6.4 Hz, 1H), 7.34 (d, *J* = 8.5 Hz, 2H), 7.24 (dd, *J* = 10.4, 15.3 Hz, 1H), 6.38 (ddd, *J* = 5.0, 9.8, 15.0 Hz, 1H), 6.31 (dd, *J* = 15.0, 10.4 Hz, 1H), 5.92 (d, *J* = 15.3 Hz, 1H), 5.65 (ddd, *J* = 5.0, 10.4, 14.8 Hz, 1H), 5.55 (br d, *J* = 11.4 Hz, 1H), 5.14 (m, 1H), 5.10 (m, 1H), 5.00–4.77 (m, 2H), 4.48 (dd, *J* = 4.4, 7.5 Hz, 1H), 4.46 (dd, *J* = 4.4, 8.0 Hz, 1H), 4.39 [4.44][1] (s, 2H), 4.29 (dd, *J* = 4.5, 7.8 Hz, 1H), 3.70–3.45 (m, 3H), 3.62-3.49 [4.21-3.95][1] (m, 16H), 3.33 (m, 1H), 3.24 (t, *J* = 6.8 Hz, 2H), 3.20 (m, 1H), 3.18 (s, 3H), 3.16 (s, 3H), 3.08 (dd, *J* = 2.8, 11.6 Hz, 1H), 2.91 (dd, *J* = 5.0, 12.8 Hz, 1H), 2.69 (d, *J* = 12.8 Hz, 1H), 2.47–2.41 (m, 1H), 2.37–2.27 (m, 5H), 2.34 [2.35][1] [2.33][2] [2.33][1,2] (s, 6H), 2.20–1.95 (m, 9H), 1.93–1.52 (m, 29H), 1.45 (s, 3H), 1.31 [1.30][2] (d, *J* = 6.7 Hz, 3H), 1.22–1.08 (m, 3H), 1.01–0.87 (m, 18H), 0.82 (d, *J* = 5.9 Hz, 3H). Chemical shifts of the minor diastereomer are within brackets: [ ][1] 7:3 at C34 stereoisomers. [ ][2] 1:1 at C29 dimethylalanine moiety. HRMS (ESI) *m/z* 885.4984 (calcd for [C$_{88}$H$_{142}$F$_3$N$_{10}$NaO$_{20}$S]/2 [M+H+Na]$^{2+}$ Δ –0.2 mmu).

References

1. Yamada, K.; Ojika, M.; Kigoshi, H.; Suenaga, K. *Nat. Prod. Rep.* **2009**, *26*, 27–43.

2. Thiede, B.; Hohenwarter, W.; Krah, A.; Mattow, J.; Schmid, M.; Schmidt, F.; Jungblut, P. R. *Methods* **2005**, *35*, 237–247.

3. Allingham, J. S.; Klenchin, V. A.; Rayment, I. *Cell. Mol. Life Sci.* **2006**, *63*, 2119−2134.

4. Wada, S.; Matsunaga, S.; Saito, S.; Fusetani, N.; Watabe, S. *J. Biochem.* **1998**, *123,* 946−952.

5. Ojika, M.; Kigoshi, H.; Yoshida, Y.: Ishigaki, T.; Nishiwaki, M.; Tsukada, I.; Arakawa, M.; Ekimoto, H.; Yamada, K.. *Tetrahedron* **2007**, *63*, 3138–3167.

6. Wilbur, D. S.; Hamlin, D. K.; Vessella, R. L.; Stray, J. E.; Buhler, K. R.; Stayton, P. S.; Klumb, L. A.; Pathare, P. M.; Weerawarna, S. A. *Bioconjugate Chem.* **1996**, *7*, 689–702.

7. Clave, G.; Boutal, H.; Hoang, A.; Perraut, F.; Volland, H.;Renard, P. Y.; Romieu, A. *Org. Biomol. Chem.* **2008**, *6*, 3065−3078.

8. Nassal, M. *Liebigs. Ann. Chem.* **1983**, 1510–1523.

9. a) Mullins, R. D.; Heuser, J. A.; Pollard, T. D. *Proc. Natl. Acad. Sci. USA* **1998**, *95*, 6181–6186. b) Blanchoin, L.; Amann, K. J.; Higgs, H. N.; Marchand, J. B.; Kaiser, D. A.; Pollard, T. D. *Nature* **2000**, *404*, 1007–1011.

10. Shevchenko, A.; Wilm, M.; Vorm, O.; Mann, M. *Anal. Chem.* **1996**, *68*, 850–858.

Chapter 3.

Study on the Interaction of Aplyronine A with Tubulin

Abstract

In vitro labeling experiments with photoaffinity biotin probes and tubulin polymerization assay showed that ApA synergistically binds to tubulin in association with actin and inhibits tubulin polymerization. Through the gel-permeation HPLC analysis, it was revealed that ApA forms a 1:1:1 heterotrimeric complex with actin and tubulin heterodimer.

3.1. Introduction

It is known that the primary target protein of ApA (**1**) is actin. As shown in chapter 2, in situ photoaffinity labeling experiments revealed that ApA-PB (**11**) also specifically binds to tubulin in cells. A lot of compounds targeting actin or tubulin have been reported (see chapter 1). To the best of my knowledge, ApA (**1**) is the first small compound which interacts with both actin and tubulin. It is unknown whether ApA (**1**) interacts with both actin and tubulin together. Also it is still unclear how ApA (**1**) affects cellular functions through the interaction with tubulin to exhibit potent antitumor activity. Therefore it is required to analyze more detail interactions between ApA (**1**) and tubulin. Fortunately both purified actin and tubulin are commercially available, and their biochemical experiments have been developed.

In this chapter, study on the interaction of ApA (**1**) with tubulin was carried out to analyze the binding mode among ApA (**1**), actin and tubulin. In vitro labeling experiments using photoaffinity probes, tubulin-polymerization assay and gel-permeation HPLC analysis were examined.

3.2. In vitro analysis of the interaction of ApA with tubulin

3.2.1. Labeling experiments of purified proteins with ApA-PB

In vitro photolabeling experiments with purified proteins were carried out to investigate specific interactions among ApA (**1**), actin, and tubulin (Figure 3-1). Tubulin and/or actin incubated in the presence of 0.67 μM ApA-PB (**11**) for 30 min. After the photoreaction, labeled proteins were detected by WB analysis with HRP conjugate streptavidin (Figure 3-2).
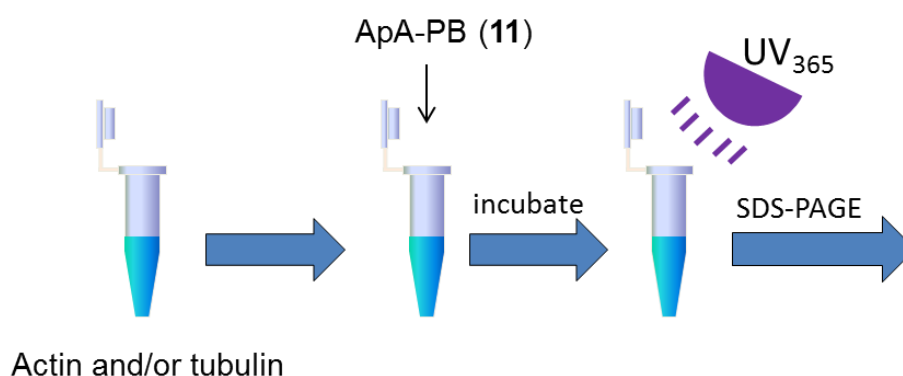

Figure 3-1. Outline of in vitro labeling experiments.

ApA-PB (**11**) formed a covalent bond with actin but not with tubulin alone (lanes 1 and 3). In the presence of actin, however, tubulin was photolabeled with ApA-PB (**11**) and detected as two biotin-labeled protein bands (55 and 58 kDa) (lane 3), as with in situ experiments (see figure 2-22). These results revealed that the 55 kDa protein also derived from α- or β-tubulin. It was found that actin is necessary for interaction of ApA (**1**) with tubulin, which suggested that ApA-actin complex interact with tubulin to form ternary complex (Figure 3-3). Although stoichiometric amounts of tubulin were used, the amount of tubulin photolabeled by ApA-PB (**11**) was far less than that of actin. Photolabeling by ApA-PB (**11**) might occur at several places following the random movement of a flexible diazirine moiety on the ternary complex. Thus it is inferred that the aryldiazirine group of ApA-PB (**11**) is located inside of actin and it is difficult to reach and interact with the tubulin.
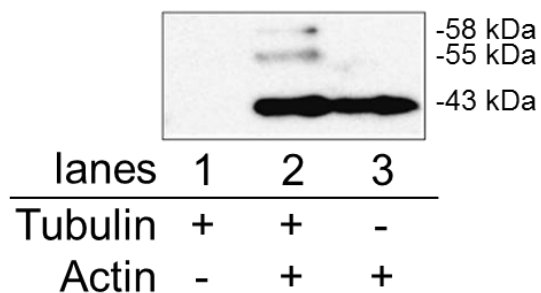
Figure 3-2. In vitro photolabeling experiment of actin and/or tubulin with ApA-PB (**11**). After photoreaction

with actin and tubulin, labeled proteins were detected by HRP conjugate streptavidin.
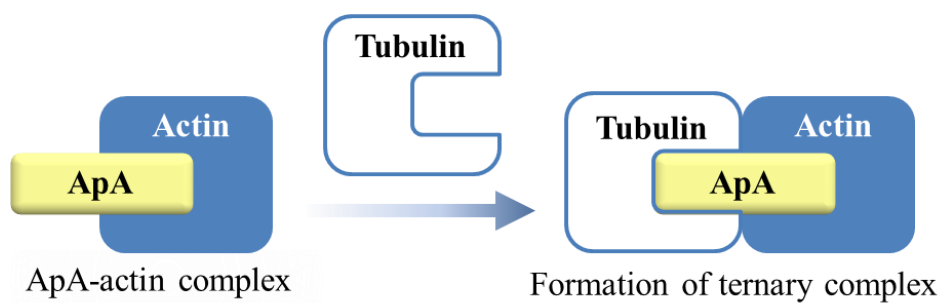

Figure 3-3. Actin-ApA complex may interact with tubulin to form the ternary complex.

3.2.2. Design, synthesis and biological activities of ApA-DPB

3.2.2.1. Conformational search of ApA-PB on actin

The C24−C34 side chain of ApA (**1**) binds to the hydrophobic cleft between SD 1 and 3 of actin, and the aryldiazirine group in ApA-PB (**11**) is thought to be located inside of actin. To confirm this hypothesis, conformational search of ApA-PB (**11**) on actin were performed using the software MOE (Molecular Operating Environment, Chemical Computing Group Inc.). The initial structure of actin-ApA-PB complex was constructed by replacing the side chain part of ApA (**1**) on the X-ray crystal structure of actin-ApA complex. Conformational search of ApA-PB (**11**) was performed at the molecular mechanics level using the Amber12-EHT force-field, under the condition that both ApA moiety of ApA-PB (**11**) and actin were fixed. Six representative conformations within 19 kcal/mol of global minimum structure were superposed in figure 3-4. As expected, the results of conformational search suggested that the diazirine moiety of ApA-PB (**11**) was peripherally located in hydrophobic cleft of SD 1 and 3 of actin. Therefore, it is difficult that the diazirine group of ApA-PB (**11**) binds efficiently to tubulin compared with actin.

a)
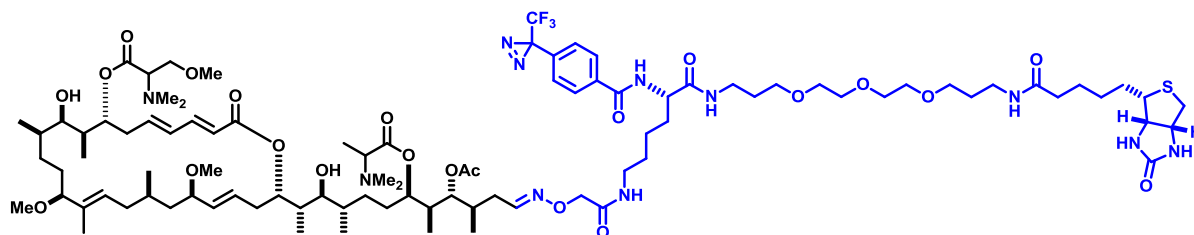
b)
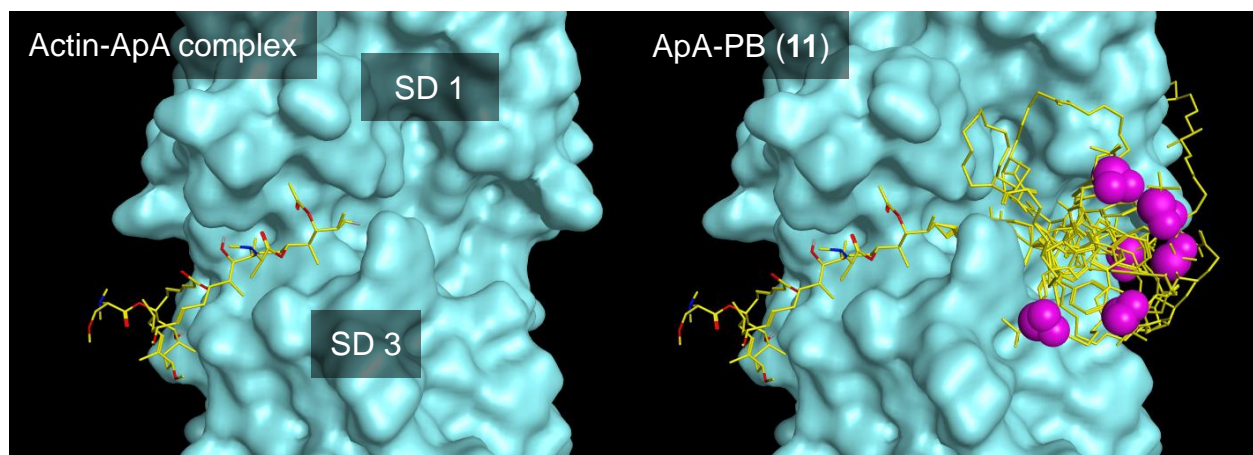
Figure 3-4. Conformational search of ApA-PB on actin by using MOE. a) Strucuture of ApA-PB (**11**). The bule-colored partial structure is movable in this conformational search. b) In the left, X-ray crystallographic structure of actin-ApA complex was shown (PDB code: 1WUA). In the right, six representative conformations were superposed in which conformation within 19 kcal/mol of global minimum structure. Diazirine groups are shown as pink spheres. Among 941 conformations within 19 kcal/mol of global minimum structure, all diazirine groups existed inside the area of representative structures.

3.2.2.2. Design of ApA-DPB

To enhance the flexibility of the photoreacting group and allow it to reach toward the C7 trimethylserine ester moiety, that was believed to be important for binding to tubulin, ApA double-PEG-linked photoaffinity biotin probe (ApA-DPB, **21**) were designed (Figure 3-5). Conformational search of ApA-DPB (**21**) on actin were carried out in the same way of ApA-PB (**11**). As shown in figure 3-6, the diazirine group of ApA-DPB (**21**) can protrude from the SD 1 and 3 cleft and locate on the wide area of actin surface. Therefore, it was expected that the diazirine group of ApA-DPB (**21**) might be more accessible to tubulin than that of ApA-PB (**11**). In accordance with this hypothesis, ApA-DPB (**21**) was synthesized and compared with its tubulin-binding property with that of ApA-PB (**11**).
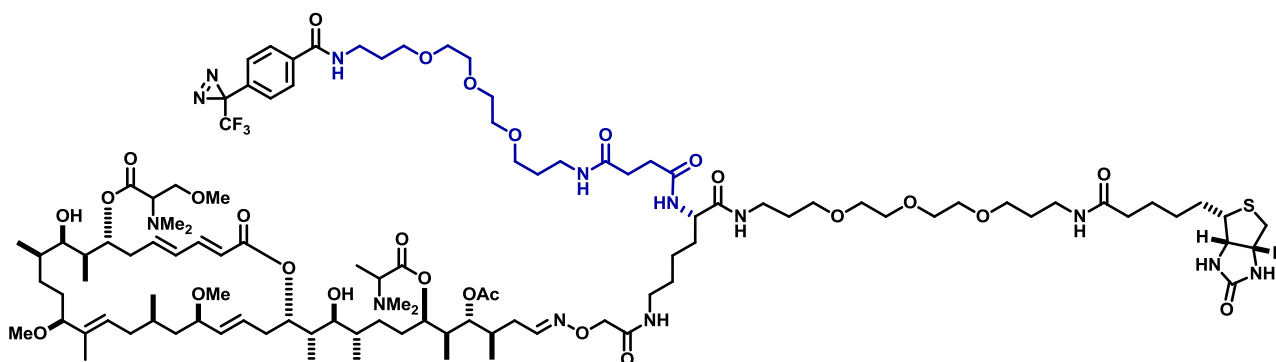

Figure 3-5. Structure of ApA-DPB (**21**).

a)
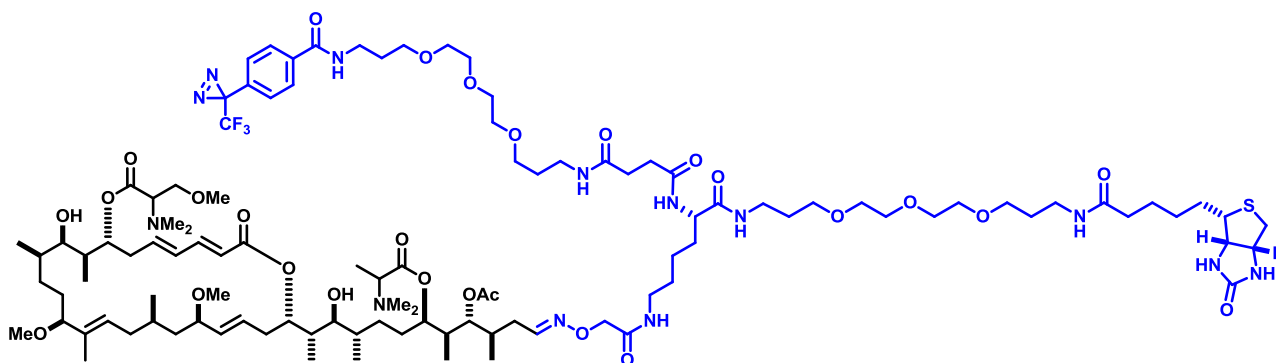
b)
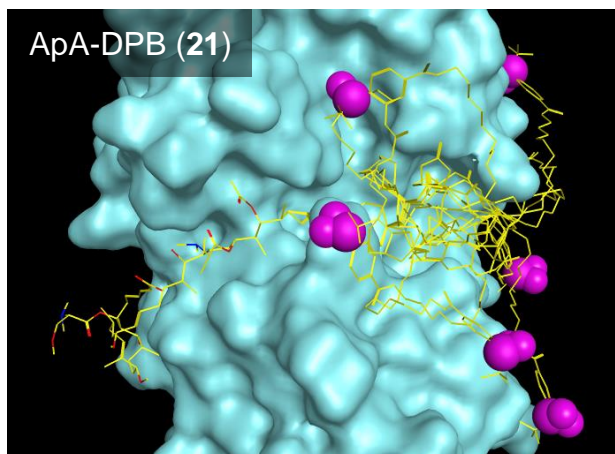
Figure 3-6. Conformational search of ApA-PB on actin by using MOE. a) Strucuture of ApA-PB (**12**). The bule-colored partial structure is movable in this conformational search. b) Six representative conformations were superposed in which conformation within 20 kcal/mol of global minimum structure. Diazirine groups are shown as pink spheres. Among 224 conformations within 20 kcal/mol of global minimum structure, all diazirine groups existed inside the area of representative structures.

3.2.2.3. Synthesis of alkoxyamine 27

To synthesize the ApA-DPB (**21**), alkoxyamine **27** was synthesized (scheme 3-1). First, succinyl ester **23** was prepared by condensation of carboxylic acid **22** with *N*-hydroxysuccinimide (NHS) (84%). Acidic cleavage of the Boc group in **15** with TFA followed by coupling with succinyl ester **23** in the presence of DIPEA yielded amide **24** (61% in 2 steps). Deprotection of the Boc group in **24** followed by condensation of amine **25** with succinyl ester **17**[1] gave amide **26** (97% in 2 steps). Finally, deprotection of Phth group in **26** yielded alkoxyamine **27** (quant.).
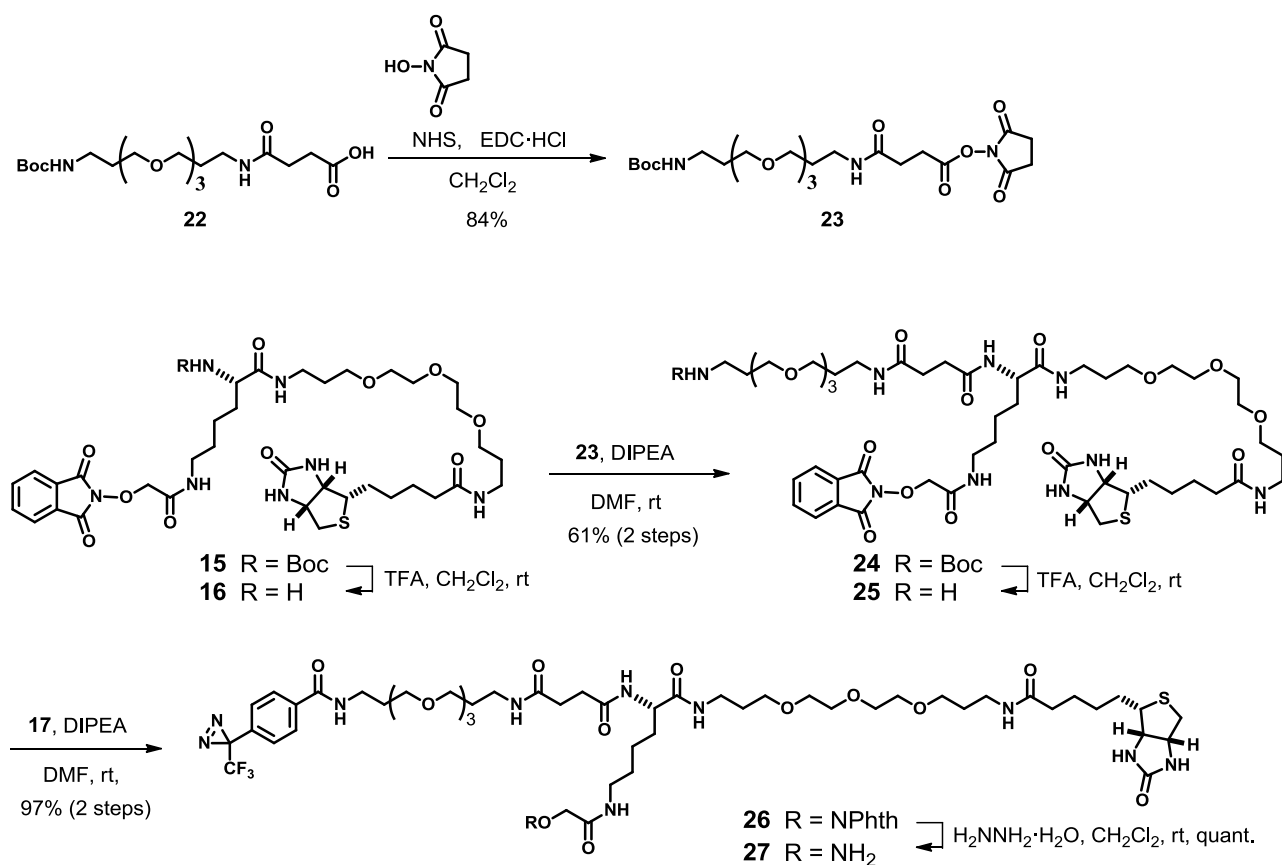
Scheme 3-1. Synthesis of alkoxyamine **27**.

3.2.2.4. Synthesis of ApA-DPB

Conversion from ApA (**1**) to aldehyde **8** by the acidic hydrolysis of the enamide group followed by the condensation reaction with alkoxyamine **27** gave ApA-DPB (**21**) (50% in 2 steps) (Scheme 3-2).
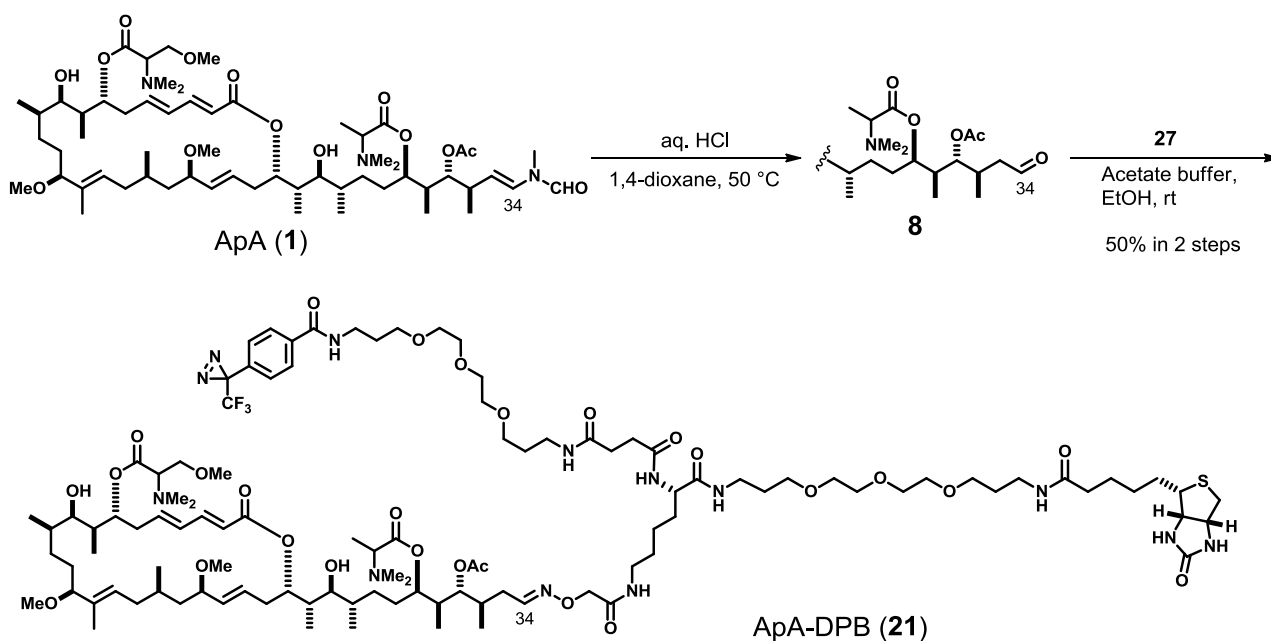
Scheme 3-2. Synthesis of ApA-DPB (**21**)

3.2.2.5. Cytotoxicity of ApA-DPB

The cytotoxicity of ApA-DPB (**21**) was compared with those of ApA (**1**) and ApA-PB (**11**) (Table 3-1). Cytotoxicity of ApA-DPB (**21**) was 50 times less than ApA (**1**) and 2-fold more than ApA-PB (**11**).

Table 3-1. Cytotoxicity of ApA-DPB (**21**)

Compound	Cytotoxicity against HeLa S3 cells IC$_{50}$ (nM)
ApA (**1**)	0.010
ApA-PB (**11**)	1.2
ApA-DPB (**21**)	0.54

89

3.2.3. Labeling experiments of purified proteins with ApA-DPB or ApC-PB.

Labeling experiments using ApA-DPB (**21**) were performed (Figure 3-7). As expected, ApA-DPB (**21**) increased the amounts of photolabeled tubulins (55 and 58 kDa) and also slightly increased the amount of photolabeled actin (lane 3), in comparison to the treatment with ApA-PB (**11**) (lane 1).

To investigate whether tubulin specifically interacts with ApA (**1**), labeling experiments using ApC-PB (**12**) were also performed (lane 2). ApC-PB (**12**) did not label tubulin even in the presence of actin as well as in situ experiments (Figure 2-22). These results suggested that the trimethylserine moiety of ApA (**1**) plays a key role in the interaction with tubulin, and that the potent antitumor activity of ApA (**1**) is due to the interaction with tubulin.
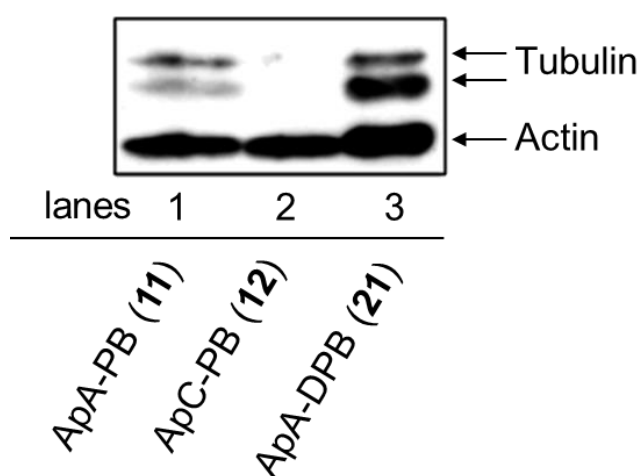

Figure 3-7. Labeling experiments with aplyronine photoaffinity probes. After photoreaction with actin and tubulin, labeled proteins were detected by HRP conjugate streptavidin.

3.2.4. Tubulin polymerizing assay

In general, tubulin-interactive agents exhibit antitumor activity through the disruption of polymerization or depolymerization of tubulin. In vitro tubulin polymerization assay[2] was examined to establish whether aplyronines affects microtubule assembly. Tubulin was polymerized with 20% glycerol at 37 °C. The polymerization of tubulin immediately started and reached plateau after 20 min under this condition (Figure 3-8. control). When 10 μM of vinblastine (VBL), known tubulin-polymerizing inhibitor, was added, fluorescent intensity did not increase, which indicated that tubulin did not polymerized. (Figure 3-9). While 10 μM of actin or ApA (**1**) alone had little effect on in vitro tubulin polymerization, their 1:1 complex (10 μM) delayed nucleation and growth phases and reduced the final polymer mass of tubulin in a dose-dependent manner (Figure 3-8). In contrast, the actin-ApC complex (9 μM) failed to attenuate microtubule growth (Figure 3-9).
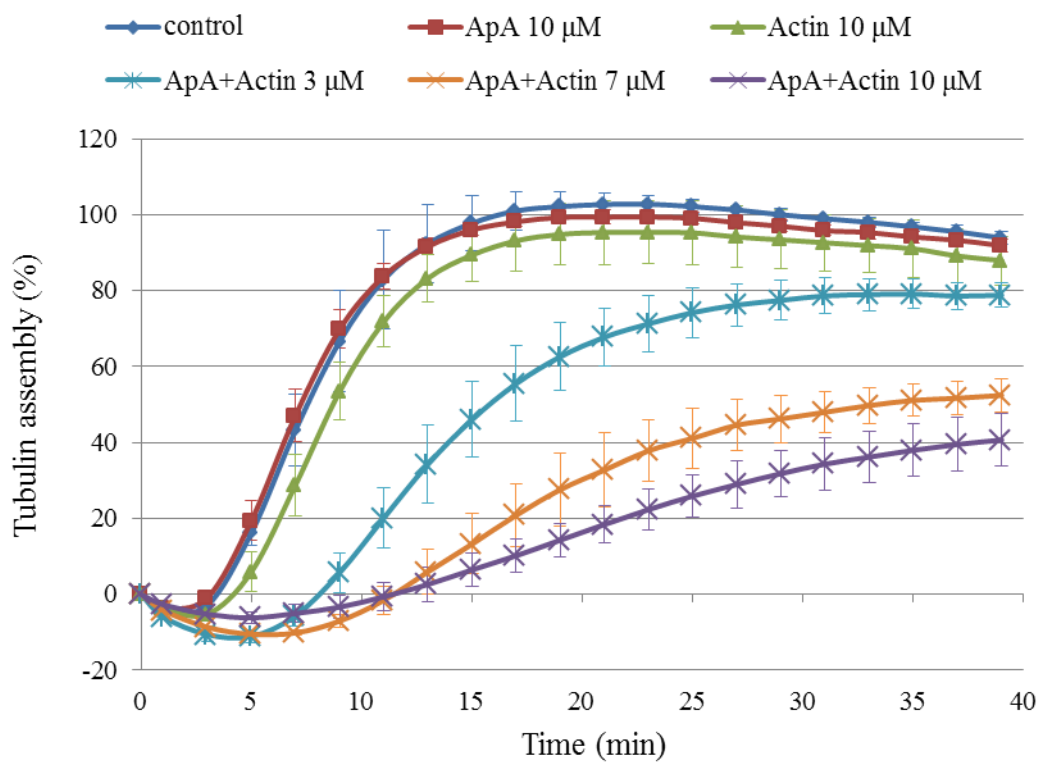
Figure 3-8. Tubulin polymerization assay. Tubulin was polymerized with 20% glycerol at 37 °C, as monitored by an increase in DAPI fluorescence ($\lambda_{ex}/\lambda_{em}$ 360/450 nm). Values are the mean ±SDs of four independent experiments.
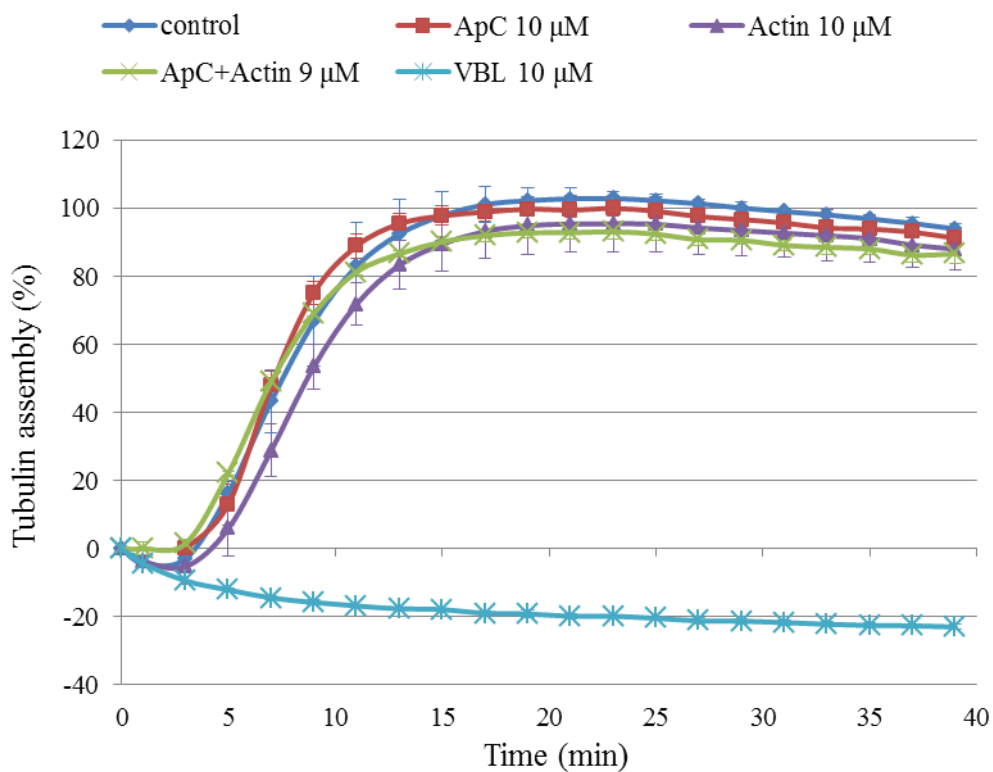
Figure 3-9. Tubulin polymerization assay. Tubulin was polymerized with 20% glycerol at 37 °C, as monitored by an increase in DAPI fluorescence ($\lambda_{ex}/\lambda_{em}$ 360/450 nm). Values are the mean ±SDs of four independent experiments.

3.2.5. Analytical ultracentrifugation

To confirm that ApA (**1**) inhibit tubulin polymerization in association with actin, ultracentrifugation experiments were carried out (Figure 3-10). Polymerized tubulin was precipitated by ultracentrifugation and dominantly detected in the precipitate (P) fraction (lanes 1), while depolymerized tubulin was detected in the supernatant (S) fraction (lane 2). In the presence of ApA (**1**) or actin, tubulin was polymerized and detected in the P fraction (lanes 3 and 4). Actin was polymerized in this tubulin stabilizing buffer condition and precipitated (lane 6), while actin was depolymerized in the presence of ApA (**1**) and detected in the S fraction (lane 7). Thus it was indicate that actin-ApA complex can be formed in this buffer condition. Only upon treatment with both ApA (**1**) and actin, the tubulin was observed mostly in the S fraction along with actin, which suggested that actin-ApA complex inhibited the polymerization of tubulin (lane 5). ApA (**1**), actin and tubulin synergistically interact to form ternary complex.
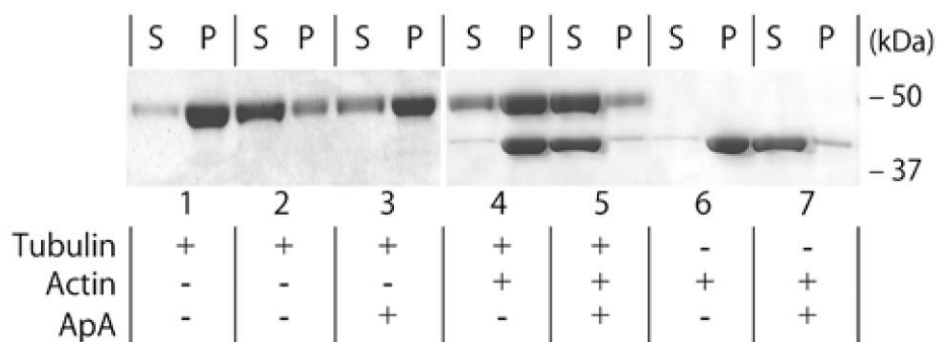

Figure 3-10. Tubulin sedimentation assay. Tubulin (3 μM) was polymerized with paclitaxel (3 μM). In lane 2, CaCl$_2$ (5 mM) was added instead of paclitaxel to inhibit tubulin polymerization. Proteins in the supernatant (S) and the precipitate (P) were analyzed by SDS-PAGE, and detected with CBB stain.

## 3.3. Analysis of the binding mode of ternary complex

Experiments of section 3.2. led to the conclusion that ApA and actin synergistically interact with tubulin and inhibit tubulin polymerization. Next my question is what kind of the ternary complex was formed to inhibit the tubulin polymerization. To analyze and detect the ternary complex, gel-permeation HPLC analysis was examined.

### 3.3.1. Gel-permeation HPLC analysis of ternary complex

Tubulin, actin and/or ApA were analyzed with gel-permeation HPLC (Figure 3-11). Tubulin was detected as a single peak (t_R 16.31 min) in the tubulin stabilizing buffer.[3] The retention time of the peak was compared with these of standard proteins (Figure 3-12), which indicated that the molecular weight was 106 kDa, so tubulin was eluted as heterodimer (100 kDa). Actin was polymerized in the tubulin stabilizing buffer, so it was difficult to analyze actin alone. When a mixture of actin and ApA was analyzed, a single peak (t_R 18.24 min) corresponding to 42.7 kDa was detected suggesting the formation of actin-ApA complex (44 kDa). When the actin-ApA complex and tubulin were coanalyzed, a mobility peak (t_R 15.42 min) appeared that was faster than both tubulin heterodimer and actin-ApA complex peaks, and the latter two were reduced. To confirm the peak is a ternary complex, components of the peaks were analyzed by SDS-PAGE. Detection with CBB stain and anti-α/β-tubulin revealed that the faster mobility peak contained both actin and α/β-tubulin. The retention time indicates that the ternary complex corresponded to the 1:1:1 complex of actin-ApA-tubulin heterodimer (145 kDa).

Gel-permeation HPLC analysis with ApC (**2**) instead of ApA (**1**) was conducted (Figure 3-13). Ternary complex was not detected, and instead, two peaks corresponding to the actin-ApC complex and tubulin heterodimer were detected. It was confirmed by SDS-PAGE analysis that these two peaks were the actin-ApC complex and tubulin heterodimer, respectively. This result was corresponding to tubulin polymerization assay and photolabeling experiments. These results suggested that ApC (**2**) cannot form the ternary complex with actin and tubulin.

a) Gel-permeation HPLC
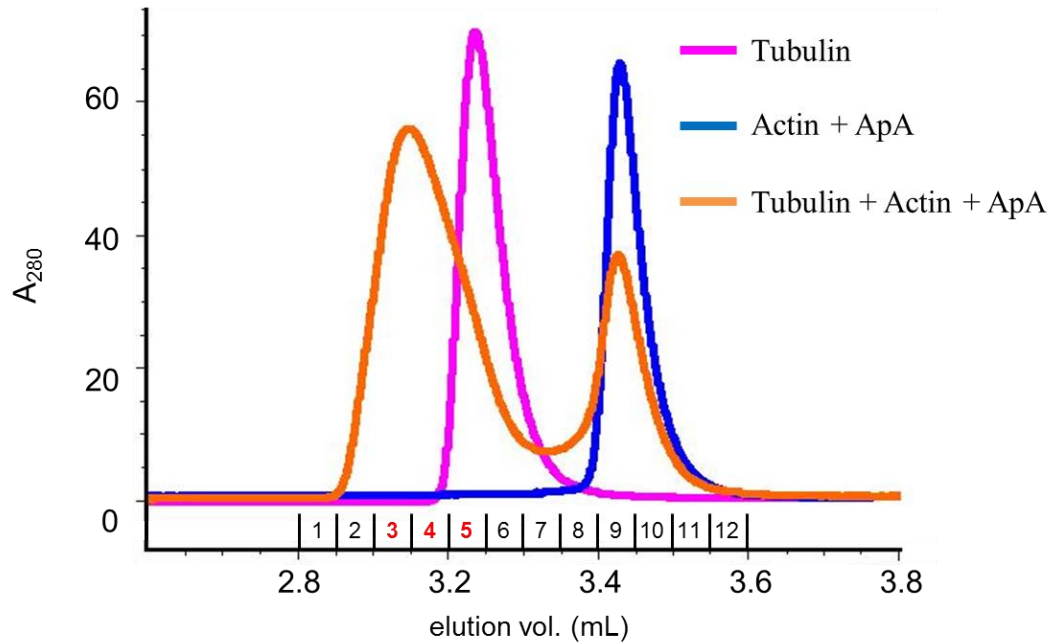
b) CBB stain
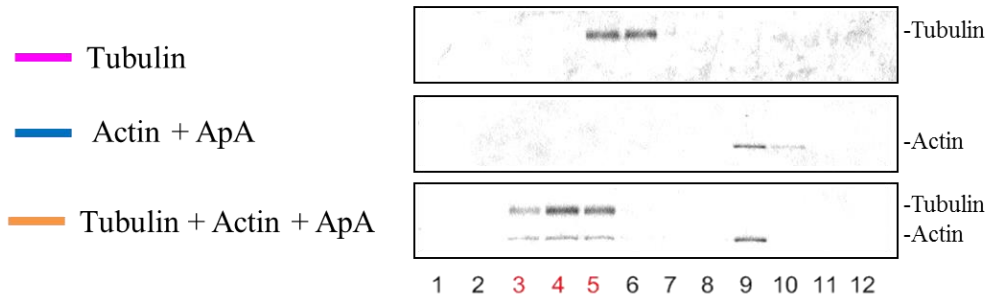
c) Immunoblotting analysis
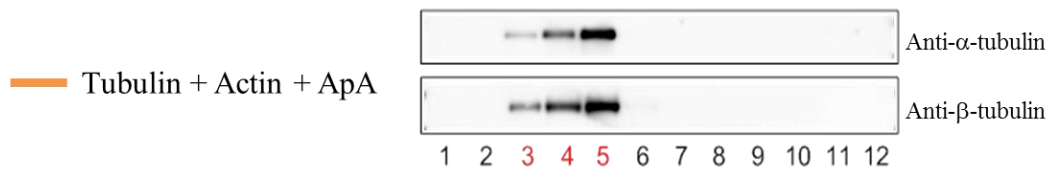
Figure 3-11. (a) Gel-permeation HPLC analysis of tubulin and/or actin-ApA complex. Column, TSKgel SuperSW3000 (φ 4.6×300 mm); flow rate, 0.2 mL/min; temp., 8 °C; detection, UV 280 nm.; Elution proteins (fractions 1−12) were detected with (b) CBB stain and (c) immunoblotting using anti-α/β-tubulin.
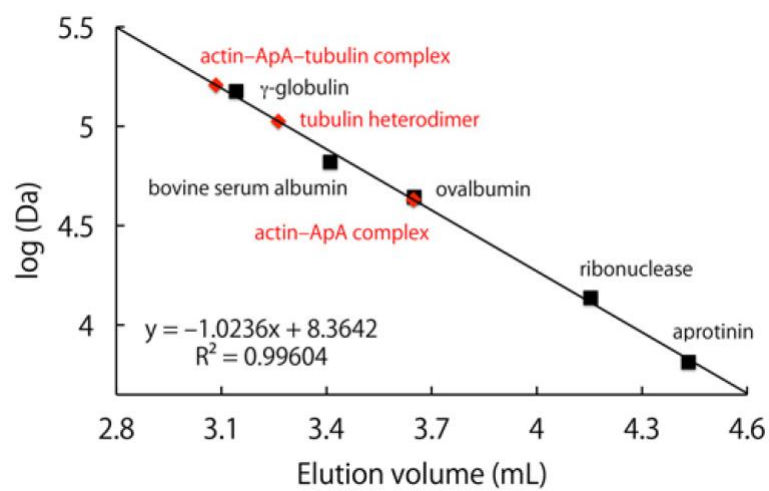
Figure 3-12. Standard curve. Column, TSKgel SuperSW3000 (ϕ 4.6 × 300 mm). Buffer, 50 mM PIPES·K (pH 6.8), 100 mM KCl, 10 mM MgCl$_2$. Temp., 8 °C. The column was calibrated using protein standards, and a standard curve is shown in the graph.

a) Gel-permeation HPLC
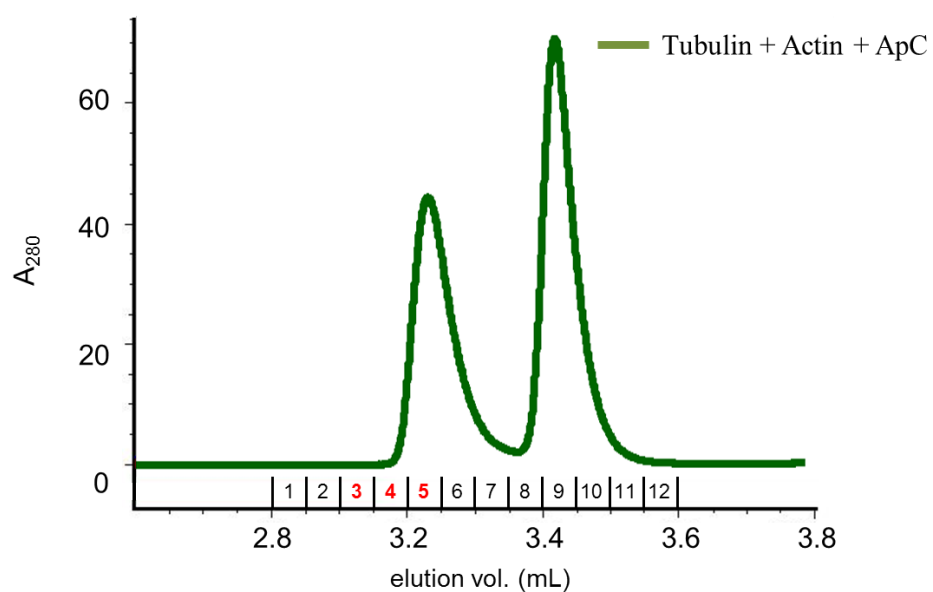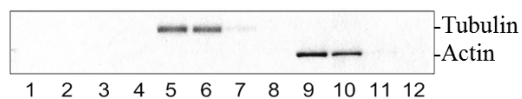
b) CBB stain

Figure 3-13. (a) Gel-permeation HPLC analysis with ApC. Column, TSKgel SuperSW3000 (ϕ 4.6×300 mm); flow rate, 0.2 mL/min; temp., 8 °C; detection, UV 280 nm.; (b) Elution proteins (fractions 1−12) were detected with CBB stain.

A densitometric analysis of the CBB-stained bands (figure 3-11, b, tubulin + actin + ApA) showed that the quantitative ratios of tubulin-actin in lanes 2 and 3 in figure 3-14 were 1.6:1 and 2.7:1, respectively. These values were consistent with the calculated value for 1:1 ratios of 100 kDa tubulin heterodimer-43 kDa actin. While we have no evidence regarding the stoichiometry of ApA in the ternary complex, it is likely that the 1:1 actin-ApA complex binds to a tubulin heterodimer on the basis of the x-ray structural analysis of the complex. This ternary complex was stable in solution for at least 1 h, despite being in equilibrium with the actin-ApA complex and the liberated tubulin heterodimer.
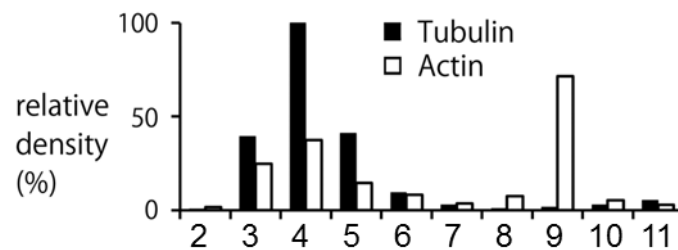
Figure 3-14. Densitometric analysis of the actin and tubulin complex bands (figure 3-10, b, tubulin + actin + ApA). The relative protein amounts were shown.

3.3.2. Scatchard plot analysis.

To examine binding modes and strength of the interaction between actin-ApA complex and tubulin heterodimer, kinetics analysis was carried out. (Figure 3-15, a). Various concentrations of actin and constant concentration of tubulin and ApA were analyzed with gel-permeation HPLC. The peak of ternary complex was increased and the peak of tubulin was decreased with increased concentration of actin. The peak of actin also appeared when actin concentration was above 0.75 equivalence. Elution proteins were stained with CBB, and the concentrations (= $[D_f]$) of actin-ApA complex unbound to tubulin (fr 1–6) were calculated based on the densitometry of CBB-stained bands. Also the ratio (= r) of tubulin that forms a ternary complex with actin–ApA to the total tubulin was calculated. The Scatchard plot was constructed by plotting the values of $r/[D_f]$ against r (Figure 3-15, b). The binding constant of the actin-ApA complex to tubulin heterodimer was estimated to be 3.0×10^6 M^{-1} on the basis of a Scatchard plot analysis. The r value converges to approximately 1, which indicates that the actin-ApA complex binds to tubulin heterodimer to form 1:1 complex.
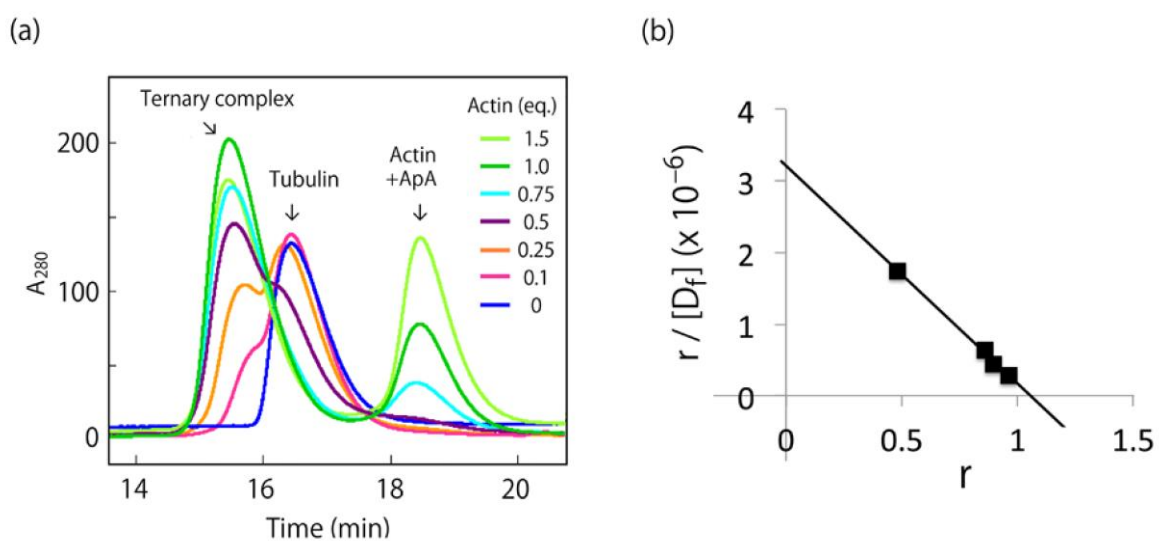
Figure 3-15. Gel-permeation HPLC analysis. (a) Dose-dependence of actin for the formation of ternary complex. Tubulin (27.5 μM for the heterodimer) and ApA (275 μM) were mixed with various concentrations of actin (0 to 41.2 μM) before injection. Buffer, 50 mM PIPES·K (pH 6.9), 100 mM KCl, 5 mM DTT, 10 mM MgCl$_2$. Column, TSKgel SuperSW3000 (φ 4.6 × 300 mm). Flow rate 0.2 mL/min., Temp. 12 °C, Detection UV 280 nm. (b) Scatchard plot analysis for the ternary complex.

3.4. Conclusion

To analyze the binding mode among ApA, actin, and tubulin, in vitro labeling experiments using photoaffinity probes, tubulin-polymerization assay, and gel-permeation HPLC analysis were conducted.

In vitro photolabeling experiments showed that ApA-PB synergistically bound to tubulin in association with actin. In contrast, ApC-PB was failed to bind to tubulin even in the presence of actin. Therefore, It was strongly suggested that trimethylserine ester of ApA is essential for the interaction with tubulin.

To enhance the labeling efficiency of tubulin, ApA-DPB, in which the photoaffinity group was connected with a long PEG linker, was synthesized and showed enhancement of labeling efficiently of tubulin.

Tubulin-polymerization assay and ultracentrifugation analysis revealed that ApA inhibited polymerization of tubulin in the presence of actin.

When tubulin, actin and ApA were coanalyzed by gel-permeation HPLC, the peak of ternary complex was observed. The retention time and SDS-PAGE analysis revealed that the ternary complex corresponded to the 1:1:1 complex of actin−ApA–tubulin heterodimer. The binding constant of the actin-ApA complex to tubulin heterodimer was estimated to be $3.0 \times 10^6 \, \mathrm{M}^{-1}$ on the basis of the Scatchard plot analysis.

These result revealed that ApA synergistically binds to tubulin in association with actin, and inhibits tubulin polymerization. To the best of my knowledge, ApA is a first compound that form the ternary complex with two cytoskeletal proteins, actin and tubulin.

3.5. Experimental

3.5.1. General

Aplyronine A was isolated from the sea hare by the methods described in chapter 2. Actin and antibodies were obtained from commercial suplies. Tubulin was isolated from the porcine brain by the method described.[3] Chemicals and solvents were the best grade available and were used as received from commercial sources. For bioassay, ApA and its derivatives were stored in DMSO at 1 mM, actin was stored in G-buffer [2 mM Tris·HCl (pH 8.0), 0.2 mM $CaCl_2$, 0.2 mM ATP, 0.5 mM 2-mercaptoethanol] at 5 mg/mL, and tubulin was stored in RB buffer [100 mM MES (pH 6.8), 0.5 mM $MgCl_2$, 1 mM EGTA] at 11 mg/mL, unless otherwise noted. To protect aryl diazirine derivatives from the light, all synthetic and biological experiments with aryl diazirine derivatives were conducted with light-shaded glass or plastic equipments, or under a yellow-filtered light hood. All of the following experiments that used cell lysate and proteins were performed on ice unless otherwise noted. The protein concentration was measured with a Bio-Rad Protein Assay Kit (Bradford's method) with BSA as a standard.

TLC analysis was conducted on E. Merck precoated silica gel 60 F_{254} (0.25 mm layer thickness) or HPTLC Silica gel 60 WF_{254}. Fuji Silysia silica gels BW-820 MH and FL-60D, Merck Aluminum oxide 90 standardized, and Nacalai tesque COSMOSIL 75C_{18}-OPN were used for open column chromatography. NMR spectra were recorded on a Bruker Biospin AVANCE 600 spectrometer (600 MHz for ^{1}H and 150 MHz for ^{13}C), or a Bruker Biospin AVANCE 400 spectrometer (400 MHz for ^{1}H and 100 MHz for ^{13}C). Chemical shifts are reported in parts per million (ppm) with coupling constants (J) in hertz relative to the solvent peaks, δ_H 3.30 (residual CHD_2OD) and δ_C 49.0 for CD_3OD, δ_H 7.26 (residual $CHCl_3$) and δ C 77.0 for $CDCl_3$, or δ_H 2.50 (residual $CHD_2S(O)CD_3$) and δ_C 39.5 for $(CD_3)_2S=O$, respectively. For the quantification of minute amounts of specimens by ^{1}H NMR analyses, benzene (10 mM in CD_3OD) was added to the sample solutions as a standard (1:60 v/v). Optical rotations were measured with a JASCO DIP-1000 polarimeter. IR spectra were recorded on a JASCO FT/IR-230 spectrometer. High-resolution electrospray ionization mass spectra

(HR-ESIMS) were measured on a QSTAR Pulsar *i* spectrometer (Applied Biosystems) or an AccuTOF CS spectrometer (JEOL). Matrix-assisted laser desorption/ionization with time-of-flight mass spectrometry (MALDI-TOF MS) was performed using a Bruker ultrafleXtreme spectrometer with α-cyano-4-hydroxycinnamic acid (CHCA) as a matrix.

3.5.2. Cell culture and cytotoxicity assay.

Culture of HeLa S3 cells and cytotoxicity assay were conducted as previously described in chapter 2.

3.5.3. In situ photolabeling experiments

General procedure

ApA–PB (**11**) or ApC–PB (**12**) were added to the HeLa S3 cells in a 6-well plate (80% confluent). For competition experiments, ApA was added simultaneously. After incubation for 2 h at 37 °C, the cells were cooled on ice and irradiated with UV light (365 nm) for 15 min, using a handheld UV lamp (0.8 mW/cm^2). The culture medium was removed, and the cells were lysed in 200 μL of lysis buffer [10 mM Tris·HCl (pH 7.4), 0.15 M NaCl, 1% Triton X-100, 10 μg/mL leupeptin]. After the freeze-thawing process, which was repeated five times, the lysate were filtered (Millipore 0.45 μm centrifugal filter), and treated with NeutrAvidin agarose resin (40 μL, Pierce), equilibrated with lysis buffer. After incubation with a rotator for 1 h at 4 °C, the resins were washed four times with 0.1% Tween 20 in PBS (PBS-T), three times with 0.1% Tween 20 in 1 M KCl, and twice with PBS, then resuspended in 2 × SDS buffer (40 μL, Sigma). The binding proteins were eluted by boiling for 5 min at 95 °C. SDS-PAGE was performed by using a precast 10% polyacrylamide gel, and the gels were stained with a Silver Stain Kit, Protein (GE Healthcare).

For immunoblot analyses, proteins in the gels after electrophoresis were transferred to PVDF membranes, using the Trans-Blot® SD semi-dry blotting system (Bio-Rad), according to the manufacturer's instructions. After transfection, PVDF membranes were blocked with 0.5% skim-milk in PBS-T. Proteins were detected with HRP-conjugated streptavidin (1:3000, cat. no. RPN1231v, GE Healthcare), rabbit polyclonal

anti-β-actin (1:200, cat. no. A2066, Sigma), anti-α-tubulin (1:500, cat. no. RB-9281, Thermo) or anti-α-tubulin (1:500, cat. no. RB-9249, Thermo). For all primary antibodies, proteins were further treated with HRP-conjugated anti-rabbit IgG (1:2000, cat. no. NA934, GE Healthcare). The HRP-conjugated bands were visualized with an ECL-prime system (GE Healthcare), and detected by a Fujifilm LAS-4000 MINI imaging scanner. Densitometry of Western blots and CBB-stained proteins were performed using ImageJ software.

3.5.4. In vitro photolabeling experiments of purified actin and tubulin with aplyronine derivatives.

Actin (0.20 nmol, from rabbit skeletal muscle, Sigma Co.) and/or tubulin (0.10 nmol as a heterodimer) were incubated with ApA-PB, ApC-PB or ApA-DPB (0.20 nmol) in 300 μL of BRB80 (Brinkley Reassembly Buffer 80) [80 mM PIPES•Na (pH 6.9), 1 mM MgCl2, 1 mM EGTA, 1 mM GTP] for 30 min in a rotator at 4 °C. The total concentrations of DMSO and G-buffer, derived from actin solutions, were <2.5%, which did not significantly affect tubulin dynamics. The resulting mixture was irradiated with UV light (365 nm) for 30 min on ice, treated with equal volumes of $2 \times$ SDS-buffer, and boiled for 5 min at 95 °C. SDS-PAGE was performed using a precast 10% polyacrylamide gel, and the probe-bound proteins were detected with CBB stain and HRP-conjugated streptavidin.

3.5.5. In vitro tubulin polymerization assay.

For the fluorescence-based tubulin polymerization assay,[2] $\times$10 samples (5 μL) were added to 50 μL aliquots of 2 mg/ml tubulin (20 μM for the heterodimer) in tubulin assay buffer [80 mM PIPES·Na (pH 6.9), 2 mM MgCl$_2$, 0.5 mM EGTA, 10 μM DAPI] with 20% glycerol (v/v) cooled on ice, in a half-volume 96-well plate according to the manufacturer's instruction for this assay kit (cat. BK011P, Cytoskeleton Inc.). Tubulin polymerization was monitored by the increase in fluorescence ($\lambda_{ex/em}$ 360/450 nm) during 30 min at 37 °C, using a TECAN Infinite 200® PRO fluorescence microplate reader.

In another assay of microtubule sedimentation (centrifugation method), 3 μM tubulin in BRB buffer was ultracentrifuged (150,000 × g, 30 min at 4 °C) to remove oligomeric tubulins. To the supernatants (500 μL) were added 2 mM paclitaxel in DMSO (0.75 μL) to induce microtubule formation, and/or 100 μM actin in G-buffer (15 μL) and 1 mM ApA (1.5 μL). As a control experiment, 1 M CaCl$_2$ aq. (2.5 μL) was added instead of paclitaxel. After incubation for 1 h at 37 °C, samples were ultracentrifuged (150,000 × g, 1 h at 37 °C). The supernatants (lyophilized) and precipitates were dissolved in 1 × SDS buffer (100 μL) and boiled for 5 min at 95 °C. SDS-PAGE was performed using a precast 10% polyacrylamide gel, and the gels were stained with a Quick-CBB kit (Wako).

3.5.6. Gel permeation HPLC analysis of the actin–ApA–tubulin complex.

Actin, aplyronines, and tubulin heterodimer were mixed at a 1:1:1 molar ratio (50 μM each). After incubation at room temperature for 10 min, 10 μL of the mixture was analyzed by gel permeation column chromatography on a TSKgel SuperSW3000 column (ϕ 4.6 × 300 mm, TOSOH Co.). The components of the mixture were eluted with tubulin elution buffer [50 mM PIPES·K (pH 6.8), 100 mM KCl, 10 mM MgCl$_2$]. at 8 °C, with a flow rate of 0.2 ml/min.[3] The absorbance of the eluting solution was monitored at 280 nm, and fractions were collected for SDS-PAGE analysis and visualized by CBB stain and immunoblotting analysis with anti α-/β-tubulin. The same experiments were repeated for tubulin, actin–ApA or actin–ApC complexes alone.

## 3.5.7. Synthesis and spectroscopic data of ApA-DPB.

Succinyl ester **23**.[5]
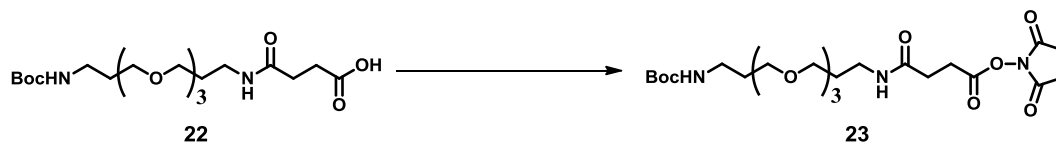
To a stirred solution of carboxylic acid **22** (22.3 mg, 53.0 μmol, commercially available) in dry dichloromethane (0.5 mL) were added *N*-hydroxysuccimide (9.7 mg, 84 μmol) and 1-ethyl-3-(3-dimethylaminopropyl)carbodiimide hydrochloride (EDC·HCl) (15.5 mg, 81 μmol). After being stirred at room temperature for 3 h, the reaction mixture was washed with sat. sodium bicarbonate aq. (4 mL × 3) and brine, dried with sodium sulfate, and concentrated. The crude material was purified with a SiO$_2$ column (0.5 g, chloroform–methanol = 1:0 → 99:1 → 0:1) to give succinyl ester **23** (23.1 mg, 84%) as a colorless oil. Compound **23**: ^{1}H NMR (600 MHz, CDCl$_3$) δ 6.51 (br s, 1H), 4.96 (br s, 1H), 3.65–3.51 (m, 12H), 3.38 (q, *J* = 6.0 Hz, 2H), 3.20 (br q, *J* = 6.0 Hz, 2H), 2.98 (t, *J* = 7.4 Hz, 2H), 2.83 (br s, 4H), 2.57 (t, *J* = 7.4 Hz, 2H), 1.79–1.72 (m, 4H), 1.43 (s, 9H); ^{13}C NMR (150 MHz, CDCl$_3$) δ 169.7, 168.9 (2C), 168.3, 156.1, 79.0, 70.50, 70.48, 70.2 (2C), 70.0, 69.5, 38.4, 38.3, 30.6, 29.7, 28.7, 28.4 (3C), 26.8, 25.6 (2C); IR (CHCl$_3$) 3453, 3388, 3010, 2929, 2874, 1818, 1789, 1742, 1709, 1668, 1511, 1367, 1215, 1210, 1170, 1090, 992, 856, 647 cm^{-1}; HRMS (ESI) *m/z* 556.2250 (calcd for C$_{23}$H$_{39}$KN$_3$O$_{10}$ [M+K]$^+$, Δ −1.7 mmu).

Double-PEG linked amide **24**.
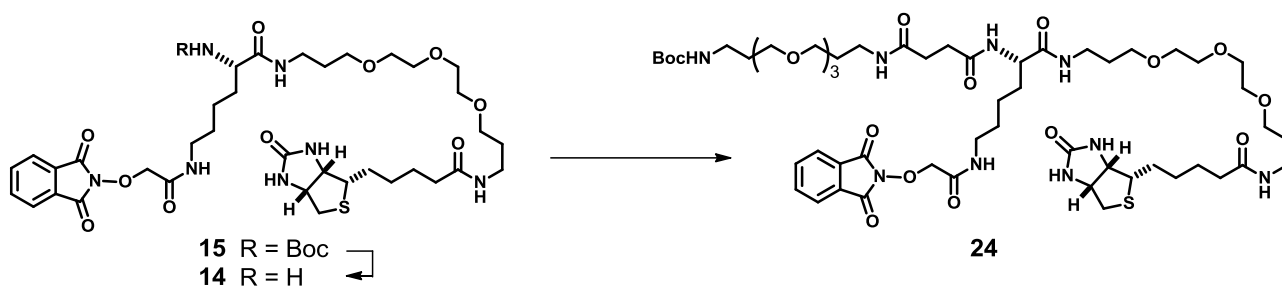
A solution of amide **15** (20.9 mg, 23.8 μmol) in a 1:1 mixture of dry dichloromethane and trifluoroacetic acid (1 mL) was stirred for 30 min at room temperature and azeotropically concentrated with toluene in vacuo to give crude amine (26.4 mg) as a trifluoroacetic acid salt. To a stirred solution of the crude amine trifluoroacetic acid salt in dry *N,N*-dimethylformamide (1 mL) were added succinyl ester **23** (23 mg, 45 μmol) and diisopropylethylamine (DIPEA, 10 μL, 58 μmol) under a nitrogen atmosphere. After being stirred for 11 h at room temperature, the mixture was azeotropically concentrated with toluene. The crude material was purified by recycling HPLC [JAIGEL-1H, JAIGEL-2H, chloroform] to give double-PEG linked amide **24** (17.1 mg, 61%) as a colorless oil. Compound **24**: $[\alpha]_D^{25}$ +2.5 (*c* 0.57, chloroform); ^{1}H NMR (600 MHz, DMSO-d_6) δ 8.14 (t, *J* = 5.7 Hz, 1H), 7.96 (d, *J* = 8.0 Hz, 1H), 7.93–7.80 (m, 6H), 7.74 (t, *J* = 5.6 Hz, 1H), 6.74 (t, *J* = 5.7 Hz, 1H), 6.42 (s, 1H), 6.35 (s, 1H), 4.60 (s, 2H), 4.30 (dd, *J* = 7.8, 5.0 Hz, 1H), 4.15–4.06 (m, 2H), 3.53–3.41 (m, 18H), 3.44–3.34 (m, 7H), 3.14–3.02 (m, 8H), 2.95 (q, *J* = 6.7 Hz, 2H), 2.81 (dd, *J* = 12.4, 5.1 Hz, 1H), 2.57 (d, *J* = 12.4 Hz, 1H), 2.40–2.25 (m, 4H), 2.04 (t, *J* = 7.4 Hz, 2H), 1.71–1.53 (m, 10H), 1.55–1.38 (m, 6H), 1.36 (s, 9H), 1.33–1.21 (m, 4H); ^{13}C NMR (150 MHz, DMSO-d_6) δ 171.9, 171.60, 171.57, 171.4, 165.7, 162.9 (2C), 162.7, 155.6, 134.9 (2C), 128.5 (2C), 123.4 (2C), 77.4, 75.8, 69.8 (4C), 69.5 (4C), 68.10, 68.08, 68.05, 68.02, 61.0, 59.2, 55.4, 52.6, 39.9–39.1 (2C, overlapped with the solvent signals), 38.3, 37.2, 35.85, 35.80, 35.7, 35.2, 31.4, 30.7, 29.7, 29.4, 29.3, 29.2, 28.6, 28.24 (3C), 28.20, 28.0, 25.3, 22.9; IR (CHCl$_3$) 3347, 3007, 2929, 2871, 1793, 1734, 1700, 1663, 1529, 1457, 1357, 1245, 1215 cm^{-1}; HRMS (ESI) m/z 1202.5960 (calcd for C$_{55}$H$_{89}$N$_9$NaO$_{17}$S [M+Na]$^+$, Δ −2.9 mmu).

Diazirine amide **26**.
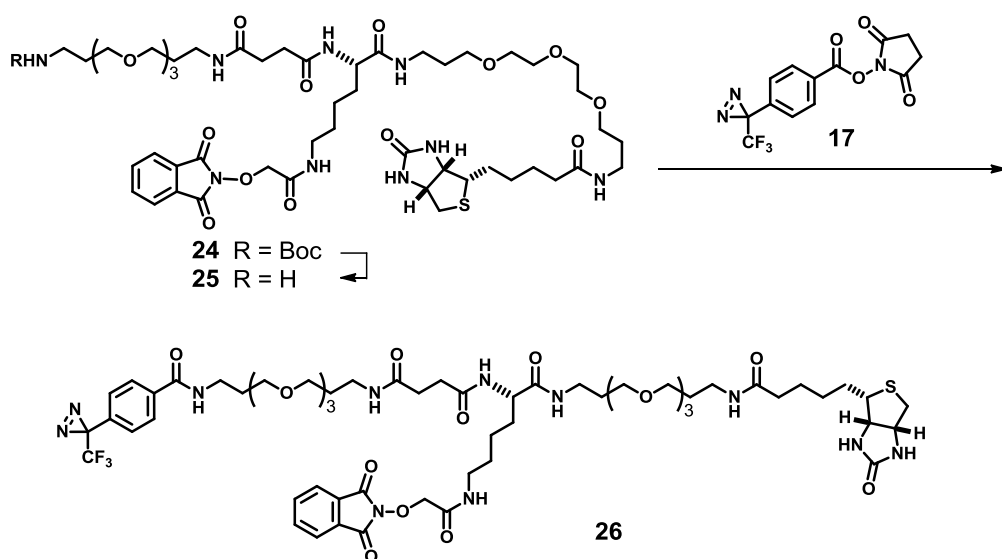
A solution of double-PEG linked amide **24** (9.9 mg, 8.4 µmol) in a 1:1 mixture of dry dichloromethane and trifluoroacetic acid (1 mL) was stirred for 30 min at room temperature and azeotropically concentrated with toluene in vacuo to give crude amine (12.9 mg) as a trifluoroacetic acid salt. To a stirred solution of the crude amine trifluoroacetic acid salt in dry *N,N*-dimethylformamide (0.4 mL) were added diazirine succinyl ester **17**[1] (9.6 mg, 29 µmol) and DIPEA (10 µL, 57 µmol) under a nitrogen atmosphere. After being stirred for 1 h at room temperature, the mixture was concentrated in vacuo. The crude material was purified by recycling HPLC [JAIGEL-1H, JAIGEL-2H, chloroform] to give diazirine amide **26** (10.5 mg, 97%) as a colorless oil.

Compound **26**: $[\alpha]_D^{23}$ +3.7 (*c* 0.19, chloroform); ^{1}H NMR (600 MHz, DMSO-d_6) δ 8.58 (t, *J* = 5.6 Hz, 1H), 8.14 (t, *J* = 5.7 Hz, 1H), 7.95 (d, *J* = 8.0 Hz, 1H), 7.93 (d, *J* = 8.3 Hz, 2H), 7.90–7.80 (m, 6H), 7.73 (t, *J* = 5.6 Hz, 1H), 7.37 (d, *J* = 8.3 Hz, 2H), 6.41 (s, 1H) 6.35 (s, 1H), 4.60 (s, 2H), 4.33–4.27 (m, 1H), 4.15–4.06 (m, 2H), 3.54–3.41 (m, 18H), 3.41–3.28 (m, 9H), 3.14–3.02 (m, 8H), 2.81 (dd, *J* = 12.4, 5.1 Hz, 1H), 2.57 (d, *J* = 12.4 Hz, 1H), 2.39–2.25 (m, 4H), 2.04 (t, *J* = 7.4 Hz, 2H), 1.74 (qui, *J* = 6.6 Hz, 2H), 1.70–1.55 (m, 8H), 1.54–1.36 (m, 6H), 1.36–1.20 (m, 4H); ^{13}C NMR (150 MHz, DMSO-d_6) δ 172.3, 172.04, 172.01, 171.9, 166.1, 165.5, 163.4 (2C), 163.1, 136.6, 135.3 (2C), 130.5, 128.9 (2C), 128.5 (2C), 126.8 (2C), 123.8 (2C), 122.2 (q, $^1J_{C\text{-}F}$ = 274 Hz), 76.2, 70.21, 70.18 (2C), 70.16, 69.99, 69.96 (2C), 69.94, 68.6, 68.53, 68.48, 68.45,

61.5, 59.6, 55.8, 53.0, 40.5, 40.3, 38.7, 37.2, 36.3, 36.2, 36.1, 35.6, 31.9, 31.1, 29.83, 29.75, 29.66, 29.65, 29.0, 28.6, 28.48 (q, $^2J_{\text{C-F}}$ = 40.5 Hz), 28.46, 25.7, 23.3; IR (chloroform) 3360, 3005, 2928, 2871, 1793, 1735, 1692, 1659, 1539, 1458, 1349, 1235, 1189, 1162, 1126 cm^{-1}; HRMS (ESI) m/z 1330.5408 (calcd for C$_{59}$H$_{84}$F$_3$KN$_{11}$O$_{16}$S [M+K]$^+$, Δ +0.6 mmu).

Alkoxyamine **27**.
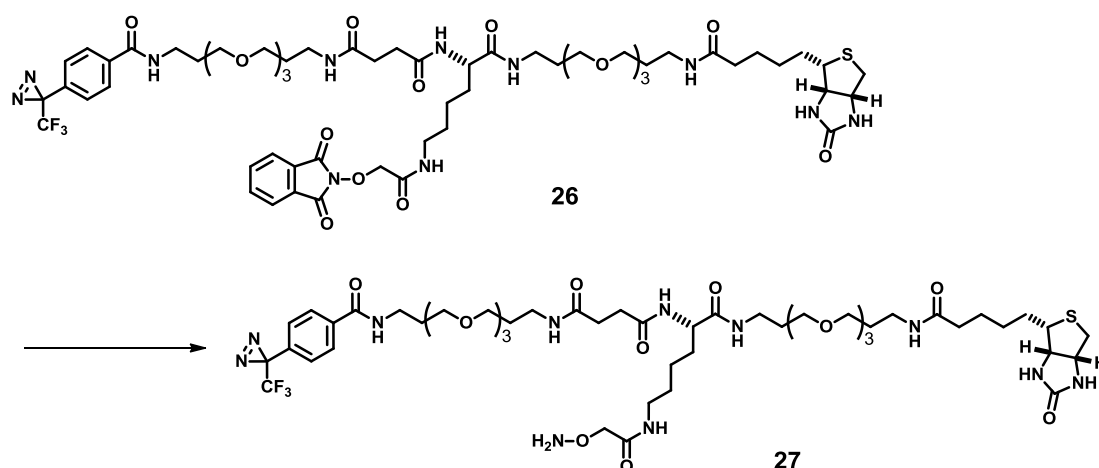
Diazirine amide **26** (1.8 mg, 1.4 μmol) was dissolved in a 21 mM solution of hydrazine monohydrate in ethanol (1.0 mL, 21 μmol). After being stirred at room temperature for 15 min, the mixture was filtered, and the filtrate was azeotropically concentrated with toluene to give alkoxyamine **27** (quant. monitored by TLC analysis: R_{f} 0.23, chloroform/methanol 4:1), which was immediately used for the next step without further purification.

ApA–DPB (**21**).
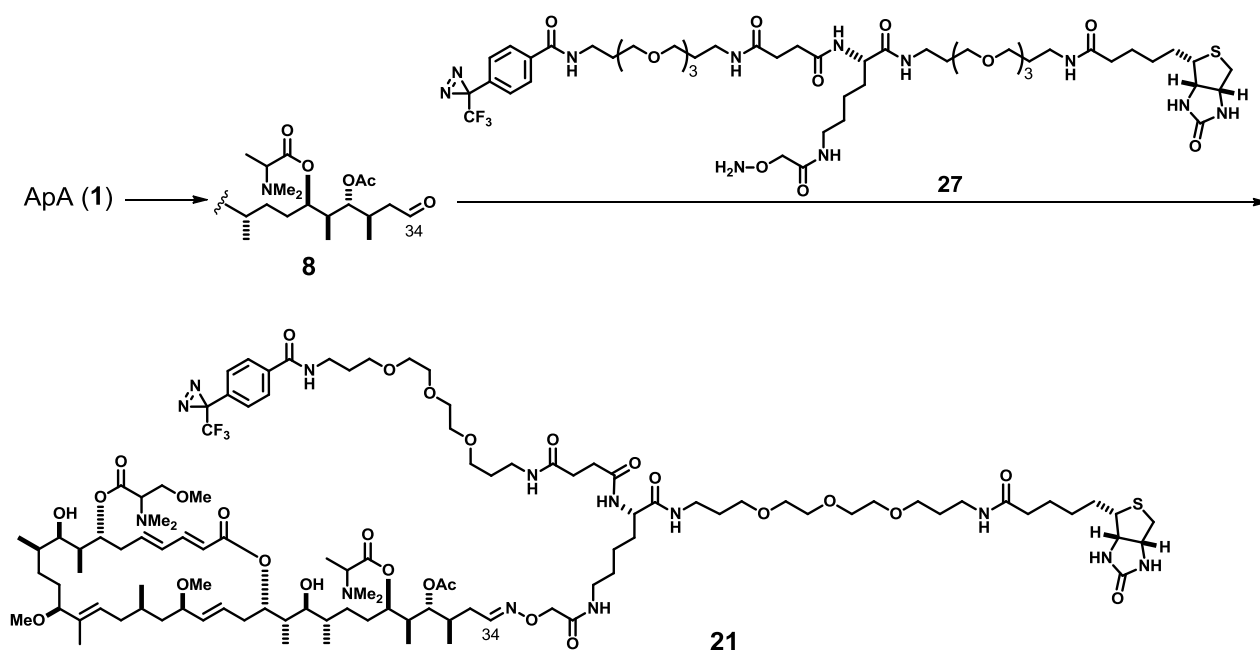
A solution of ApA (0.32 mg, 300 nmol) in a 3:1 mixture of 1,4-dioxane (150 μL) and 2 M aq. HCl (50 μL) was stirred for 1 h at 50 °C. The resulting mixture was diluted with sat. sodium bicarbonate aq. (250 μL) and water (2 mL), and extracted with chloroform (1 mL × 5). The combined extracts were washed with brine and concentrated to give aldehyde **8** (quant. monitored by HPTLC analysis: R_f 0.49, chloroform–methanol 9:1), which was used for the next step without further purification. A solution of the aldehyde **8** and the alkoxyamine **27** prepared as above in a 9:1 mixture of ethanol and 50 mM acetate buffer (pH 4.0) (0.3 mL) was stirred at room temperature for 118 h. The reaction mixture was directly applied twice to a Develosil ODS-HG-5 HPLC column (ϕ 20 mm I.D. × 250 mm). Samples were eluted with methanol–20 mM ammonium acetate (80:20) at a flow rate of 5 mL/min, with monitoring at 254 nm (t_R = 45–50 min) to give ApA–DPB (**21**) (149 nmol, 50%, based on NMR quantification, E/Z = 5.7:1 for the C34 isomers). The purified ApA-DPB (**21**) was freeze-dried, dissolved in water, and freeze-dried again twice to remove remaining ammonium acetate. Compound **21** : ^{1}H NMR (600 MHz, CD3OD) δ 7.90 (d, J = 8.4 Hz, 2H), 7.57 [6.86][1] (t, J = 6.4 Hz, 1H), 7.34 (d, J = 8.4 Hz, 2H), 7.20 (dd, J = 10.9, 15.3 Hz, 1H), 6.38 [6.38][2] (dd, J =

10.9, 14.8 Hz, 1H), 6.22 (ddd, J = 4.4, 9.8, 14.8 Hz, 1H), 5.97 (d, J = 15.3 Hz, 1H), 5.64 (ddd, J = 3.9, 10.9, 14.8 Hz, 1H), 5.55 (d, J = 11.2 Hz, 1H), 5.15–4.55 (m, 5H), 4.48 (dd, J = 4.8, 7.9 Hz, 1H), 4.41 [4.47][1] (s, 2H), 4.29 (dd, J = 4.5, 8.6 Hz, 1H), 4.21 (dd, J = 4.9, 8.6 Hz, 1H), 3.70–3.45 (m, 2 8H), 3.41–3.07 (m, 15H), 3.34 [3.33][2] (s, 3H), 3.18 (s, 3H), 3.15 (s, 3H), 2.92 (dd, J = 4.9, 12.7 Hz, 1H), 2.70 (d, J = 12.7 Hz, 1H), 2.55–2.25 (m, 5H), 2.38 [2.39][2] (s, 6H), 2.34 [2.33][3] (s, 6H), 2.20–1.95 (m, 10H), 2.04 [2.05][1] [2.03][3] [2.04][1,3] (s, 3H), 1.90–0.80 (m, 54H), 0.92 (d, J = 6.6 Hz, 3H), 0.91 (d, J = 6.3 Hz, 3H), 0.77 [0.76][2] (d, J = 5.8 Hz, 3H). Chemical shifts of the minor diastereomers are within brackets: [ ][1] 5.7:1 at C34 stereoisomers. [ ][2] 1.8:1 at C7 trimethylserine moiety. [ ][3] 1.2:1 at C29 dimethylalanine moiety. HRMS (ESI) m/z 741.7487 (calcd for $C_{108}H_{179}F_3N_{13}Na_2O_{27}$ S [M+H+2Na]$^{3+}$ 741.7495, Δ −0.8 mmu).

References

1) Nassal, M. *Liebigs. Ann. Chem.* **1983**, 1510–1523.

2) Bonne, D.; Heusele, C.; Simon, C.; Pantaloni, D. *J. Biol. Chem.* **1985**, *260*, 2819–2825.

3) Szyk, A.; Deaconescu, A. M.; Piszczek, G.; Roll-Mecak, A. *Nat. Struct. Mol. Biol.* **2011**, *18*, 1250–1258.

4) Castoldi, M.; Popov, A. V. *Protein Expr. Purif.* **2003**, *32*, 83–88.

5) Rajopadhye, M.; Edwards, D. S.; Harris, T. D.; Heminway, S. J.; Liu, S.; Singh, P. R. PCT Int. Appl. WO 9958162.

Chapter 4.

Discussions and Conclusions

In this research, to clarify the mode of action of ApA, the author has carried out the identification of new target proteins of ApA and the analysis the interaction between ApA and its target proteins.

In chapter 2, the author searched the target proteins of ApA by using aplyronine biotin probes.

1) ApA-biocytin and ApA-bio were synthesized by converting the *N*-methyl enamide moiety of ApA. These two probes maintained the both cytotoxicity and actin-depolymerizing activity of ApA, and a known target, actin, was affinity-purified by using these probes (described in section 2.2).

2) By using ApA-bio, 40 kDa and 47 kDa proteins were specifically purified from tumor cell lysate as with actin. These proteins were identified as Arp2 and Arp3 (actin-related proteins) (described in section 2.3.1).

3) ApA-PB and ApC-PB, which have photoaffinity groups, were synthesized. They did not covalently bind to Arp2 or Arp3. Thus, actin-related proteins might indirectly bind to ApA as the ternary adducts of the actin-ApA complex or through the oligomeric actin (described in section 2.3.2).

4) Through in situ photolabeling experiments with ApA-PB, two proteins (55 kDa and 58 kDa) as well as actin were specifically labeled. The major constituents of two bands were α-/β-tubulin. The 58 kDa protein was identified as β-tubulin which binds with ApA-PB (described in section 2.4).

In chapter 3, the author analyzed the interaction among tubulin, ApA and actin through the use of in vitro experiments.

1) In vitro photolabeling experiments showed that ApA-PB synergistically binds to tubulin in association with actin. In contrast, ApC-PB did not bind to tubulin even in the presence of actin (described in section 3.2).

2) Tubulin polymerization assay and ultracentrifugation analysis revealed that ApA inhibits tubulin

polymerization in the presence of actin (described in section 3.3).

3) Through the use of gel-permeation HPLC analysis, it was revealed that ApA forms a 1:1:1 heterotrimeric complex with actin and a tubulin heterodimer (described in section 3.4).

As described in chapter 1, it has been suggested that ApA does not interact with known molecular targets of antitumor agents, such as DNA, microtubules, and cell cycle regulating proteins. The author established that ApA interacts with tubulin in association with actin, thereby inhibiting microtubule assembly. To the best of my knowledge, there have been no previous reports that small actin-binding agents disturb microtubule assembly.

Now, tubulin has been identified as the second target of ApA. Here the author considers what factors were important for the identification of tubulin. Initial pull-down experiments using ApA-bio showed that Arp2 and Arp3 were affinity-purified as binding proteins from HeLa S3 cell lysate. However, Arp2 and Arp3 did not covalently bind to ApA-PB or ApC-PB. It is noted that no tubulin in the cell lysate was photolabeled or affinity-purified with ApA-PB. In contrast, in situ photolabeling experiments established that the cellular targets of ApA are both actin and tubulin. These critical differences between in vitro and in situ photolabeling experiments might be due to the instability of tubulin under the lysis conditions the author used.

Through the use of in situ photolabeling experiments, it was demonstrated that ApA binds selectively to actin and β-tubulin in cells. In contrast to β-tubulin, the amount of affinity-purified α-tubulin with ApA-PB was similar to that of the control. This result suggests that the tight association of the subunits of the tubulin heterodimer need to be dissociated, which is incompatible with gel permeation HPLC analysis. A possible explanation is that ApA-PB covalently bound to β-tubulin might destabilize the association of tubulin subunits. Alternatively, it is possible that α-tubulin is more labile than β-isomer under the cell lysis or affinity-purification conditions we used, which might enhance its dissociation from the resin.

It was reported by co-workers that the treatment of HeLa S3 cells with 100 pM ApA caused abnormal spindle formation and inhibition of mitosis[1], which finally induce apoptosis in HeLa S3 cells.[2] These results

suggest that ApA affects microtubule assembly in cells. ApA exhibited cytotoxicity at sub-nM concentration. The total actin concentration in eukaryotic cell is approximately 100 μM,[3] and the K_d value for the actin-ApA interaction was shown to be 100 nM.[4] Therefore, most of ApA might be trapped within cells as an actin complex at the sub-nM concentration. Based on these information, plausible mode of action of ApA are shown in Figure 4-1. First, ApA interacts with actin to form an actin-ApA complex without causing the depolymerization of F-actin at sub-nM concentration. Next, the actin-ApA complex might interact with tubulin heterodimer to inhibit microtubule dynamics. Finally the inhibition of microtubule dynamics would cause cell cycle arrest through the abnormal spindle formation and apoptosis. Compared to the tubulin concentration in eukaryotic cells (~20 μM),[5] the effective concentration of actin-ApA complex would be too low to form the ternary complex with a tubulin heterodimer by the complete decomposition of microtubule. Generally, vinblastine binds to microtubule ends to prevent further polymerization, and colchicine binds to heterodimer which can be incorporate in the microtubule and induce the dynamic instability.[6] Thus, they affect microtubule dynamics even at low concentration. Actin-ApA complex might have the similar mechanism that actin-ApA complex or the ternary complex bind to or incorporate in microtubule in order to inhibit microtubule dynamics.
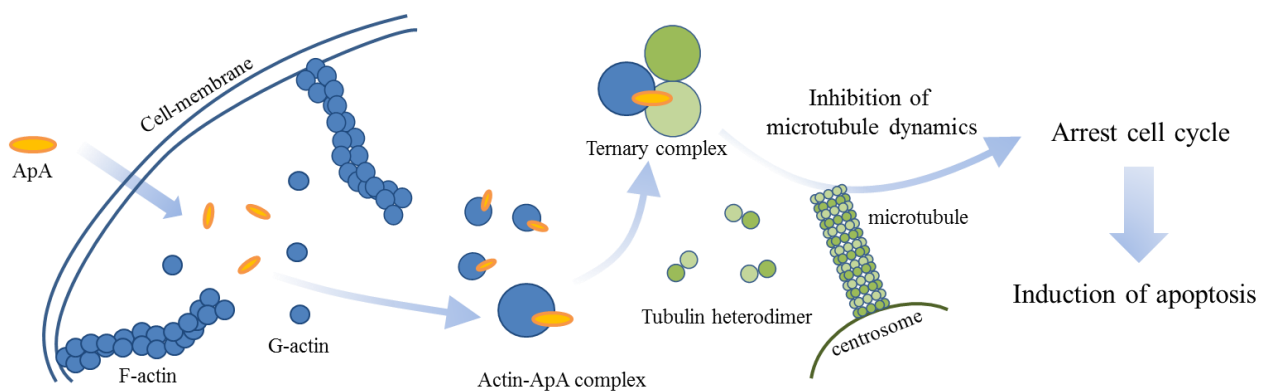

Figure 4-1. Plausible mode of action of aplyronine A.

Dynamics of microtubule and microfilaments regulate the various cellular functions. These dynamics were also regulated by various cellular proteins.[7] A variety of proteins mediates microtubule-actin interactions and regulates their dynamics. Among those, mammalian diaphanous-related (mDia) formin proteins not only nucleate and assemble linear actin filaments but also directly bind to microtubules and regulate their stabilization.[8] A member of the mDia family, mDia3, associates with the kinetochore and contributes to chromosome alignment in the M-phase.[9] Another F-actin-associated protein, drebrin, binds to EB3 to coordinate the F-actin-microtubule interactions responsible for neurogenesis.[10] It is possible that ApA modulates the coordination between the microtubules and actin and affects cytoskeleton dynamics by mimicking such microtubule-targeting, actin-binding proteins.

Thus, ApA represents a relatively rare type of compound, which binds to two different cytoplasmic proteins and forms a ternary complex. A lot of actin-targeting agents have been reported and its modes of action were still unclear. It is possible that actin-targeting agents also interact with multiple cellular targets via protein-protein interactions (PPI). Actin is an abundant cytoplasmic protein and has important roles in various cellar functions in cells. The studies of compounds that induce PPI based on the actin interaction have potential for the design and development of newly classified pharmacological tools and therapeutic agents. The author expected that the studies on ApA pioneer in these studies.

References

1) Kita, M.; Hirayama, Y.; Yoneda, K.; Yamagishi, K.; Chinen, T.; Usui, T.; Sumiya, E.; Uesugi, M.; Kigoshi, H. *J. Am. Chem. Soc*. **2013**, *135*, 18089–18095.

2) Kita, M.; Yoneda, K.; Hirayama, Y.; Yamagishi, K.; Saito, Y.; Sugiyama, Y.; Miwa, Y.; Ohno, O.; Morita, M.; Suenaga, K.; Kigoshi, H. *ChemBioChem* **2012**, *13*, 1754−1758.

3) Korn, E. D. *Physol. Rev*. **1982**, *62*, 672–737.

4) Saito, S.; Watabe, S.; Ozaki, H.; Kigoshi, H.; Yamada, K.; Fusetani, N.; Karaki, H. *J. Biochem.* (Tokyo) **1996**, *120*, 552−555.

5) Gard, D. L.; Kirschner, M. W. *J. Cell Biol*. **1987**, *105*, 2191–2201.

6) Dumontet, C.; Jordan, M. A. *Nat. Rev. Drug Discov.* **2010**, *9*, 790–803.

7) Rodriguez, O. C.; Schaefer, A. W.; Mandato, C. A.; Forscher, P.; Bement, W. M.; Waterman−Storer, C. M. *Nat. Cell Biol*. **2003**, *5*, 599−609.

8) Ishizaki, T.; Morishima, Y.; Furuyashiki, T.; Kato, T.; Narumiya, S. *Nat. Cell Biol*. **2001**, *3*, 8−14.

9) Yasuda, S.; Oceguera−Yanez, F.; Kato, T.; Okamoto, M.; Yonemura, S.; Terada, Y.; Ishizaki, T.; Narumiya, S. *Nature* **2004**, *428*, 767−771.

10) Geraldo, S.; Khanzada, U. K.; Parsons, M.; Chilton, J. K.; Gordon−Weeks, P. R. *Nat. Cell Biol*. **2008**, *10*, 1181−1189.

List of publications

1. Kita, M.; Hirayama, Y.; Sugiyama, M.; Kigoshi, H. *Angewandte Chem. Int. Ed.* **2011**, *50*, 9871–9874.

2. Kita, M.; Hirayama, Y.; Yamagishi, K.; Yoneda, K.; Fujisawa, R.; Kigoshi, H. *J. Am. Chem. Soc*. **2012**, *134*, 20314–20317.

3. Kita, M.; Hirayama, Y.; Yoneda, K.; Yamagishi, K.; Chinen, T.; Usui, T.; Sumiya, E.; Uesugi, M.; Kigoshi, H. *J. Am. Chem. Soc*. **2013**, *135*, 18089–18095.

Supplementary list of publication

1. 平山　裕一郎 *ファルマシア* **2011**, *47*, 250–251.

2. Kobayashi, K.; Fujii, Y.; Hirayama, Y.; Kobayashi, S.; Hayakawa, I.; Kigoshi, H. *Org. Lett.* **2012**, *14*, 1290–1293.

3. Kita, M.; Yoneda, K.; Hirayama, Y.; Yamagishi, K.; Saito, Y.; Sugiyama, Y.; Miwa, Y.; Ohno, O.; Morita, M.; Suenaga, K.; Kigoshi, H. *ChemBioChem* **2012**, *13*, 1754–1758.